

POLITECNICO DI TORINO

Corso di Laurea in Ingegneria Civile

Tesi di Laurea Magistrale

Auxetic materials in civil construction: state of the art and preliminary experimental investigation



Relatori:

prof. Davide Dalmazzo

prof. Fabrizio Barpi

prof. Pier Paolo Riviera

prof. Orazio Baglieri

Candidato:

Dino Odobasic

Luglio 2020

ABSTRACT

This work suggests a possible direction towards the diffusion of a different kind of materials for civil engineering applications. These materials are called “Auxetic materials” and their peculiarity is to have a negative Poisson’s ratio.

In this work are analyzed the behavior and properties of these materials and their possible applications through one of the newest technologies: 3D printing.

In the first part auxetics are classified by the different geometries and the different kind of uses they can be adopted, for example as sheets, solids and foams. To understand in a better way this classification some nowadays interesting applications are listed.

Then they analyzed by a mechanical point of view. One of the most interesting aspects analyzed is how the unitary cell of the auxetic element affects the deformation of the entire element under and applied load. This analysis is done by changing different parameters such as shape, size and thickness of the elementary cell.

The analysis is done by doing a FEM analysis on the software Autocad Inventor Nastran. Than the analysis is compared to a mechanical laboratory test witch is done on the same element analyzed on the software, but created with a 3D printer.

Index

1	AUXETIC MATERIALS	6
1.1	Introduction	6
1.2	Poisson's ratio	6
1.2.1	Definition.....	6
1.2.2	Demonstration of Poisson's ratio's range	7
1.3	Definition and history of auxetic materials.....	8
1.4	Classification of auxetic materials	9
1.4.1	Natural auxetic materials.....	9
1.4.2	Man-made auxetic materials.....	9
1.4.3	Auxetic honeycombs.....	10
1.4.4	Auxetic foams	12
1.4.5	Auxetic polymers	13
1.4.6	Fiber composite	14
1.5	Structures.....	14
1.5.1	Non-affine deformation	15
1.5.2	Non-central forces	15
1.5.3	Noncentrosymmetry.....	17
1.6	Properties.....	17
1.6.1	Shear modulus and resistance.....	18
1.6.2	Resistance to indentation	18
1.6.3	Fracture resistance	19
1.6.4	Acoustic absorption	21
1.6.5	Synclastic behavior	22
1.6.6	Variable permeability.....	23
1.6.7	Shape memory auxetic	23
1.6.8	Other auxetic properties	24
1.7	Applications.....	24
2	SOFTWARE ANALYSIS	28
2.1	Introduction	28
2.2	Geometry analysis	28
2.3	Dependence between deformation and structural packing.....	45
2.4	Models for laboratory tests	55
2.5	Conclusions	57
3	3D PRINTING.....	58

3.1	Introduction	58
3.2	MakerBot Replicator +	58
3.3	Printing process.....	59
3.4	Conclusions	61
4	LABORATORY TEST	62
4.1	Introduction	62
4.2	Equipment and software	62
4.2.1	Laboratory equipment	62
4.2.2	Tracker video analysis software	63
4.3	Laboratory set up	64
4.4	Laboratory and software results compared	64
4.5	Conclusions	67
5	Conclusions.....	68
6	APPENDIX	70
6.1	FEA.....	70
6.2	Linear and nonlinear analysis.....	70
6.2.1	Geometric nonlinearity	71
6.2.2	Material nonlinearity	71
6.2.3	Boundary condition nonlinearity	72
7	REFERENCES.....	73

1 AUXETIC MATERIALS

1.1 Introduction

This chapter is an introduction to the auxetic materials. The analysis of such materials starts with their definition through the Poisson's ratio and a brief segment of the history of auxetics. It's given a description of their structure and a classification of auxetic materials is draft, based on their manufacturing. To better understand the behavior of auxetic materials is offered a list of their main properties with a comparison with "normal" materials. Finally is given a list of different field applications where auxetic materials are used.

1.2 Poisson's ratio

1.2.1 Definition

In physics the Poisson's ratio, indicated with the greek letter "v", is the measure of the Poisson effect, that describes the expansion or contraction of a material in directions perpendicular to the direction of loading. The value of Poisson's ratio is the negative of the ratio of transverse strain to axial strain. The Poisson's ratio can be expressed in the following formula:

$$\nu = - \frac{\varepsilon_{trans}}{\varepsilon_{axial}}$$

where ν is the Poisson's ratio, ε_{trans} is the transverse strain (positive for tension, negative for compression), ε_{axial} is the axial strain (positive for tension, negative for compression). For most materials the Poisson's ratio is a positive number between 0 and 0,5, usually close to 0,33. The reason why is that most materials can resist a change in volume (determined by the bulk modulus) more that they can resist a change in shape (determined by the shear modulus). However in the last years it was discovered that there are some anisotropic materials and some designed materials that could have a negative Poisson's ratio. The designed materials are called Auxetic materials and they have this specific behavior thanks to their geometry. By considering this kind of materials the Poisson's ratio range increases by going from -1 to 0,5.

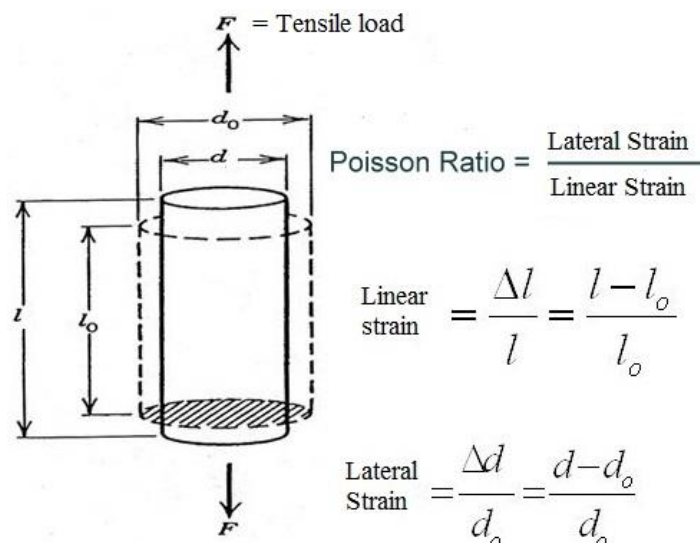


Figure 1 Poisson's ratio formulation

By analyzing the Poisson's ratio in different materials and situations is possible to reach some conclusions. For isotropic solids (properties non dependent on the direction) the Poisson's ratio is related to the bulk modulus, shear modulus and elastic modulus by the following equations:

$$\nu = (3K - 2G)/(6K + 2G)$$

$$E = 2G(1 + \nu)$$

$$E = 3K(1 - 2\nu)$$

For anisotropic solids the Poisson's ratio and elastic moduli depend on the direction. Moreover the Poisson's ratio can have high positive or negative values. For orthotropic materials the Poisson's ratio and elastic modulus are bounded by the following equation:

$$|\nu_{ij}| = (E_i/E_j)^{1/2}$$

With i and j indicating the considered directions.

In viscoelastic materials the Poisson's ratio is depending on time in the context of transient tests such as creep and stress relaxation. If the deformation is sinusoidal in time, the Poisson's ratio could depend on frequency, and could have an associated phase angle. Specifically, in viscoelastic solids, the transverse strain could be out of phase with the longitudinal strain. Considering polymers in glassy regime, the Poisson's ratio is close to 0,33, however at a higher temperature, sufficient for rubber behavior, there's a decrease in stiffness and the Poisson's ratio is close to 0,5. Usually, in case of phase transformation, the bulk modulus decreases and the shear modulus tends to stay the same. In this cases the Poisson's ratio decreases while approaching the phase transformation and can even get to negative values.

As seen there are many cases where the Poisson's ratio can differ from the usual values. One of the most interesting it's the auxetic behavior because there's a significant improvement of the structure properties, all related to the negative value of ν .

1.2.2 Demonstration of Poisson's ratio's range

In order to have a more precise mathematical description of the modification obtained by the auxetic body that undergoes a field of forces, many other physical quantities factors have to be taken into consideration. These are useful in measuring the stiffness of the materials. They all arise from the generalized Hooke's law, which is a principle that states that the force (F) needed to extend or compress a spring by some distance (X) scales linearly with respect to that distance by a factor (K) which is a constant characteristic of the spring (material).

$$F = kx$$

To understand the demonstration is natural to introduce the four constants ν , Poisson's ratio, E, Young's modulus, G, shear modulus and K, bulk modulus witch are not independent for an isotropic material [1].

The Young's modulus "E" is also known as "tensile modulus" or "elastic modulus" and it's a mechanical property of linear elastic solid materials. It is defined as the ratio of the stress along an axis to the strain along that axis in the range of stress in witch Hooke's law holds.

$$E = \frac{\sigma}{\varepsilon}$$

The shear modulus "G" is taken into account when on an element there are two opposing forces on two opposite faces. Usually "G" is defined as the ratio of shear stress to the shear strain, but employing the Hooke's law relations is known that G must be related to E and ν through:

$$G = \frac{E}{2(1 + \nu)}$$

Each engineering modulus E and G must be positive if a free block of the material is to be in stable equilibrium, therefore $\nu > -1$

Summing the normal components of stress and defining the bulk modulus as the ratio of pressure to volumetric strain provides a definition for bulk modulus

$$K = \frac{E}{3(1 - 2\nu)}$$

Requiring both K and E positive for stability gives $\nu < 0,5$. Combining these gives the range of ν from -1 to $0,5$. If one modulus were to be exactly zero, a condition of neutral stability would obtain, associated with Poisson's ratio exactly attaining one of the limits.

1.3 Definition and history of auxetic materials

The Poisson's ratio of a material is a dimensionless constant that depends on the direction of an applied load, and describes the ratio of negative transverse strain to the longitudinal strain of a body submitted to a tensile load [2, 3]. It is used to make a comparison between the structural performance of real homogeneous and non-homogeneous materials [4]. In the past it was believed that in nature isotropic materials could not have a negative Poisson's ratio [5], so it was implicitly assumed to be positive [6]. However, there are materials that present an inverse behavior. These materials expand their transverse dimension when submitted to an axial tensile strength and decrease it when compressed [7], so they have a negative Poisson's ratio. The materials that revealed this behavior have been called anti-rubber [8] and dilatational materials [9], till Ken Evans coined the currently accepted term: "auxetics" [10]. This name, derived from the Greek word αὐξητικός (auxetikos), meaning "that which tends to increase" [11].

This kind of behavior does not contradict the classical theory of elasticity as seen in the previous demonstration [12, 13]. In the theory, for isotropic materials the Poisson's ratio can assume values between -1 and $0,5$ for 3D structures [14] while for 2D structures it can assume values from -1 to 1 . The violation of these limits gives rise to instability [15].

In isotropic systems, the Poisson's ratio is independent of the direction, but in the case of anisotropic materials the determination of this elastic constant is depending on the direction of the stretch [16] and the other transverse directions [17]. There are materials that have an auxetic behavior in some directions and a non-auxetic behavior in the others (for example in α -Cristobalite) [18,19]. These kinds of materials are known as partial auxetics. Despite common sense, partial auxetics [20,21] are quite common, as 69 % of cubic elemental metals present an auxetic behavior in at least one direction [22]. This kind of interaction between the different directions of deformations may generate interesting values [23, 24] of Poisson's ratio that exceed largely the presented isotropic values for orthotropic and anisotropic materials [25].

Even though the existence of auxetic materials has been admitted for more than 150 years [26], only a few natural examples have been found. In 1882 the case of iron pyrite monocrystals was reported by experiments on the twisting and bending of mineral rods [27]. This was the first study that proved the existence of auxetic material in nature and it was estimated a Poisson's ratio of about $-1/7$ [28]. Since then there have been other considered cases, such as polymorphic silicones [29], zeolites [30] and silicates [31]. One of the first artificially produced auxetic materials was the RFS structure (diamond-fold structure) which was invented in 1978 by the Berlin researcher K. Pietsch. Even if he didn't use the term "auxetic", he reported for the first time their lever mechanism and non-linear mechanical reaction, therefore he was considered the inventor of the

auxetic net.

There were found some examples of auxetic behavior in biological tissues. The classical examples are cat skin [32], cow teat skin [33] and cancellous bone [34]. Additional studies suggest that some inorganic and biological fibrous materials present auxetic behavior in general [35]. Due to the absence of auxetic materials in nature and the difficulty in attributing them a specific application, an effort was made to synthesize them [36]. This objective was completed and described in the article entitled "Foam structures with a Negative Poisson's Ratio" by R.S. Lakes from the University of Wisconsin Madison, who succeeded for the first time in 1987, to manufacture the first auxetic foam [37]. This was possible by analyzing the way in which the structure was deforming when subjected to a load and manipulating its internal structure [38].

1.4 Classification of auxetic materials

Overall, auxetic materials can be classified into two groups: natural auxetic materials and man-made auxetic materials. If compared to conventional materials, auxetic materials are relatively rare, but there are some examples of natural materials that have a negative Poisson's ratio. However most of auxetic materials are man-made. These materials are made from nanoscale to macroscale through a large quantity of engineering methods such as: laser cutting machine, 3D printing, foaming, folding/spinning methods and through a combination of assembly methods for composites.

1.4.1 Natural auxetic materials

The natural auxetic materials can be classified as organic or inorganic materials. It was found one type of inorganic auxetic material, α -cristobalite, a type of silicon dioxide [39]. Several analyses were done to discover its elastic stiffness. At the end a laser Brillouin spectroscopy permitted to obtain its adiabatic single-crystal elastic stiffness coefficients. The tensorial analysis on the silicon dioxide demonstrated that this type of natural material could reach a maximum negative Poisson's ratio of -0,5 in some directions, while the average Poisson's ratio for single-phased aggregate was -0,16 [40].

The first organic natural material that was found was animal skin, a polymer with an auxetic behavior. The first proved animal skin with an auxetic behavior was cat skin. By doing some tests on cat skin, Verona and Westmann proved that its Poisson's ratio was negative. After that it was discovered that cow teat skin showed an auxetic behavior too. In this case, by conducting a biaxial tensile test, it was discovered that cow teat skin would have a negative Poisson's ratio when the testing samples would have a certain ratio between length and width.

1.4.2 Man-made auxetic materials

Most of the man-made auxetic materials are from bulk-scale materials and specially engineered structures. Some of the most typical auxetic materials made with this method are auxetic polymers, auxetic fabrics and auxetic composites. For the fabrication of these materials are used conventional technologies, but some new technologies are also reported. One of the best technologies currently used to create auxetic structures is the laser writing, by which is possible to produce complicated 3D auxetic structure with high precision. In Fig. 6 are listed the fabrication methods used to produce auxetic structures.

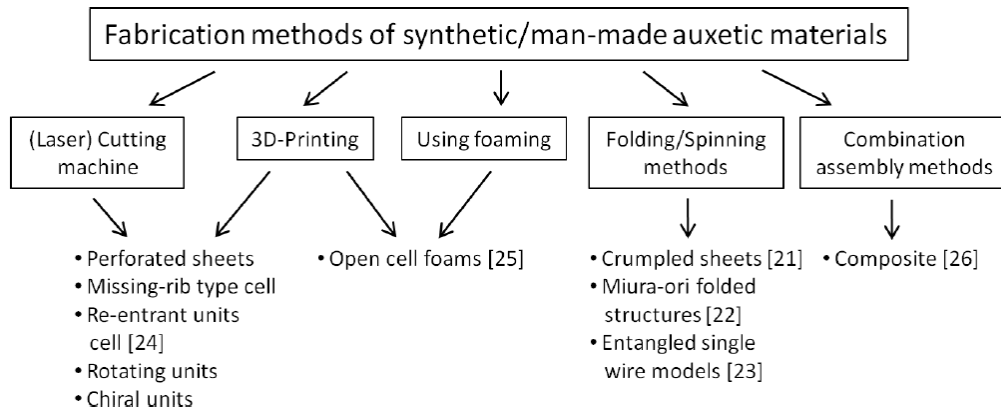


Figure 2 Fabrication methods of auxetic structures

Auxetic materials can be divided in to four main group as the following:

- Auxetic honeycombs
- Auxetic foams
- Auxetic polymers
- Fibre composite

1.4.3 Auxetic honeycombs

The first example of auxetic honeycomb was developed in the 80s and it's the tessellating re-entrant hexagon shown schematically in fig. 3 [41-42]. It's shown that the deformation is due to the hinging of the diagonal cell walls in response to the applied load. As shown in the figure when the load is applied in the horizontal direction, the diagonal cell walls tend to open up and align in the horizontal direction. Due to this deformation, the vertical cell walls tend to move apart from one to another. All this mechanism results in having the auxetic behavior of the whole structure. In reality, most honeycombs of this type deform predominantly by flexure of the diagonal ribs, with hinging and axial stretching of the ribs also occurring simultaneously [43-44]. Flexure of the ribs also leads to auxetic behavior in the re-entrant hexagonal honeycomb system.

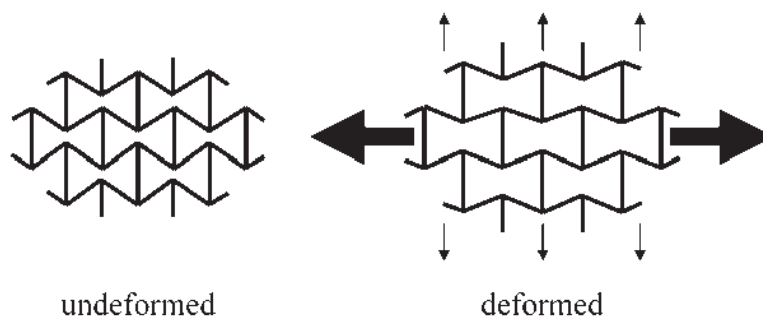


Figure 3 Re-entrant honeycomb structure undeformed and deformed

Figure 4 shows some alternative honeycomb topologies to the tessellating re-entrant hexagon motif which give rise to auxetic behavior.

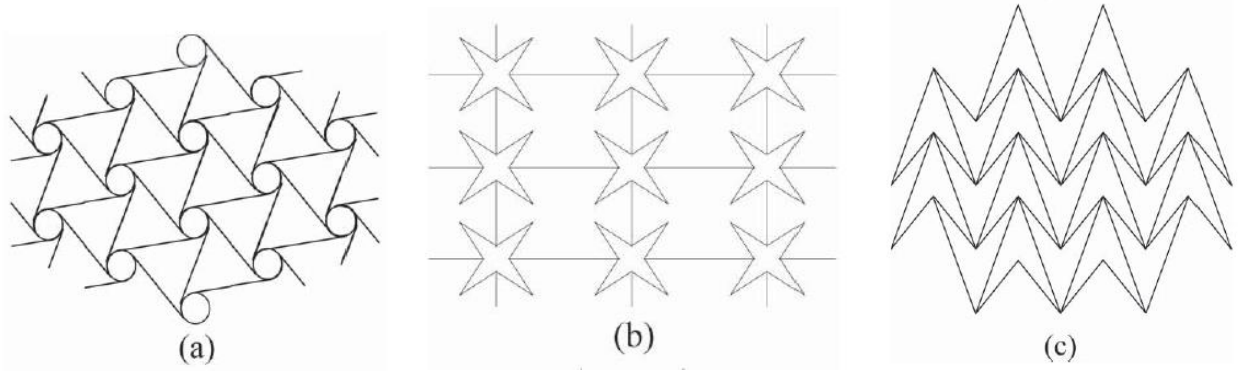


Figure 4 Auxetic honeycomb topologies: (a) chiral; (b) star; (c) double arrowed

Chiral structures are consisted by central nodes which are connected between straight ligaments (ribs). Most of the times the geometry used for central nodes is a circle, however there are some other possible geometries which can be used. The difference between the various topologies of honeycomb structures is the deformation mechanism. As shown in fig. 4a [45], when a force is applied, the deformation occurs through the rotation of the circular central nodes and the wrapping or unwrapping of the ligaments around them. In the case of star honeycomb (fig. 4b) [46] and double arrow-head honeycomb (fig. 4c) [47], the auxetic behavior is due, respectively, to the opening or closing of the stars and arrowheads. In addition to the benefits associated with the auxetic property, the chiral honeycomb has potential due to the particular structural features inherent in the geometry. The cylinders have been shown to lead to improved out-of-plane compressive strength under flatwise loading [48,49], while the ligaments provide resistance to out-of-plane shear loading [50], which is important in relation to the flexural stiffness of sandwich panels. Thanks to this is proven that chiral cellular solid have a better compressive and shear strength than the conventional hexagon honeycombs.

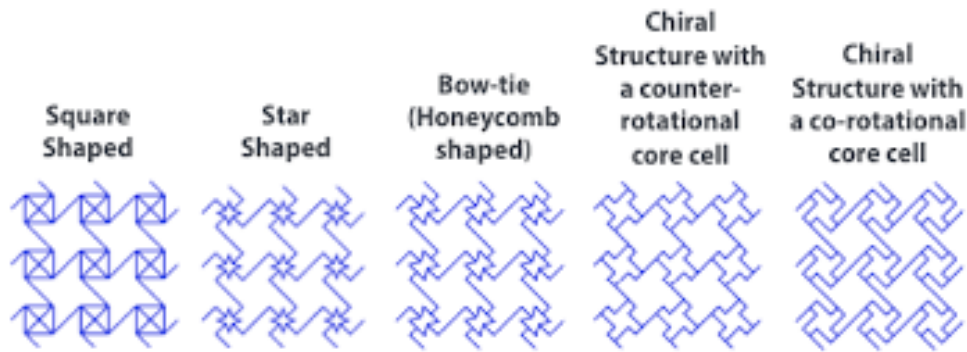


Figure 5 Different chiral geometries

All the previously described geometries are 2D structure which achieve a negative Poisson's ratio. While auxetic responses have been demonstrated in many crystals, very few designs of synthetic 3D auxetic materials have been proposed. Analytical studies have identified 3D auxetic systems consisting of networks of beams, multipods and rigid units. However in all of these systems the auxetic behavior is displayed only in the limit of small strains. Designing 3D auxetic systems able to maintain these properties, in terms of large strains, is still very challenging. Since the 3D auxetic behavior is induced by elastic buckling, these new materials are named "Bucklicrystals" [51].

These Bucklicrystals open new design paths for the development of 3D auxetic materials over a wide range of length scales. Firstly is recognizable that the structural unit capable of isotropic volume reduction represents the ideal building block to design 3D auxetic metamaterials whose response can be controlled by

the application of a stimulus. This kind of response has been recently demonstrated for patterned spherical shells, where an elastic instability produced a significant change in volume. The hole arrangement of the spherical shell has been studied and it showed that only five patterns comprising of 6, 12, 24, 30 and 60 holes are possible for such building blocks. These five spherical structures can be classified into two symmetry groups: the shells with 6, 12 and 24 holes have octahedral symmetry and the 30 and 60 holes which have an icosahedral symmetry.

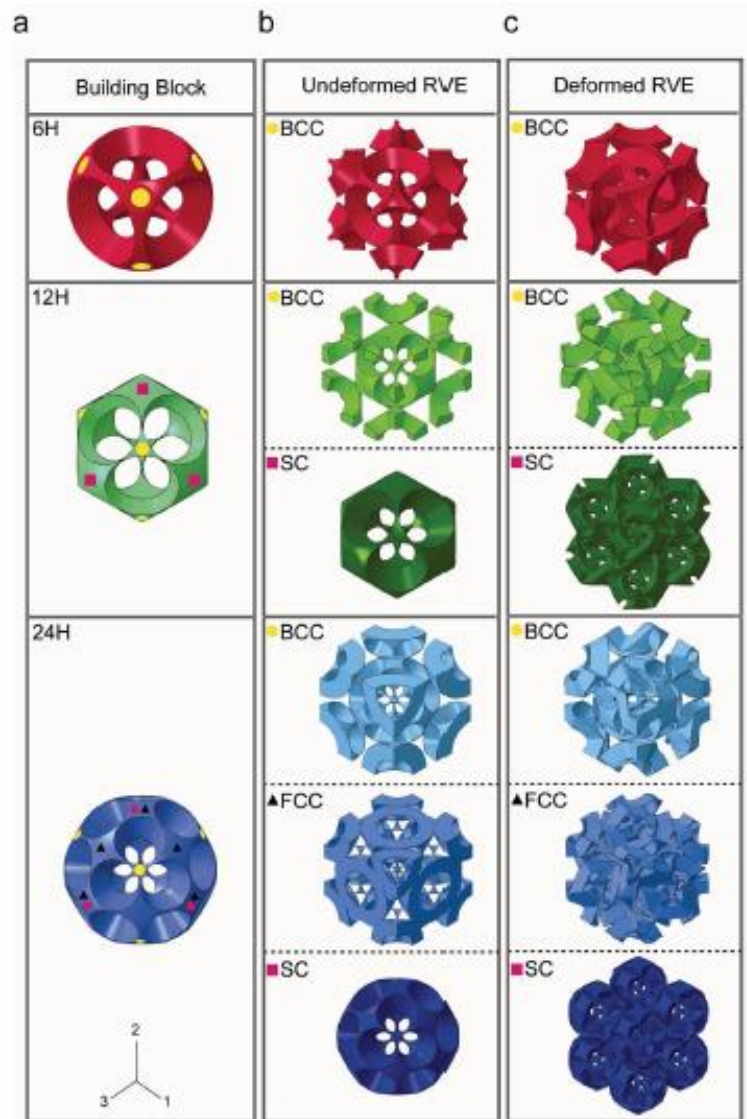


Figure 6 List of Bucklicrystals; bcc, fcc, sc are the packing configurations; RVE is representative volume elements

1.4.4 Auxetic foams

Auxetic foam materials were firstly developed by Lakes and then further studies were developed. The negative Poisson's ratio foams are developed from conventional foams. By impressing an isotropic permanent volumetric compression on a conventional foam is achieved a re-entrant cell structure. Foams can be polymeric, metallic or ceramic.

The Poisson's ratio is governed by the shape of the cells, not by the cell rib composition. The method of controlling the cell shape depends on the starting material. For polymer foams [52], the foam is compressed in three orthogonal directions by the same quantity and it's packed in a mold, then it's heated above the

softening temperature and cooled to room temperature to preserve the altered cell shape. For ductile metal foams such as copper foam [53], the material is deformed in one direction by compressing it by a small quantity and then it's similarly compressed in the other two orthogonal directions. The process is repeated until it's achieved a permanent change in volume of a factor of three to five. If the starting material is not perfectly isotropic, the final auxetic foam can be adapted to full isotropy by applying some adjustments to the permanent compression procedure [54].

Figure 7 shows micrographs of a polyurethane foam before and after conversion to auxetic form, showing a contorted three-dimensional re-entrant topology for the auxetic foam compared to the regular convex cell structure of the conventional starting foam material [55]. Auxetic foam displays synclastic curvature, improved resilience, indentation resistance, shear resistance, fracture toughness, and vibration control.

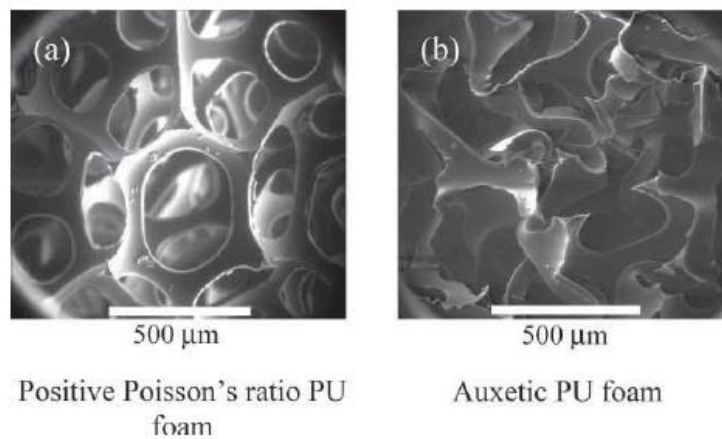


Figure 7 PU foams: (a) unconverted (positive Poisson's ratio) foam; (b) converted (auxetic) foam

1.4.5 Auxetic polymers

The auxetic effect was first observed in microporous polymeric material in 1989 [56,57]. In this case, an expanded form of polytetrafluoroethylene (PTFE) was found to exhibit a highly anisotropic negative Poisson's ratio as low as $\nu = -12$. This is due to its complex microstructure which consists of nodules interconnected by fibrils and is shown in the micrograph of fig. 8.

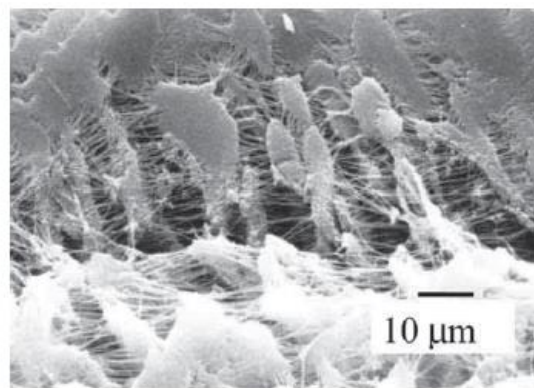


Figure 8 Nodule-fibril microstructure of auxetic PTFE

This kind of structure can be seen as a translation of the usual re-entrant structure of honeycombs and foams. The auxetic deformation mechanism is due to the hinging of the fibrils [58]. By studying the auxetic effect in PTFE is understandable that other polymers could be processed in the same way to achieve the same

particular microstructure. The role of the compaction stage is not essential for the auxetic behavior, however is essential to have a better structural integrity of the extrudate. In fact if this stage should be omitted the final structure would have low mechanical properties and low density.

Equally, the extrusion stage could be replaced by compaction followed by multiple sintering, resulting in a material with excellent structural integrity and some auxeticity. In addition there was found that these materials have a high improvement over conventional materials for indentation resistance and the absorption of ultrasound.

1.4.6 Fiber composite

It is possible to create auxetic laminate composites by using two different techniques. The first one is by using the manufacturing technique of vacuum bagging. The auxetic effect is produced by selecting suitable stacking sequences. To achieve this, the lamina material should be highly anisotropic. To determine the stacking sequence is used a software which can determine the final mechanical properties of the composite. In different studies it was determined that through this process the auxetic lamina composites would reach higher fracture toughness and higher resistance to indentation than normal laminates.

The second method is to use auxetic reinforcements to make a auxetic fiber-reinforced composite. By having an auxetic fiber there's a higher resistance to fiber pull-out because of the fiber behavior. When the auxetic fiber is pulled, it expands inside the matrix and locks itself into it. By testing auxetic polypropylene (PP) fibers [59], embedded in a softened epoxy resin it was demonstrated that the auxetic fiber can carry more than twice the maximum load than positive Poisson's ratio fiber. Also, energy absorption capability of auxetic fiber is more than three times than positive Poisson's ratio fiber [60].

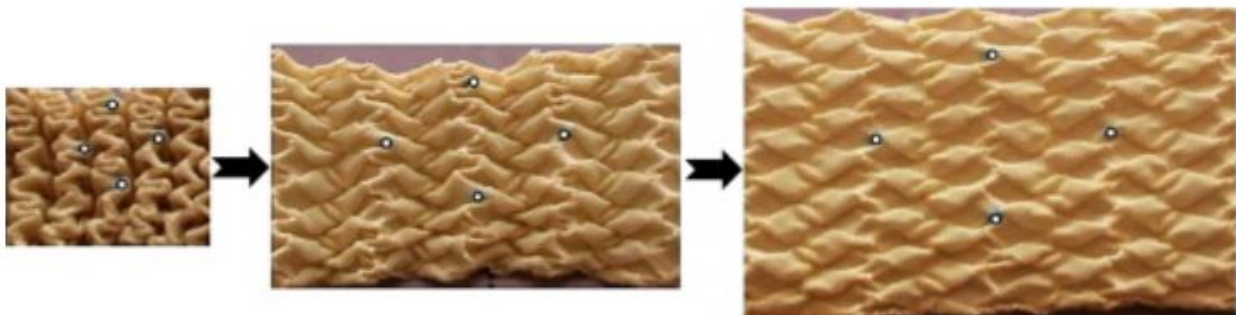


Figure 9 High performance auxetic fabric

1.5 Structures

In the early development of the theory of elasticity, it was believed that isotropic materials could be described by only one elastic constant and that Poisson's ratio was 0,25 for all isotropic materials. The basis for this view (so-called uniconstant theory) was an atomic model in which the atoms as point particles in a centrosymmetric lattice interacted by central forces depending only on distance. Experiments revealed that for most common isotropic materials Poisson's ratios was close to 0,33, therefore resulting in the abandonment of uniconstant elasticity theory governed by the Cauchy relations. The classical theory of elasticity now used incorporates two independent elastic constants for isotropic materials, and it's clear that the earlier described model doesn't have general applicability.

Poisson's ratios differing from 0,25 can arise from deviations from the above assumptions, specifically (1)

non-central forces between particles in the solid, (2) forces which do not depend on distance alone, or (3) anisotropy, including noncentrosymmetry. For this purpose are described several microstructures with the aim of showing the different kinds of interaction which are most important to achieve a negative Poisson's ratio. Most of these structures are two-dimensional and isotropic in plane in their classical elastic properties either by virtue of the choice of the elastic stiffness of the microelements or by symmetry. The range for Poisson's ratio, ν , for isotropic materials is $-1 < \nu < 1/2$ in three dimensions and $-1 < \nu < 1$ in two dimensions.

Furthermore it's important to underline that under static conditions, noncentral forces must be accompanied by a moment, to satisfy the equilibrium equations. The kinematical variable conjugate to a moment is a rotation angle. As for forces which do not depend on distance but instead connect only selected pairs of particles, the corresponding kinematical deformation is a non-affine one. This is in contrast to affine deformation in which the particles in the solid move in a way corresponding to a uniform strain plus a rotation in a continuum.

1.5.1 Non-affine deformation

A honeycomb composed of regular hexagonal cells (fig. 10, left) has a Poisson's ratio of $+1$ [61,62]. Its cell ribs withstand bending if the honeycomb is stretched or sheared and the deformation is not affine because some pairs of nodal points move apart during stretching, while others do not. Indeed, a honeycomb without any bending can be made of elastic (spring) elements free to rotate at the joints. This can be done because the elements would rotate without stretching if the honeycomb were under tension. To develop an elastic honeycomb further soft elements could be inserted to supply the restoring force and the Poisson's ratio would be slightly less than 1. Re-entrant honeycomb cells such as those shown in fig. 10 (right) produce a negative Poisson's ratio [63]. The ligaments undergo bending and the deformation is notably a non-affine one since the cells unfold during stretching of the honeycomb. In particular, points A and B move further apart than expected from the global strain, while points C and D maintain their separation during stretching. Again, bending is not essential since a similar effect can be achieved with stretchable (spring) elements only, which are free to pivot without rotational constraint. The structure is orthotropic, however by appropriate choice of the rib widths and angles, it can be obtained an elastically isotropic honeycomb with a Poisson's ratio of -1 .

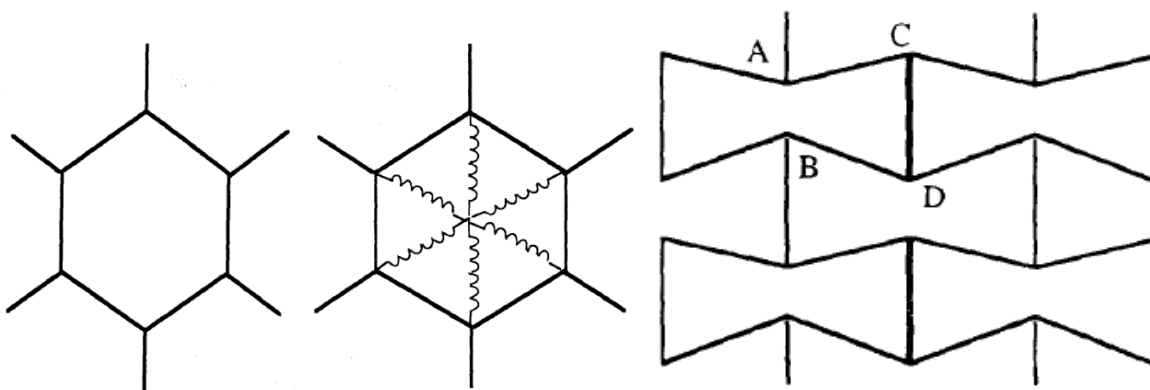


Figure 10 Hexagon honeycomb structure of bendable ligaments (left) and re-entrant auxetic honeycomb structure (right)

1.5.2 Non-central forces

We now consider the effect of non-central forces alone, with affine deformation. A two-dimensional structure of rigid rotatable nodes linked by elastic ligaments, originally examined in a study of generalized continuum mechanics [64], is of interest in this vein and is shown in fig. 11. The structure is cubic, nonetheless

it is possible to achieve elastic isotropy by changing the stiffnesses of the elastic ligaments. Given the Lamé and Cosserat elastic constants, it's proven isotropy (which results in a relationship between stiffnesses), so it can be set up the lattice without pre-strain in any of the ligaments, and calculated the engineering elastic constants in terms of the node size and the relative magnitude of the noncentral forces. Calculated Poisson's ratios are shown in fig. 11.

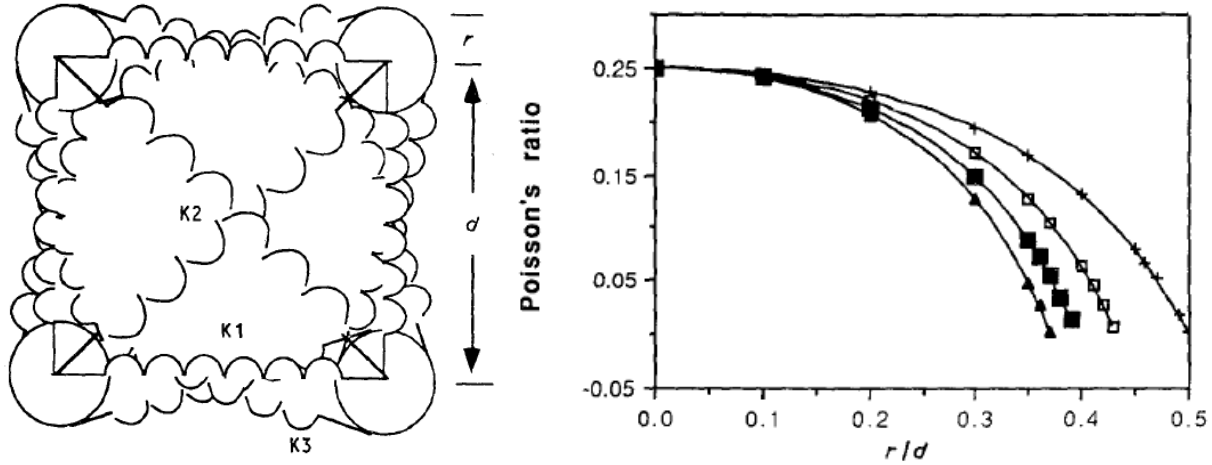


Figure 11 Lattice of rigid rotatable nodes linked by elastic ligaments (left) and its behavior (right). Poisson's ratio versus rotatable node size, r , divided by lattice spacing, d , and spring stiffness ratio k_1/k_3 , which is a measure of the relative magnitude of the noncentral forces. Poisson's ratio is positive if all the ligament stiffnesses are positive. The ratio k_1/k_3 is decreasing from left to right. Respectively 5, 2, 1 and 0,5 for each curve.

Observe that a rotatable node size of zero or a zero stiffness for the ligaments, k_3 , which are attached to the rotatable node periphery, results in a lattice governed by purely central forces; the Poisson's ratio is 0,25 as is the case in three dimensions. Introduction of non-central forces reduces the Poisson's ratio; however, negative Poisson's ratios are not achieved unless one of the ligament stiffnesses becomes negative. Such a ligament would be unstable if isolated, however the stability criterion for the entire lattice remains $-1 < \nu < 1$.

For the structure in fig. 11, it's introduced a pre-strain in the vertical and horizontal ligaments, k_1 . The corresponding pre-strain is then determined for the ligaments, k_3 , based on equilibrium considerations. Ligament stiffness is again kept positive and Poisson's ratio can be made either greater or less than 0,25 or can be made negative as shown in fig. 12. End points on the curves in figs 11 and 12 represent the admissible range for positive stiffness of all ligaments under the restriction of elastic isotropy. The model can also yield Poisson's ratios lower than -1; in that case the lattice would be unstable to small perturbations. Observe that the negative Poisson's ratios can be achieved only if both non-central forces and pre-strain are present simultaneously.

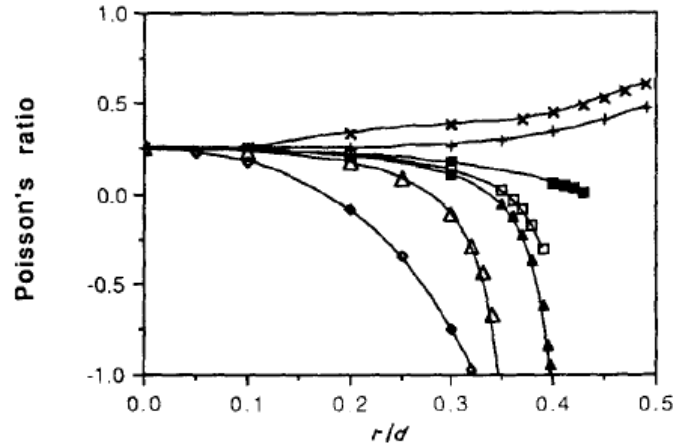


Figure 12 Poisson's ratio versus rotatable node size, r , divided by lattice spacing, d , for non-central force lattice shown in fig. 11, with pre-strain in the ligaments. Pre-strain factor, f is the ratio of natural length of the vertical and horizontal ligaments to their length in the lattice, the lattice spacing, k_1/k_3 is a ratio of ligament stiffnesses. The represented curves, from left to right, have these values of parameters: $k_1/k_3=8, f=8$; $k_1/k_3=0,125, f=0,125$; $k_1/k_3=0,25, f=0,5$; $k_1/k_3=0,5, f=0,5$; $k_1/k_3=1, f=1$; $k_1/k_3=0,5, f=2$; $k_1/k_3=0,25, f=2$;

1.5.3 Noncentrosymmetry

An unusual type of anisotropy is displayed by the hexagonal structure given in fig. 13. The structure has a negative Poisson's ratio as can be identified by visualization or by making a model. The structure is not equivalent to its mirror image, so it lacks a center of symmetry. Such structures are known as noncentrosymmetric, hemitropic, or chiral; they can be isotropic depending on the direction but by definition are not isotropic with respect to handedness. In opposition to the centrosymmetric lattice in fig. 12, no pre-strain is needed. The centers of the rigid nodes move in an affine manner. However, if the structure is represented as an assemblage of point particles, the "points" in the rigid nodes become connected by very stiff ligaments; in such a view the deformation becomes non-affine.

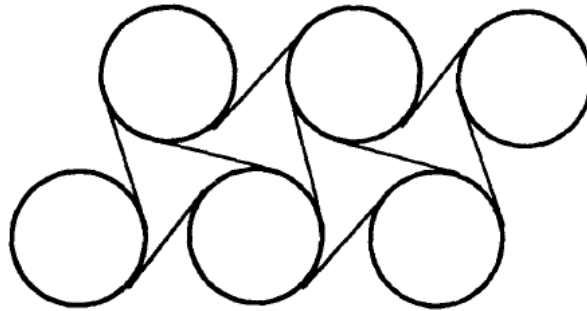


Figure 13 Chiral (noncentrosymmetric) hexagonal microstructure of rotatable nodes and bendable ligaments.

In conclusion it can be said that negative Poisson's ratio can be obtained by a non-affine deformation geometry alone, from a combination of non-central forces and pre-strain and from a chiral structure with rotational degrees of freedom combined with non-central force or non-affine deformation.

1.6 Properties

Auxetic materials are characterized by a peculiar behavior and, as a consequence, they have peculiar and rare mechanical properties [65]. These characteristics are very different from the usual materials; in fact some of them tend to contradict common sense, when compared to "regular" materials. Some of these peculiar properties are presented in the following sections.

1.6.1 Shear modulus and resistance

Auxetic materials are more resistant to shear forces than “regular” materials [66]. According to the theory of elasticity for isotropic materials, the bulk modulus and the shear modulus can be determined by two equations involving the four constants: the Young’s modulus (E), the shear modulus (G), the bulk modulus (K) and the Poisson’s ratio (ν) [67].

$$K = \frac{E}{3(1 - 2\nu)}$$

$$G = \frac{E}{2(1 + \nu)}$$

From these two equations is clear that when the Poisson’s ratio is negative the shear modulus would be significantly higher than the bulk modulus. All the materials that possess a superior shear modulus are expected to possess high indentation resistivity, high torsional rigidity, high bending stiffness, shear resistance and high energy absorption efficiency [68]. Furthermore Auxetics materials are also good candidates for use as cores in sandwich panels. In this case by analyzing the bending of a sandwich panel is noticed the difference between Auxetic and non-auxetic materials. When the panel is bent the section is subjected to a compression stress in the inner half and a tensile stress in the outer half. While the compressed section tends to expand in the case of non-auxetic materials, in case of Auxetics it tends to shrink.

As seen from the previous equations at the increasing of negative Poisson’s ratio the shear modulus increases and therefore the shear resistance increases too. All the correlation between bulk modulus, shear modulus and Poisson’s ratio can be seen on fig. 14. It can be observed that for stable unconstrained solids the shear modulus must be positive and in case of extreme negative values of Poisson’s ratio the shear modulus tends to infinity.

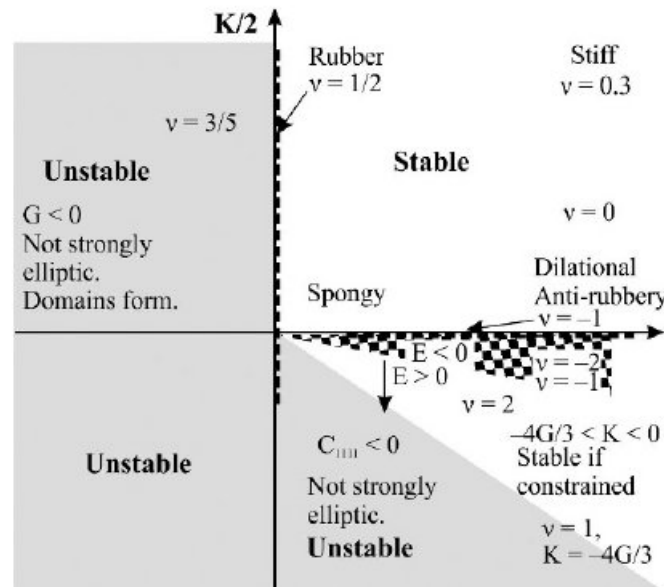


Figure 14 Correlation of the bulk modulus and shear moduli with Poisson’s ratio and stability

1.6.2 Resistance to indentation

When a regular material is subjected to a load applied by an indenter a deformation occurs. There is a compression of the material under the applied load and consequently, to compensate this compression, the material tends to open out in a perpendicular direction to the applied load [69]. However, when a load is

applied on an isotropic auxetic material, a local contraction is observed. Instead of expanding the deformation, the material accumulates under the applied load creating an area of denser material which improves the resistance to deformation (fig. 15) [70,71].

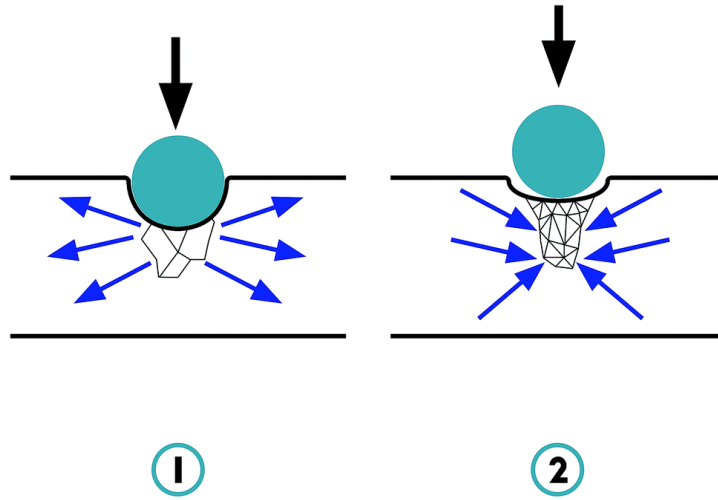


Figure 15 Non auxetic (1) and Auxetic (2) behavior due to an applied load

In this way, auxetic materials have a higher indentation resistance than conventional materials. The increase in indentation resistance can be explained by the theory of elasticity and associated to the material hardness (H). This property is correlated to the Poisson's ratio by the equation:

$$H \propto \left[\frac{E}{(1 - \nu^2)} \right]^\gamma$$

where E is the Young's modulus, ν is the Poisson's ratio of the base materials and γ is the constant that assumes the value 1 or 2/3 in the case of uniform pressure distribution or hertzian indentation, respectively. By analyzing the equation there are two limit values to check for 3D isotropic materials: when the Poisson's ratio tends to values near -1, the hardness of the material tends to infinity [72]; instead for the upper limit 0,5, the observed values are considerably lower. However, the upper limit of the Poisson's ratio for 2D isotropic systems is 1 [73,74]. Thus, the materials with such positive Poisson's ratio values can also have infinite hardness values.

1.6.3 Fracture resistance

By some studies done on auxetic and convention foams has been seen that materials that possess a negative Poisson's ratio have a better resistance to fracture than "regular" materials, even if the auxetics have a smaller Young's modulus [75,76]. To expand the cracks in auxetic materials is needed more energy, because they have a lower crack propagation than "regular" materials [77]. Thus, these kinds of materials have a fragile fracture.

In his work on the crack growth, Maiti demonstrated that the stress intensity factor for conventional foams (K_{IC}^*) is proportional to the normalized density and can be described by the equation [78]:

$$\frac{K_{IC}^*}{\sigma_f \sqrt{\pi l}} = 0.19 \left(\frac{\rho^*}{\rho_s} \right)$$

where σ_f is the fracture stress of the cell rib, l is the rib length, ρ^* is the foam density and ρ_s is the density of the foam based material. Following the same procedure that was used for conventional foams, the fracture toughness of re-entrant foams was obtained. The re-entrant structure was modelled as a re-entrant

polyhedron of the cell ribs connecting the square faces (fig. 16), so the crack tip radius r_{tip} was approximately:

$$r_{tip} = \left\{ 1 + \sin\left(\frac{\pi}{2} - \varphi\right) \right\} l \quad \frac{\pi}{4} < \varphi < \frac{\pi}{2}$$

The angle φ determines the extent of the permanent volumetric compression ratio achieved in re-entrant transformation of negative Poisson's ratio foams. The stress σ_b due to bending for the re-entrant model is:

$$\sigma_b = 10.10 K_{IC}^r \frac{1 + \cos(2\varphi)}{\sqrt{1 + \sin\left(\frac{\pi}{2} - \varphi\right)}} \frac{1}{\sqrt{\pi l}} \left(\frac{l}{t}\right)^2$$

Where K_{IC}^r is the stress intensity factor for this kind of foams and t the rib width. Since the crack will extend when $\sigma_b = \sigma_f$ the fracture toughness K_{IC}^r of re-entrant structure becomes:

$$\frac{K_{IC}^r}{\sigma_f \sqrt{\pi l}} = 0.1 \frac{\sqrt{1 + \sin\left(\frac{\pi}{2} - \varphi\right)}}{1 + \cos(2\varphi)} \frac{\rho^*}{\rho_s}$$

Using the previous equation it can be established the relationship between stress intensity factors could be established according to the equation:

$$\frac{K_{IC}^r}{K_{IC}^*} = 0.53 \frac{\sqrt{1 + \sin\left(\frac{\pi}{2} - \varphi\right)}}{1 + \cos(2\varphi)}$$

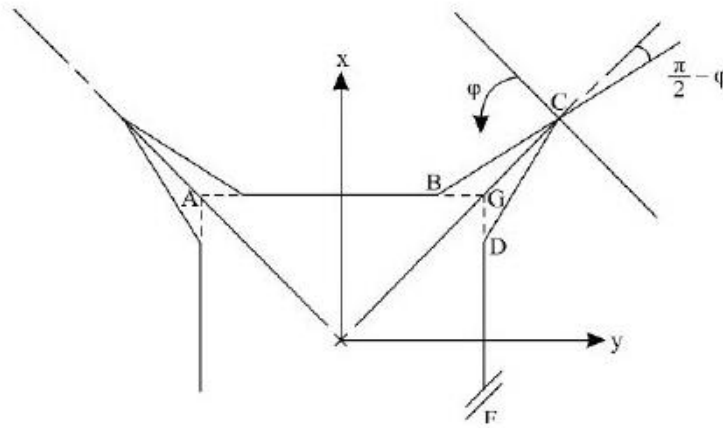


Figure 16 Schematic cross-section view of re-entrant foam cell

Experimental results also showed that for higher values of volumetric compression, reentrant foams revealed an increased fracture toughness, as demonstrated in fig. 17.

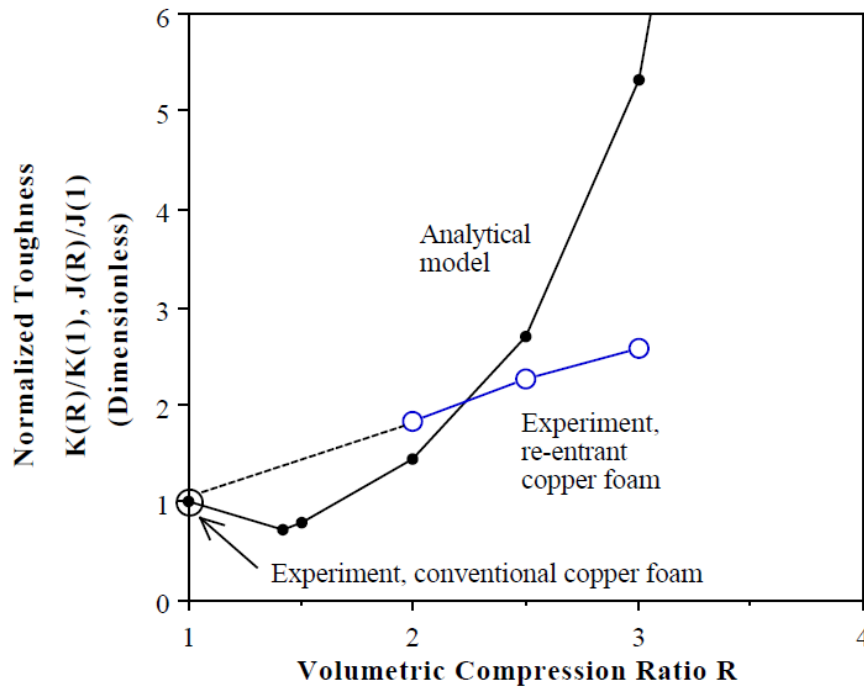


Figure 17 Experimental fracture toughness of re-entrant foams normalized with conventional foams

This phenomenon can be explained by the basic definition of auxetic materials. When these materials are submitted to a tensile strength, they increase their dimensions. This dimensional growth is verified macroscopically. However, the visualized growth is only the result of the dimensional increase of each individual auxetic cell. This way, whenever a crack is formed, the expansion of the cell will tend to close it.

1.6.4 Acoustic absorption

In many investigations regarding auxetic properties the materials that were analyzed were foams. To determine if auxetic foams had better acoustic absorption properties than “regular” foams, there were some studies using polyurethane foams [79,80]. The auxetic structure plays a relevant role in the attenuation of acoustic vibrations. Their performance was shown to be better than “regular” materials over the entire range of 100-1600 Hz. At frequencies below 200 Hz, all absorption curves converged and showed poor absorption, but an unattached polyethylene covering on the foam improved absorption below 500 Hz. At frequencies above 630 Hz, auxetic foams were superior and the foam with the smallest pore size showed the best absorption.

An example of the magnitude of this effect was the study of ultra-high-molecular weight polyethylene. This material presents an ultrasonic attenuation value 1.5 times higher than a sintered foam and 3 times higher than a conventional foam, composed of the same base material [81]. Another example of the superior performance of auxetic materials was observed by Ruzzene while studying the attenuation of elastic waves over certain frequency bands (stop bands) and the directional characteristics in hexagonal honeycombs and auxetic (bowtie) lattices [82]. The studied periodic structures are presented in fig. 18.

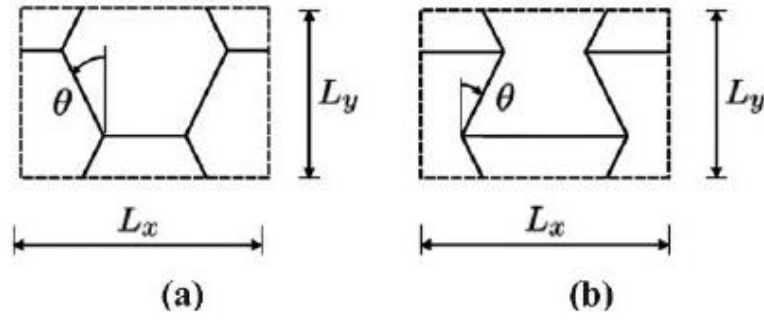


Figure 18 Hexagonal honeycombs (a) and auxetic (bowtie) lattice unit cells (b)

Numerical results demonstrated that for a rib angle $\vartheta = 30^\circ$ ($\vartheta = -30^\circ$, for auxetic cells), the auxetic structures showed a superior wave attenuation in the great majority of that structures orientation angles (Φ) and wave frequencies (ω), as shown in fig. 19.

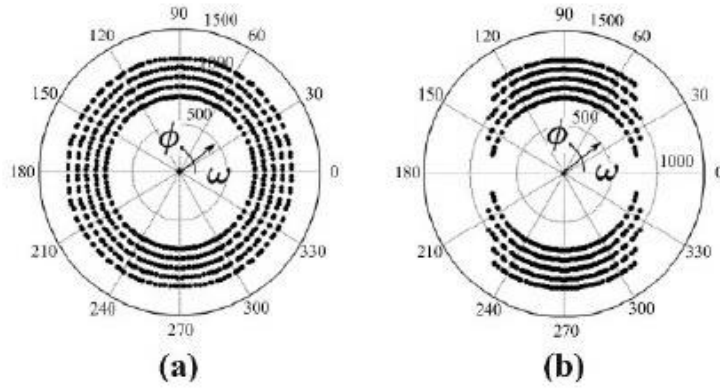


Figure 19 Band gap representation in hexagonal honeycombs (a) and auxetics (bowtie) lattice (b)

1.6.5 Synclastic behavior

Synclastic surfaces are those in which the centers or curvature are on the same side of the surface. Synclastic behavior is a body's ability to deform in a shape of a dome when it is bent [83]. Reviewing the basic concepts of mechanics of materials, when a body is bent, it is submitted to tensile and compression stresses. When a bending deformation is applied to an auxetic material a concavity is formed with an expansion of the material in the external part and a contraction of the material in the interior part [84]. While bending the auxetic material, a dome is formed, as a result of expansion of the pulled material and the contraction of the compressed portion. In fig. 20 is shown the different behavior of an hexagonal honeycomb (anticlastic) and a re-entrant hexagonal structure (synclastic):

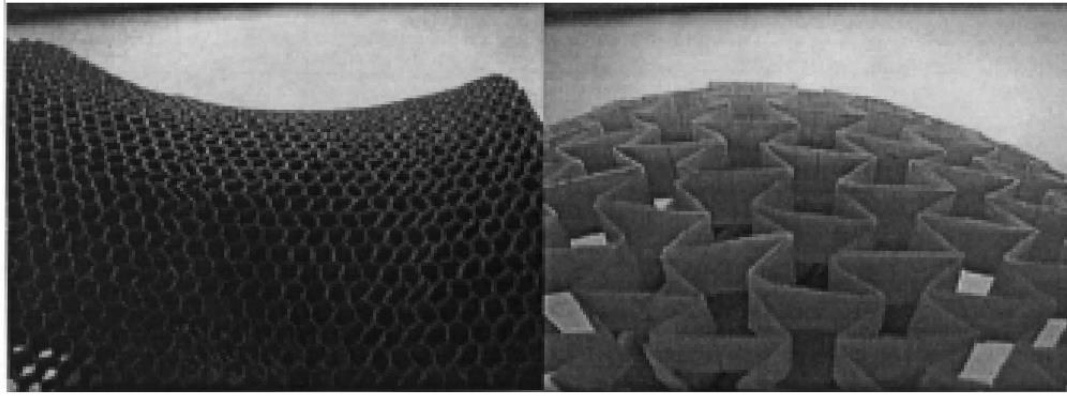


Figure 20 Hexagonal honeycomb (left) and re-entrant hexagonal structure (right)

The ability to form the doubly curved shapes is useful, because it provides a way to fabricate this kind of complex structures through a relatively small number of machine steps, avoiding the waste of material, and consequently with low manufacturing cost [85,86]. This feature is most typical for structures with re-entrant unit cells.

1.6.6 Variable permeability

In auxetic materials the variation of permeability is due to the change in dimensions and shape of the singular unit cells [87]. Each single unit cell can be seen as a pore that can be opened and closed in the more convenient way by the application of a tensile or compression stress. This kind of behavior can be seen mostly in auxetic foams, where the variation of the structure dimensions is the reflection of the change of the dimensions of each individual cell. This characteristics can be observed in fig. 21.

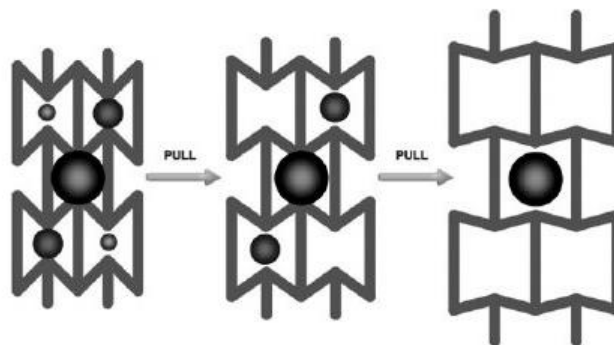


Figure 21 Variable permeability due to pulling effect

1.6.7 Shape memory auxetic

Shape memory is the ability of a material subjected to a plastic or semi-plastic deformation to remember and return to its initial shape and size, when submitted to a specific thermal stimulation [88,89]. Studies in this field show that auxetic foams subjected to a specific temperature profile returned to their original dimensions and they were showing positive Poisson's ratio. Then it was demonstrated that it's possible to reconvert the return specimen to an auxetic state, called second auxetic. With statistical analysis on the mechanical properties of the two foam phases it was shown that the second auxetic foam was able to dissipate more than the first one [90,91]. The shape memory property is extremely useful because it opened new possibilities for applications in situations that require auxetic and non-auxetic variable mechanical

properties [92], where the variation of temperature is involved [93].

1.6.8 Other auxetic properties

The improved fracture toughness and hardness of auxetic materials suggest that these materials can have better tribological attributes than conventional materials. This can be justified by the properties that reduce the abrasive wear in auxetic materials. This possibility was confirmed in the work by Uzun who showed that auxetic based weft knitted fabric had an increase of 15 – 35 % of abrasive wear resistance when compared to conventional polypropylene knitted fabrics [94]. Another interesting property of auxetics is the dielectric behavior in chiral honeycombs. It was suggested by Kopyt that the panels composed of hexa-chiral honeycombs may act like a homogenous medium, despite their complex and heterogeneous geometry [95].

1.7 Applications

Thanks to all those properties of auxetic materials that are described before, these materials could be used in many applications in different areas. Since these materials are very new currently they are not widely used, but because of their potential there are many researches about them in many fields, to revolute the materials currently used in the world.

One possible application of these materials is the manufacturing of piezoelectric devices and composites. Due to the low bulk modulus and the capacity to obtain an auxetic matrix that can follow the deformation of the piezoelectric rods, sensors more sensible to the variation of pressure can be made [96]. This behavior can be observed in fig. 22.

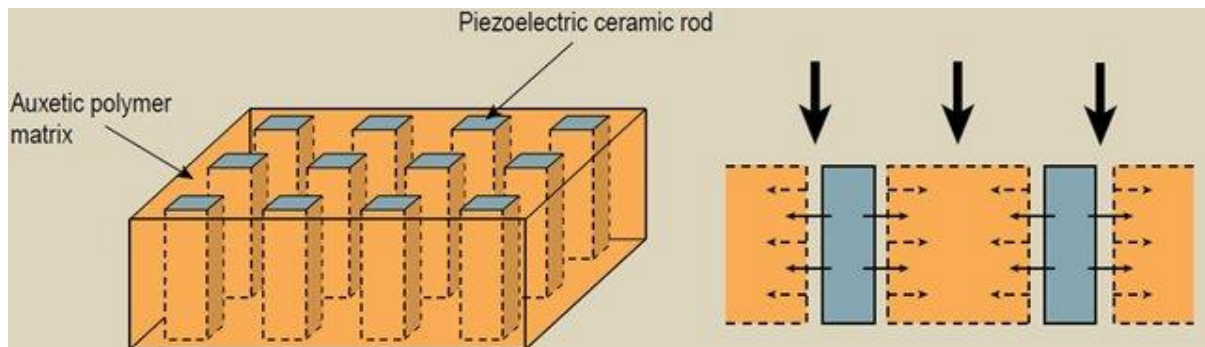


Figure 22 Auxetic piezoelectric sensor

As it was mentioned earlier, one of the most desirable properties of these materials is the variable permeability. This property can be used in manufacturing of intelligent filters, which can be designed with different sizes and particular geometries to control the passage pressure while filtering [97].

An interesting field of application for these materials is biomedical engineering. One of the most important uses will be about manufacturing of blood vessels that will tend to increase in wall thickness in response to a pulse of blood, thus preventing rupture of the vessel [98]. As shown in the example in fig. 23, where is presented the difference of a blood vessel dilator with auxetic and non-auxetic material.

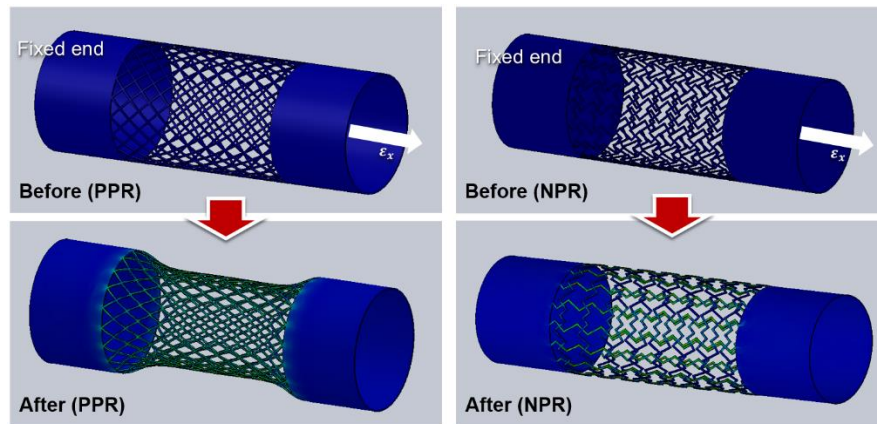


Figure 23 Blood vessel with non-auxetic (PPR) and auxetic (NPR) material

Another biomedical application is the smart bandage [99]. The typical functions of conventional wound dressings and bandages are to provide protection against infection, absorbing blood and exudate from the wound, promoting wound healing and applying medication when required. But to apply a medicine to heal the wound it's required to change the bandage. With smart bandages made of auxetic material there's no need to change the bandages and there will be better results on wound humidity and comfort too. An example is shown in fig. 24.

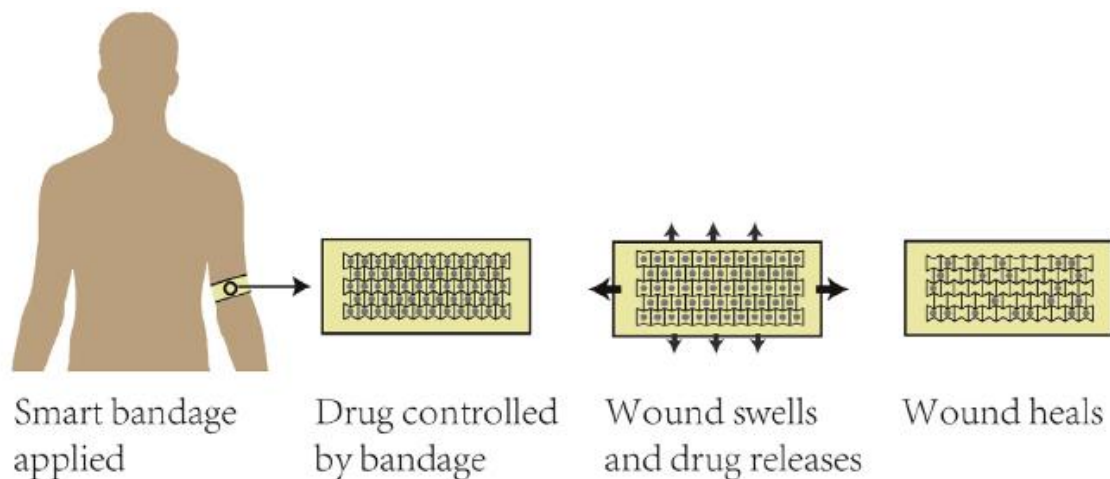


Figure 24 Smart bandages made of auxetic material

Another biomedical application is dental floss. If conventional yarns are substituted with auxetic ones there's an improvement in the cleaning effect because the expansion effect of the auxetic material, due to the hand tensile stress, would fill the gap between the teeth. Other applications in this area are stents, surgical implants, auxetic scaffolds, health monitoring sensors, artificial skin, prosthetic linings, sutures and ligament/muscle anchors.

Taking into account that the most obvious characteristics of these materials is their expansion when submitted to a tensile load, there can be found common applications that use this as an advantage. One studied application is the use of auxetic fasteners. The best quality of these fasteners is that they contract when inserted and they tend to expand when removed. Because of the expansion on the attempt of removal the required load to extract them is much bigger [100]. In fig. 25 is illustrated this behavior.

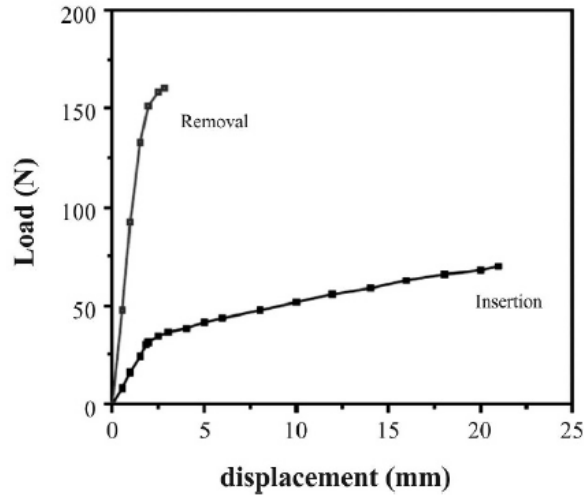


Figure 25 Behavior of auxetic fastener

Another example of the application of auxetic materials is the manufacturing of a chiral-based honeycomb deployable antenna for deep-space missions, using the shape-memory properties. This antenna is folded while transported, as there is a very limited area for rocket launchers. Once in space, the shape memory structure uses the thermal energy of the sun to unfold to its original size, as shown in fig. 26.

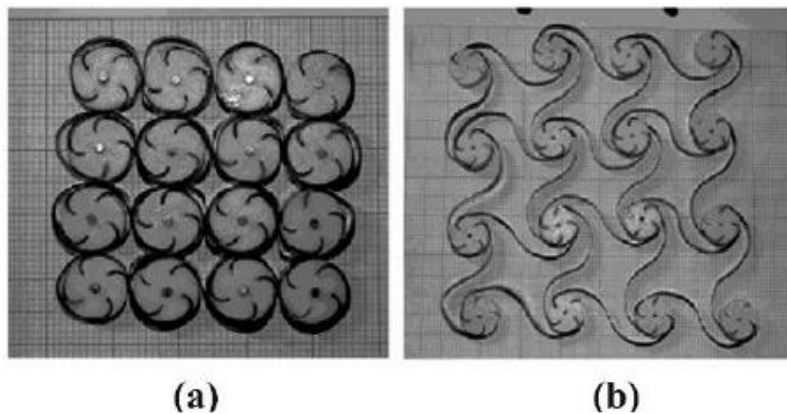


Figure 26 Folded (a) and unfolded (b) auxetic cellular antenna

Auxetic textile structures are also a fast growing field. Their development should lead to the fabrication of materials with improved energy absorption, high volume change, wear resistance and drapeability. We can see some applications in this way in the aerospace field where auxetics are used for aircraft engine vanes, aircraft thermal protecting system, wing panels, aircraft nose-cones, rivets, sound and vibration absorbers. In the automotive sector auxetics are used as energy absorption devices, cushions and jounce bumpers. One of the biggest field of uses of auxetics regarding their high impact resistance is the military sector where they are used for lighter protective materials, blast curtains, vehicle armor for ballistic protection, helmets, bulletproof vests, protective gears and knee pads [101,102].

The production of this kind of textiles can be executed by two basic methods. The first one is the use of auxetic based fibers directly in the knitting and weaving of the textiles. The other one is the production of auxetic textiles using conventional fibers weaved or knitted into a structure that is auxetic by itself.

The use of auxetic textiles can already be found commercially, for example in applications that use GoreTex and polytetrafluorethylene. They are also largely applied as packing materials for their good absorption

resistance and durability. In fig. 27 is shown the difference between non-auxetic and auxetic materials in terms of energy absorbed.

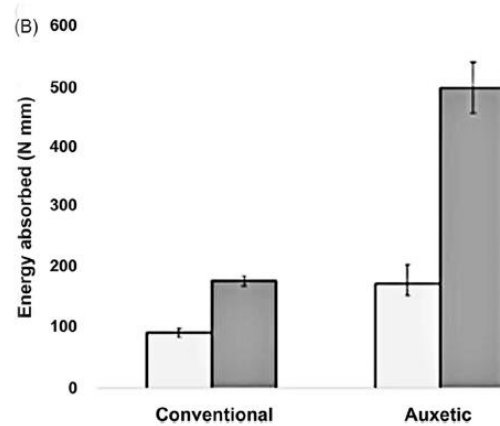


Figure 27 Compression testing results for non-auxetic and auxetic material

One of the most promising fields is the development of auxetic materials at a nanoscale, for example in the applications with carbon nanotubes. These kinds of materials are basically made of the molecules composed of a monolayer of carbon atoms arranged in a cylindrical lattice. One of the applications of this nanostructured auxetics can be the molecular variable permeability filters. The simulations that represent these nanostructures suggest that under certain geometric and force conditions, when the stretching deformation in the cell walls dominates, it is possible to obtain negative values of Poisson's ratio.

Finally one of the closest applications to civil engineering of auxetics is geotextiles. The filtration function of geotextile may be the most widely known and used function. The use of geotextiles can prevent aggregation of the particles under the road, which damages the road surface in raining days [103]. As shown in fig. 28, by placing the geotextile as a layer between particles it can be prevented the passage of soil particles without blocking the passage of water. By the usage of auxetic geotextiles it can be even adjusted the speed of the liquid flow. Taking advantage of the pore-opening effect, in those extreme weather conditions such as rainstorm and flood, the filter will let more water pass through to reduce water on the road surface, which can reduce potential dangers to pedestrians.

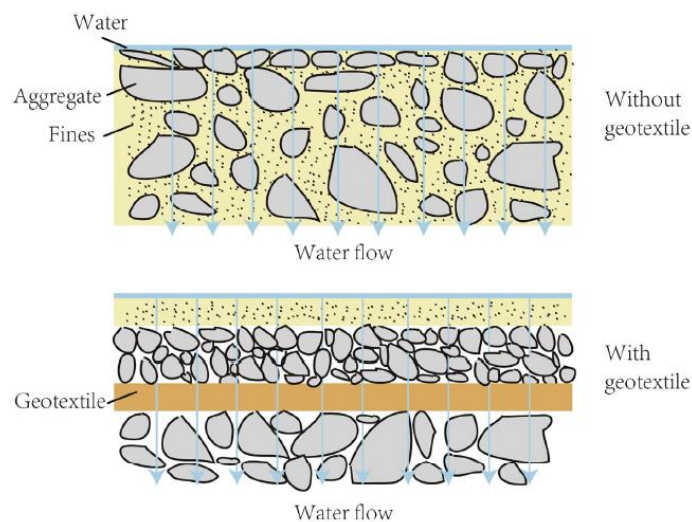


Figure 28 Filtration function of geotextiles

2 SOFTWARE ANALYSIS

2.1 Introduction

In this part of the thesis are analyzed the different kinds of auxetic structures that could be used to be printed and tested in laboratory. The analyzed structures are 2D extruded auxetic geometries formed by different kinds of unit cells.

Firstly are made the models for each type of unit cell geometry to understand every deformation mechanism. Each model is realized with the software Autodesk Inventor Nastran and its deformation mechanism is evaluated with a compression test.

After identifying which is the best unit cell geometry, other tests are made to understand how the different packing of the structure affects the deformation mechanism.

At the end it's decided which are the final models that will be printed with the 3D printer. For these models are run the last analyses that will be used to compare the laboratory test results.

2.2 Geometry analysis

The objective of this thesis is to demonstrate that some structures subjected to a load have a negative Poisson's ratio, so an auxetic behavior. This was done by printing with a 3D printer a PLA model that later was tested with a compression test. Since the auxetic behavior is due to the geometry of the structure the first step was to identify the best geometry to be tested in laboratory. Every geometry was drawn with AutoCad and built as a solid structure in the Autodesk Inventor Nastran 2019 software. To understand which auxetic structure would be the best one to be printed and tested was to analyze different auxetic geometries. To have better analysis results and a better comparison between different structures the parameters of the 3D printer were taken into consideration. The first parameter was the thickness of the structure. It was decided to have all the structure with a thickness of 0,4 millimeters which was the smallest measure that the printer could use. This decision was made because later in the test, by having a thinner wall thickness, it would be easier to have larger deformations. Then it was decided that the shortest side of the single unit cell would be at least of 20 millimeters, because with smaller dimensions would be more difficult to analyze the displacements that would occur. After that were set the minimum measures of the entire structure. For the height was decided to be at least 40 millimeters and for the length around 100 millimeters.

The first geometries which were analyzed were chiral circular, tetrachiral and lozenge grid square. In the next figures are presented the single unit geometries and the whole structure measurements.

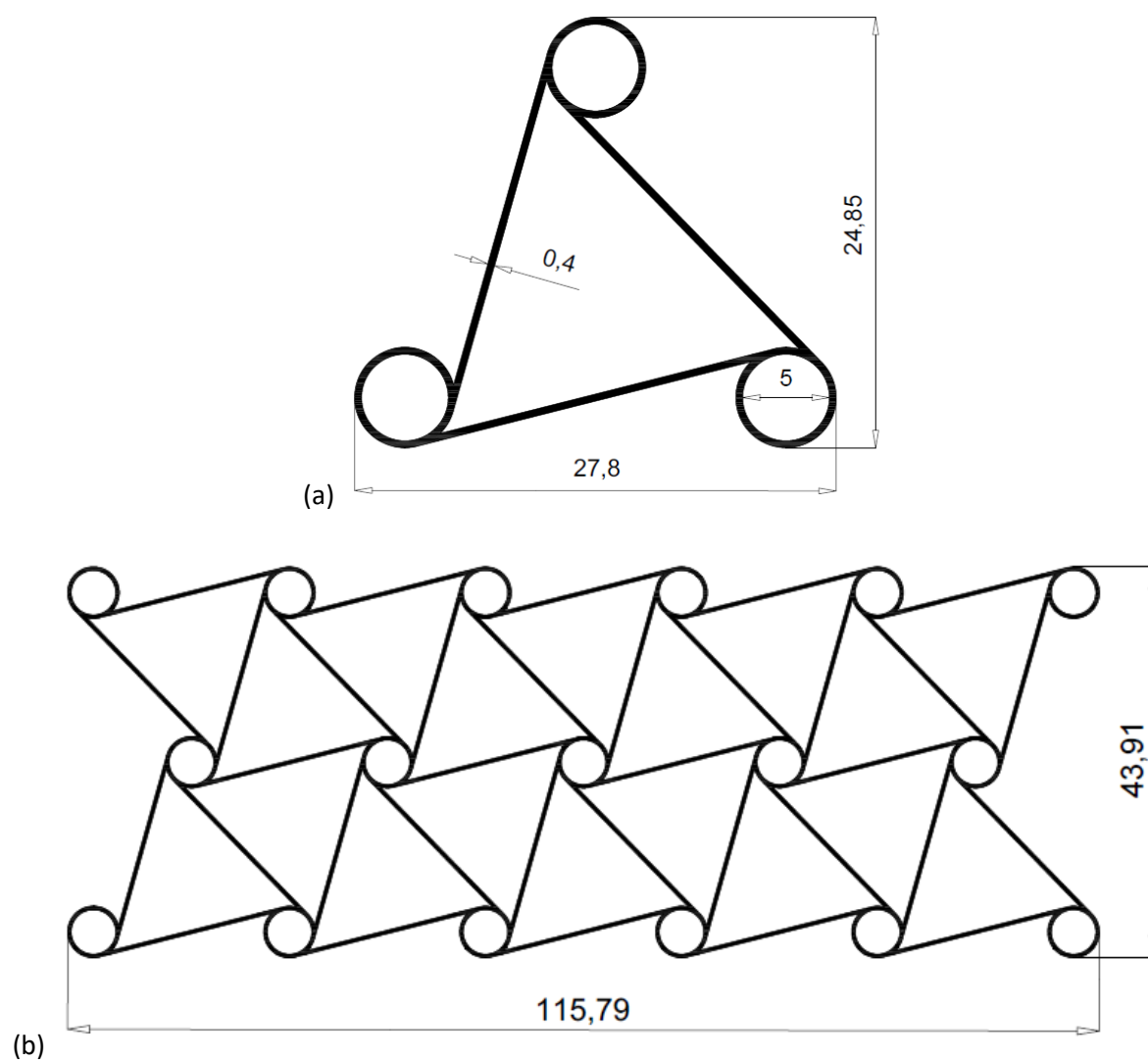
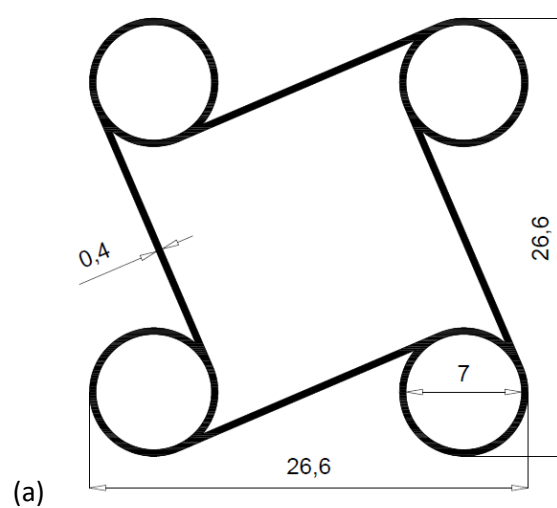


Figure 29 Chiral circular unit (a) and structure (b)



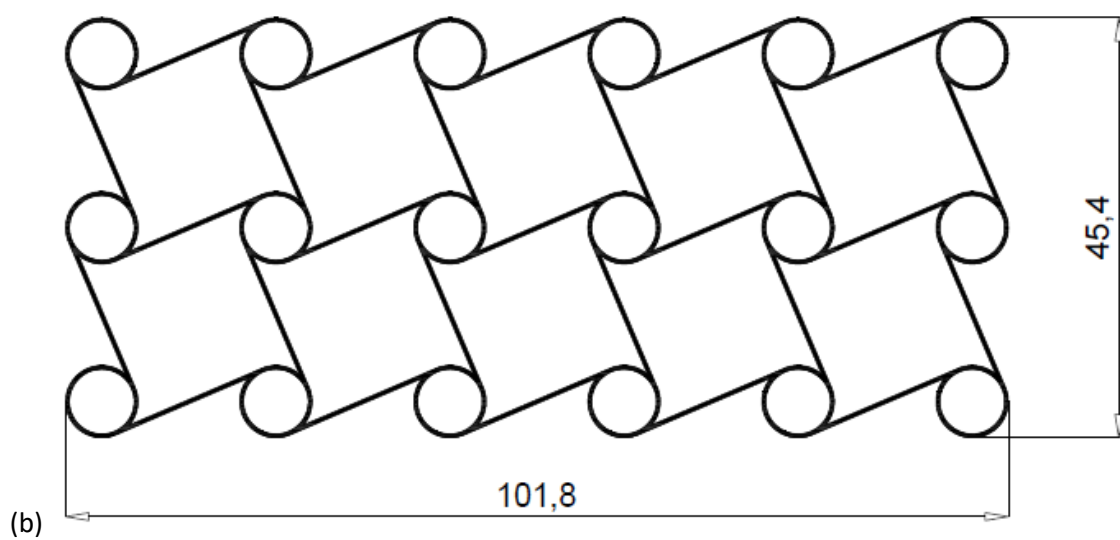


Figure 30 Tetrachiral unit (a) and structure (b)

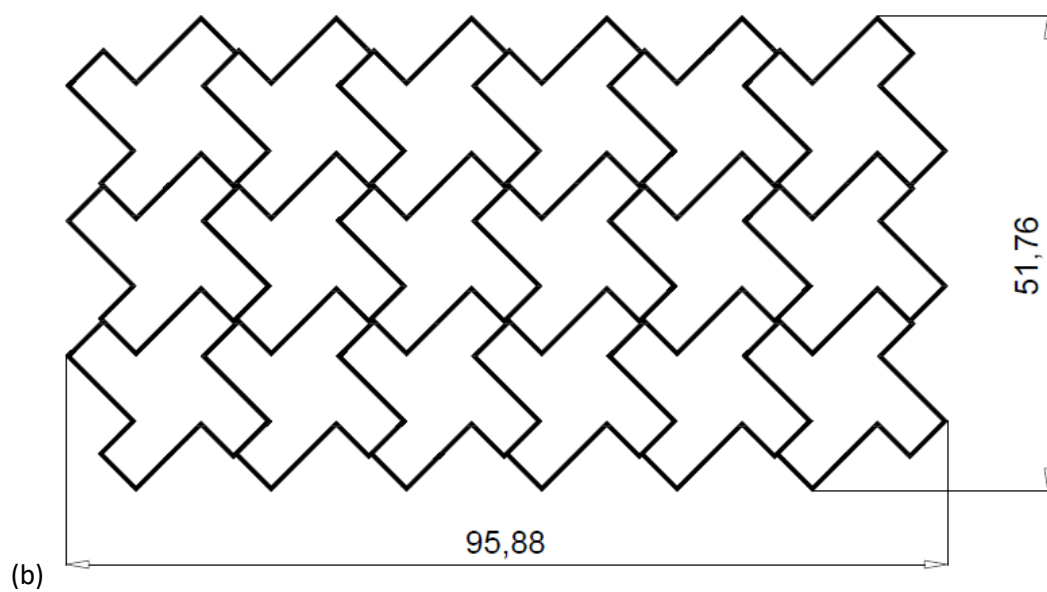
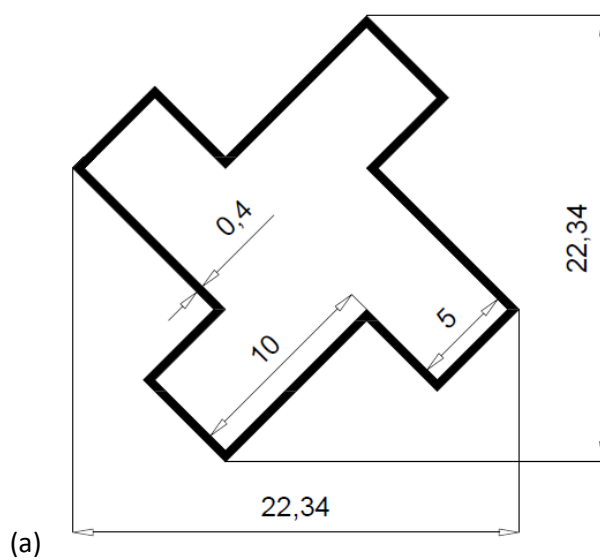


Figure 31 Lozenge grid square unit (a) and structure (b)

To check each structure behavior it was made an analysis with the software Autodesk Inventor Nastran. All the geometries were drawn in the software as a 2D structure and then they were extruded to form a 3D structure. Each structure was extruded 40 millimeters. The solid structures that were made are shown in the Fig. 31, 32.

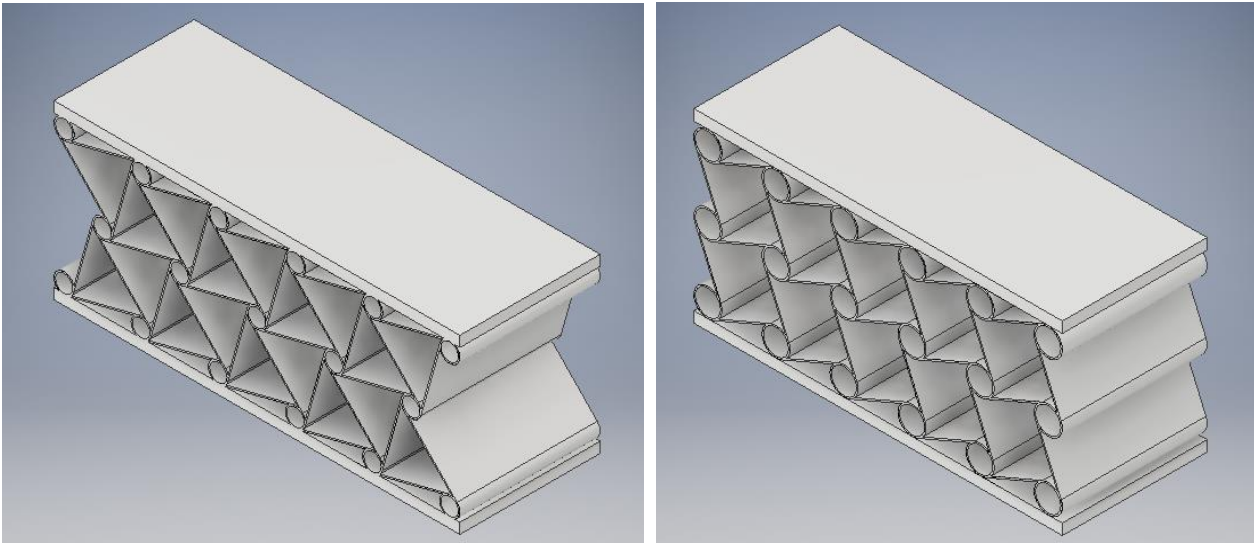


Figure 32 Chiral circular 3D structure (left) and Tetrachiral 3D structure (right)

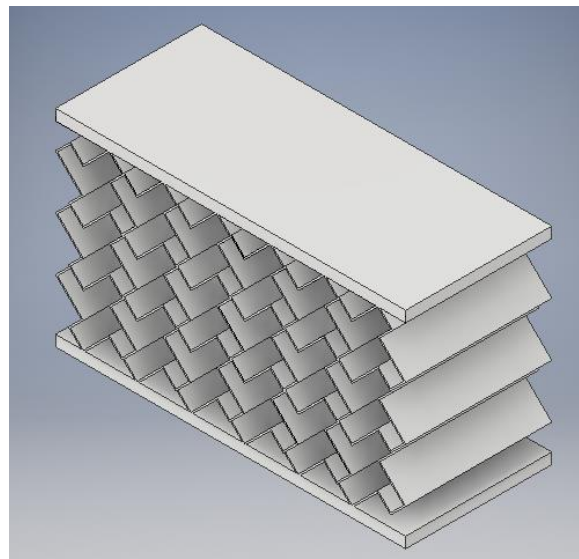


Figure 33 Lozenge grid square 3D structure

For the analysis it was important to select some parameters: type of analysis, material, constrains and applied load.

For the first samples it was chosen to make just a linear elastic analysis as a first analysis to understand the behavior of each geometry. After a geometry was selected it was used a non-linear elastic analysis to determine the results. In this way the results would much closer to reality and the comparison between software and laboratory analysis would more accurate.

For the material it was chosen to use the same material that would be used by the 3D printer, a ABS plastic. The characteristics of this material are described in fig. 34.

Editor materiali: Plastica ABS	
Identità	Aspetto ↔ Fisico ↔
▼ Informazioni	
▼ Comportamento	Comportamento: Isotropico
▼ Proprietà termiche di base	
Conducibilità termica	1,600E-01 W/(m·K)
Calore specifico	1,500 J/(g·°C)
Coefficiente di espansione termica	85,700 µm/(M · °C)
▼ Proprietà meccaniche	
Modulo di Young	2,240 GPa
Coefficiente di Poisson	0,38
Modulo a taglio	805,000 MPa
Densità	1,060 g/cm³
Coefficiente di smorzamento	0,00
▼ Resistenza	
Sollecitazione di snervamento	20,000 MPa
Resistenza alla trazione	29,600 MPa

Figure 34 Characteristics of the ABS plastic used in the software analysis

For the constraints was tried to make the situation closer to reality so the only constraint was the inability of vertical movement of the base. Later, since some of the geometries would develop horizontal displacement in just one direction, was decided to add a lateral constraint to check the differences of displacement with and without impossibility of movement in the horizontal direction.

To choose the applied load was done one important reflection based on the material and structure characteristics. Since the material that would be used was not very resistant and the models had to be a small thickness to have larger deflections, to decide which would be the applied load it was used a safety factor:

$$FS = \frac{N_d}{N_a}$$

Where FS is the safety factor, N_d is the tensile strength (maximum tensile load), N_a is the applied load. For the different loads was checked to have a safety factor greater than 1, in this way it was sure that the structure would not break under the applied load. For every model it was applied a load that would be very close to the tensile strength (FS close to 1), so that we could get the highest deformations possible. Finally the loads that were applied were all applied as a pressure and not as a concentrated force, still to have a situation closer to the laboratory one.

For the first three cases which are analyzed it was noticed that all the structures, after the load was applied, have the tendency to have an horizontal movement of the upper slab. For this reason it was done a double test: one without and one with horizontal restrictions. The horizontal restriction was applied to the upper slab so that it could move just vertically.

The first shown case is the chiral circular:

(For this case the applied load was 0,015 MPa)

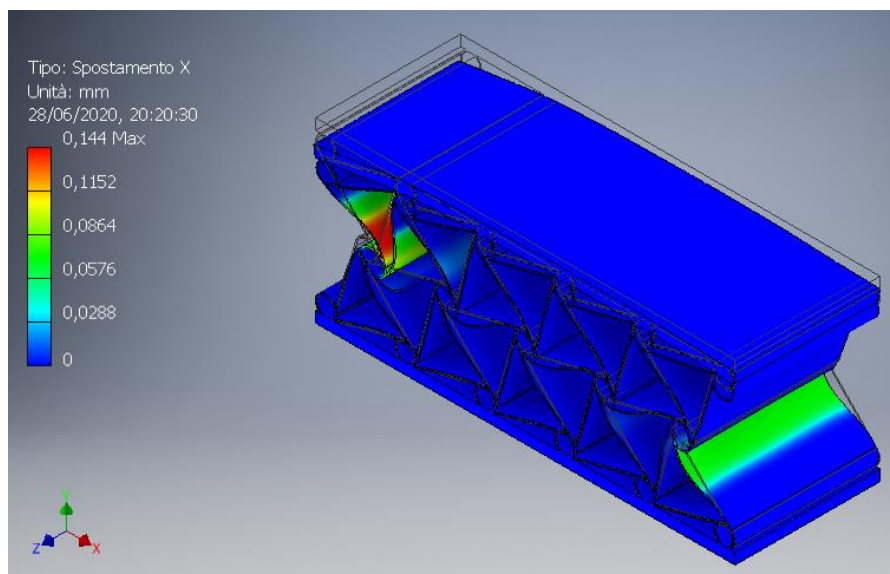


Figure 35 Horizontal deflection of the chiral circular model without restriction

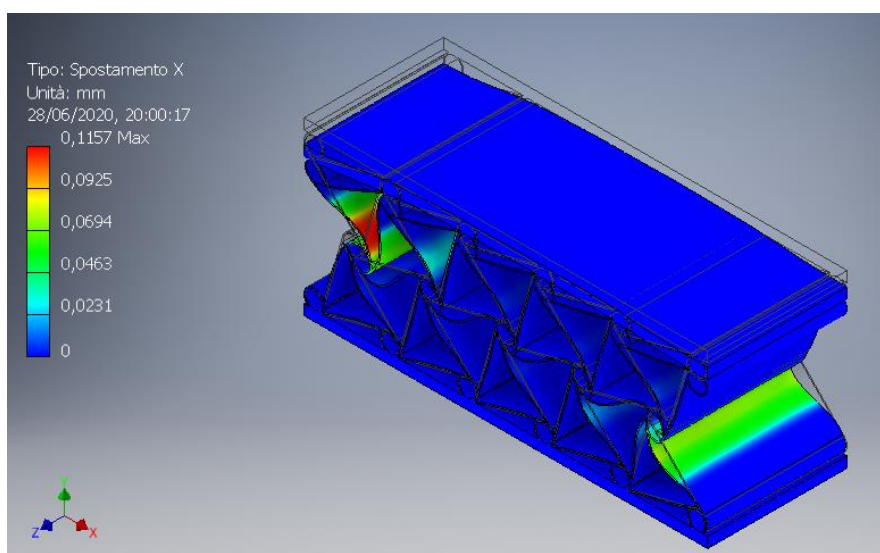


Figure 36 Horizontal deflection of the chiral circular model with restriction

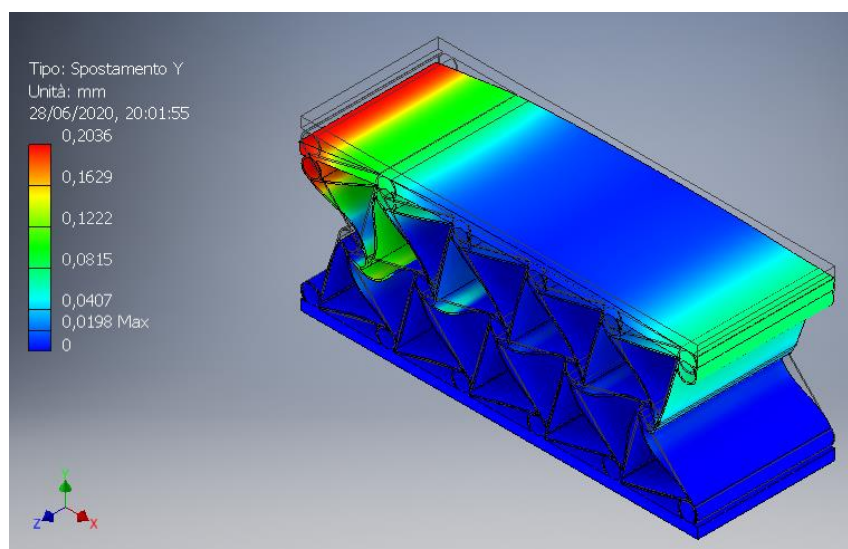


Figure 37 Vertical deflection of the chiral circular model without restriction

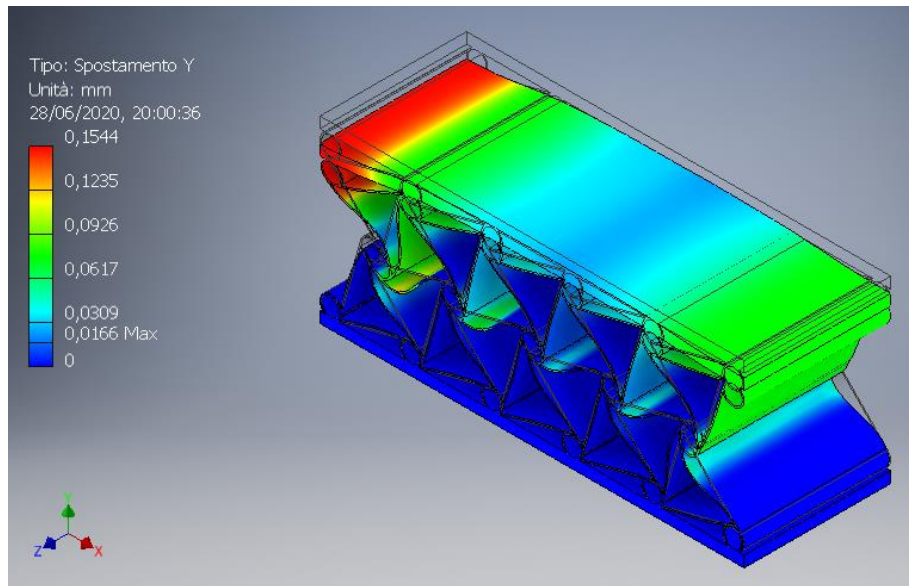


Figure 38 Vertical deflection of the chiral circular model with restriction

In this case when the load is applied the circles which connect the whole structure tend to rotate and it starts a torsional effect on the connecting sheets which give the deformation. As seen this structure is very stiff and the deformations are very low. In the center part of the structure the horizontal deformations are almost zero. All the deformation occurred is at the extreme lateral part and is due just to the torsional effect. For the vertical deformations we have a similar situation, all the deformations occur in the upper side, while in the bottom are zero. The difference between horizontally constrained and not it not very big in this case. The non constrained structure has a maximum deformation 20-30% higher than the constrained one. Finally in the not constrained model the vertical displacement is concentrated in the outer parts of the slab while in the constrained is spread almost in all the upper slab.

The second case is the Tetrachiral model:

(For this case the applied load was 0,015 MPa)

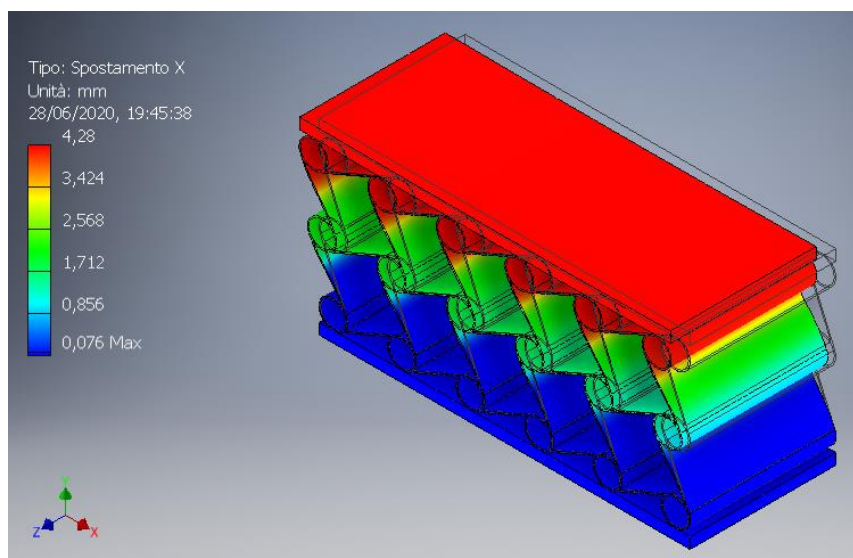


Figure 39 Horizontal deflection of the tetrachiral model without restriction

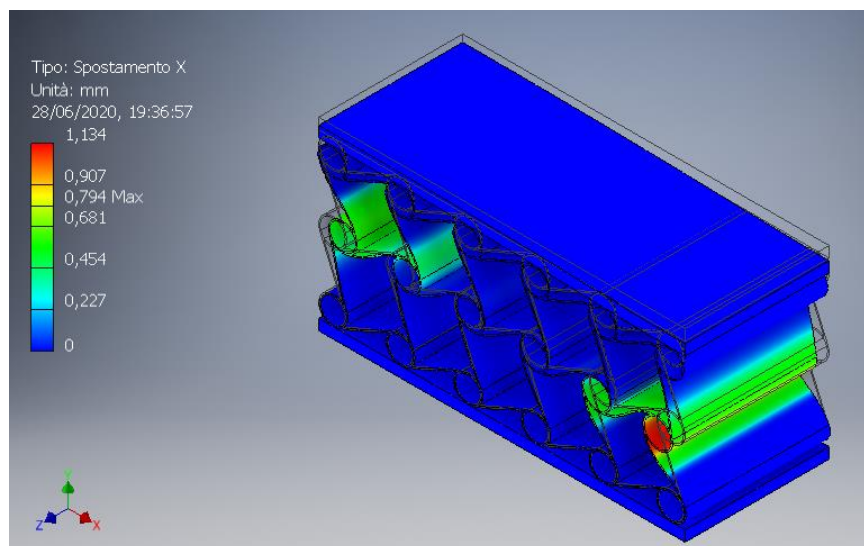


Figure 40 Horizontal deflection of the tetrachiral model with restriction

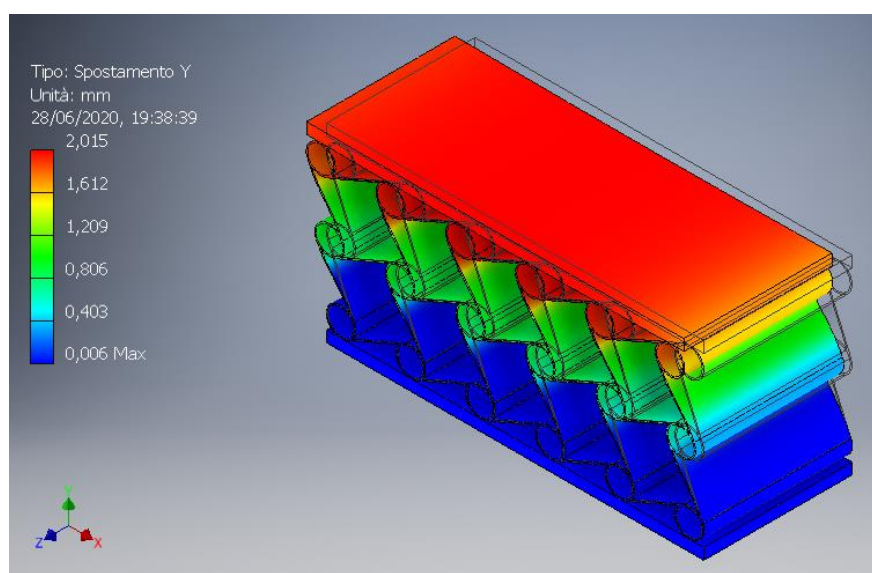


Figure 41 Vertical deflection of the tetrachiral model without restriction

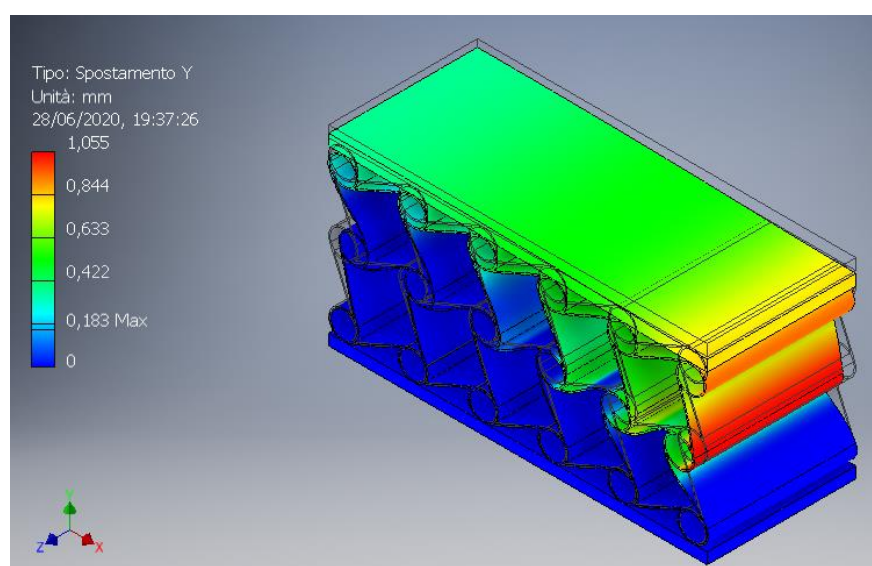


Figure 42 Vertical deflection of the tetrachiral model with restriction

As in the previous case the deformation is given by the rotation of the circles which gives a torsion effect to the single unit cells. In this case is more visible the difference between the restricted and non restricted model: actually the horizontal restriction it's like if it was giving the structure more stiffness. In fact for the non restricted model the maximum vertical displacement is double than the restricted one and for the horizontal displacement is even four times higher.

Due to the slope of the unit cell (inclined to the left) the whole structure tends to move on the left side when the load is applied, and for that reason the maximum horizontal deflection in the non constricted model appears in the upper slab and every unit cell connected to the slab has the same horizontal displacement.

The third case is the Lozenge grid square model:

(For this case the applied load was 0,01 MPa)

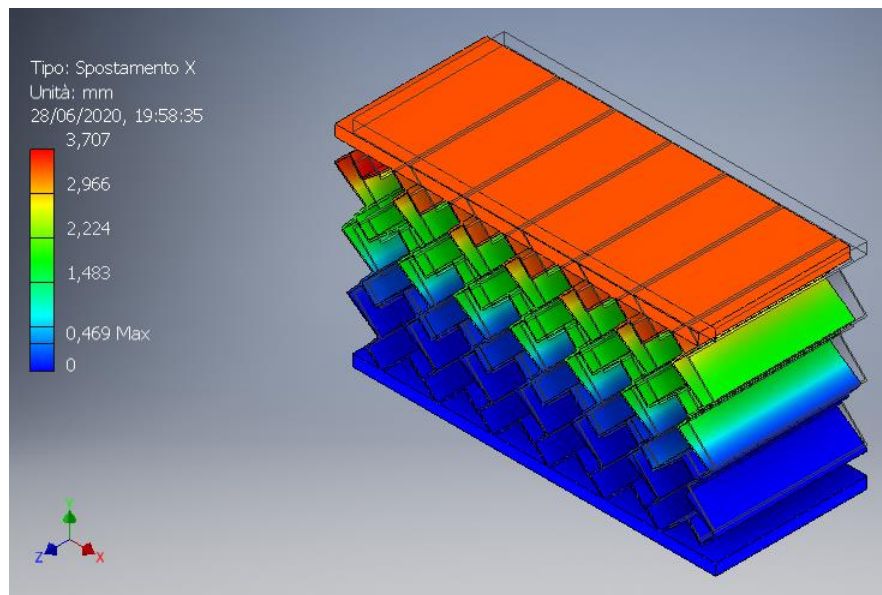


Figure 43 Horizontal deflection of the Lozenge grid square model without restriction

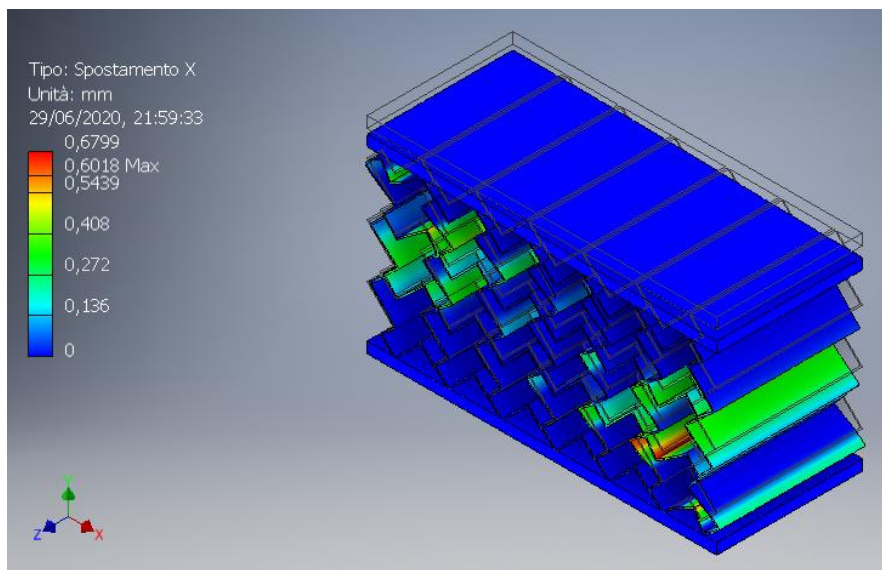


Figure 44 Horizontal deflection of the Lozenge grid square model with restriction

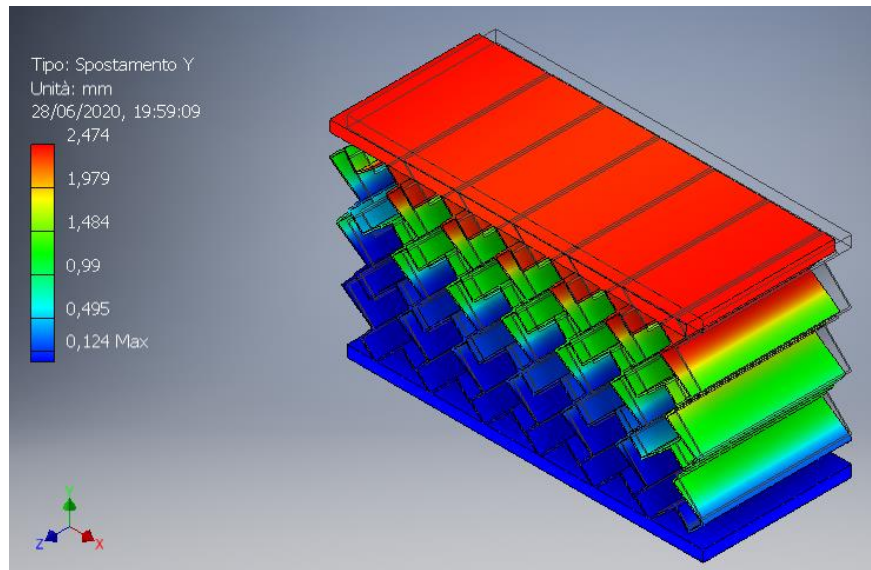


Figure 45 Vertical deflection of the Lozenge grid square model without restriction

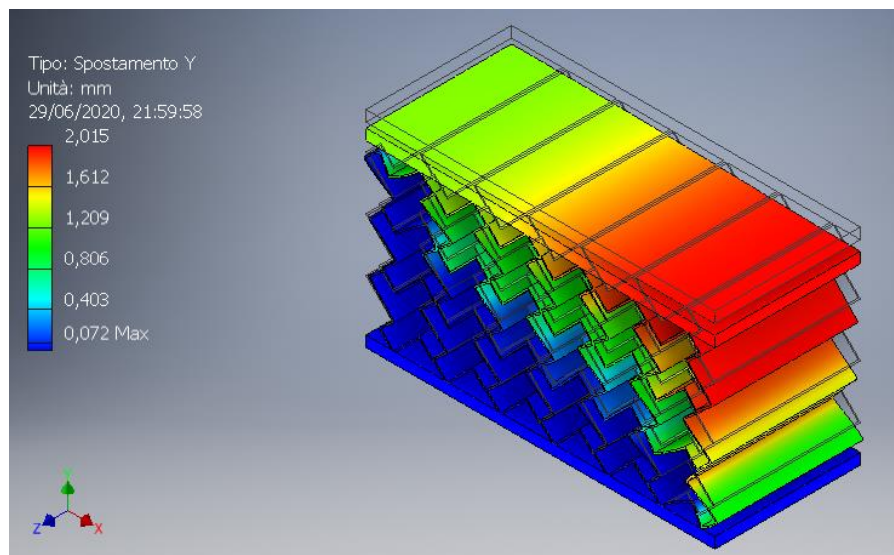


Figure 46 Vertical deflection of the Lozenge grid square model with restriction

For this case, similarly to the previous one, the horizontal constrain is giving more stiffness to the structure. However in this case the vertical displacement is concentrated in the upper section for the non constrained model, while for the constrained one the impediment to move to the left is shifting the vertical stress from the left to the right. In fact the depth of the vertical displacement increases by going to the right: on the left the displacement is concentrated in the slab while going to the right the displacements appear even in the bottom unit cells.

For horizontal displacement we have the same behavior of the tetrachiral model: a very low displacement for the constrained model and high values for the non constrained model with the maximum displacement given by the movement of the upper slab.

After studying these models it was seen that the displacements are not very relevant with constrained conditions, but without horizontal constrains there would be good displacements to measure. Theoretically they could be used but when we would try to measure the Poisson's ratio and we would test them in the laboratory there would some problems. The first one is that maximum displacements occur into the slab and not in the structure. The second one is that by having a movement of the structure to one side there are high

total displacements but the Poisson's ratio is still not very high. For this reason it was decided to proceed the study of other geometries.

In the next figures are presented the new geometries which were analyzed: Chiral square symmetric, Re-entrant triangular and Re-entrant honeycomb.

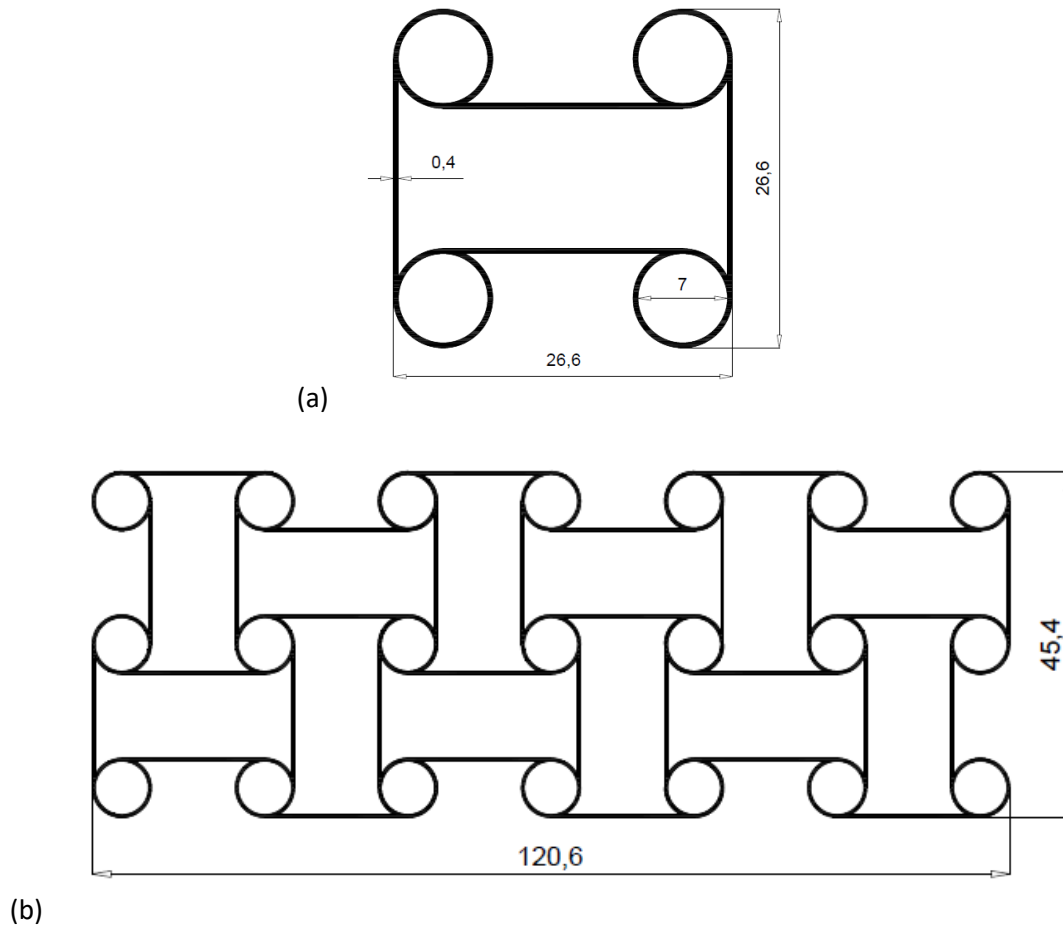
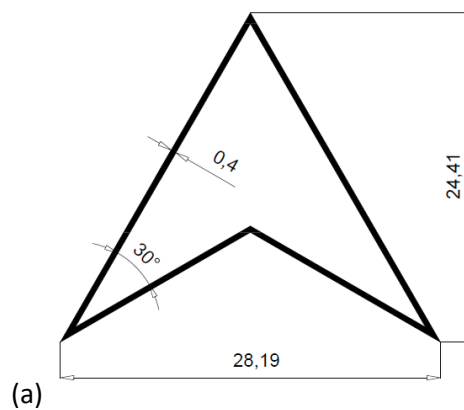


Figure 47 Chiral square symmetric singular unit (a) and structure (b)



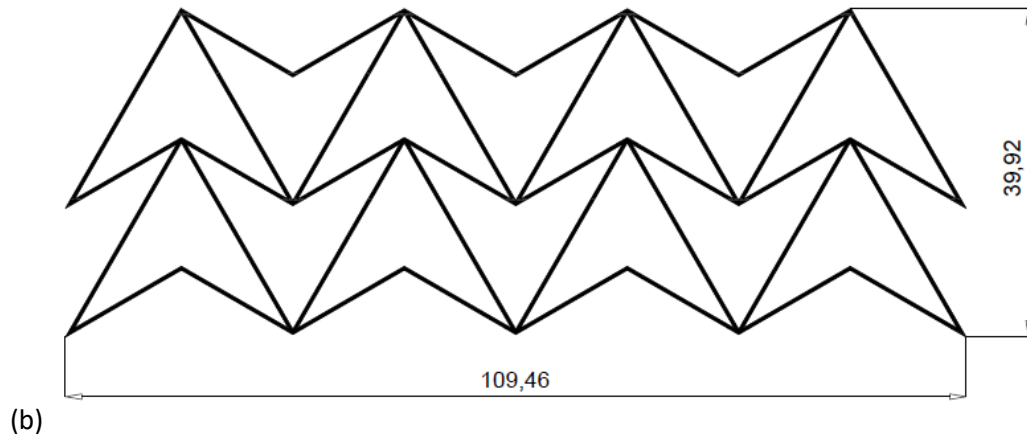


Figure 48 Re-entrant 39riangular singular unit (a) and structure (b)

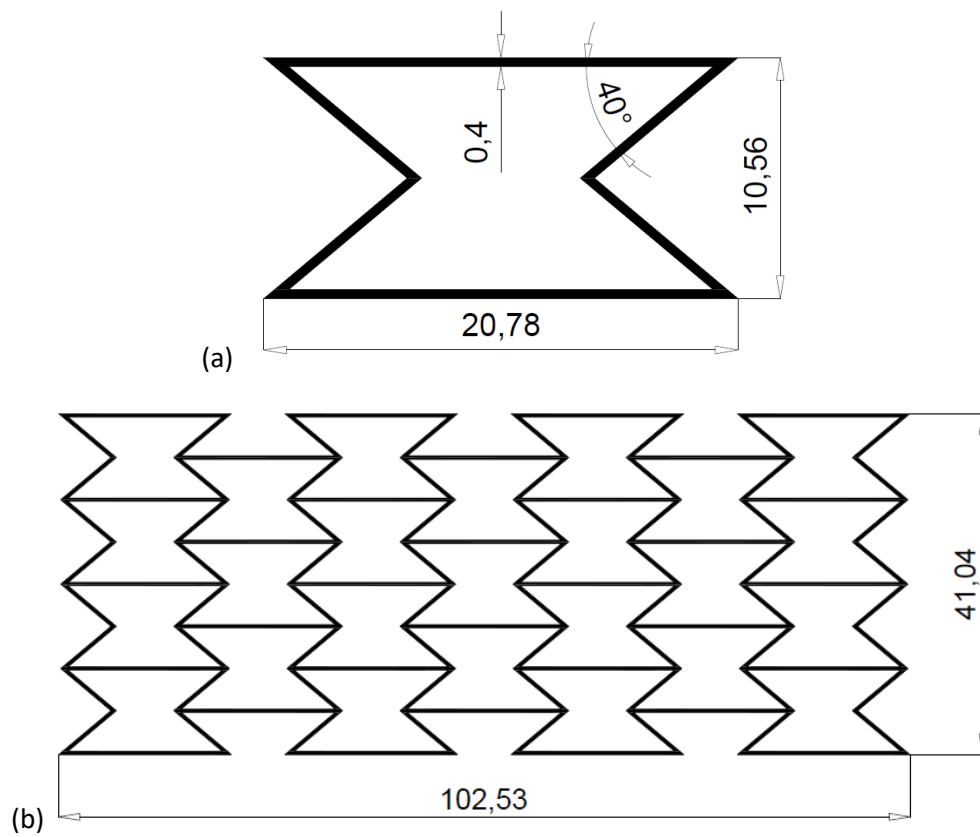


Figure 49 Re-entrant honeycomb singular unit (a) and structure (b)

For each of these models it was used the same approach that was used for the previous ones.

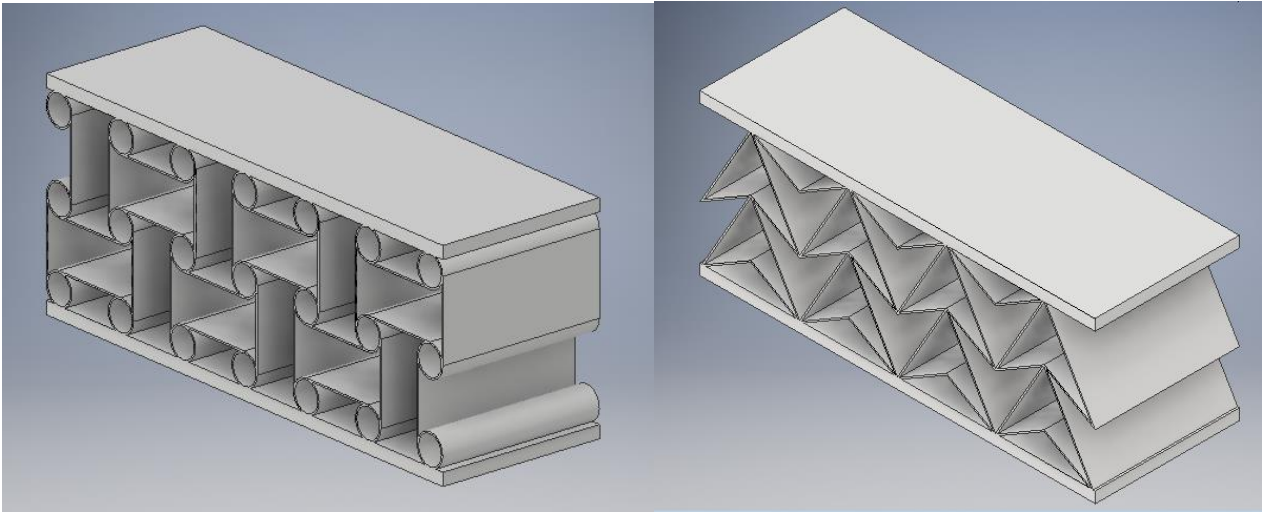


Figure 50 Chiral square symmetric 3D structure (left) and Re-entrant triangular 3D structure (right)

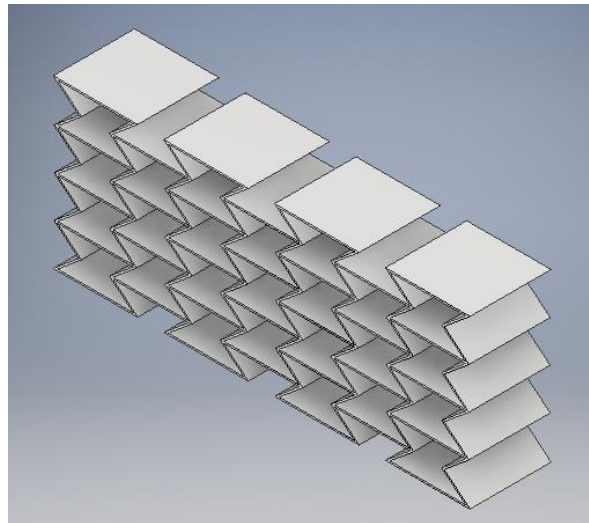


Figure 51 Re-entrant honeycomb 3D structure

The first shown case is the chiral square symmetric model:

(For this case the applied load was 0,01 MPa)

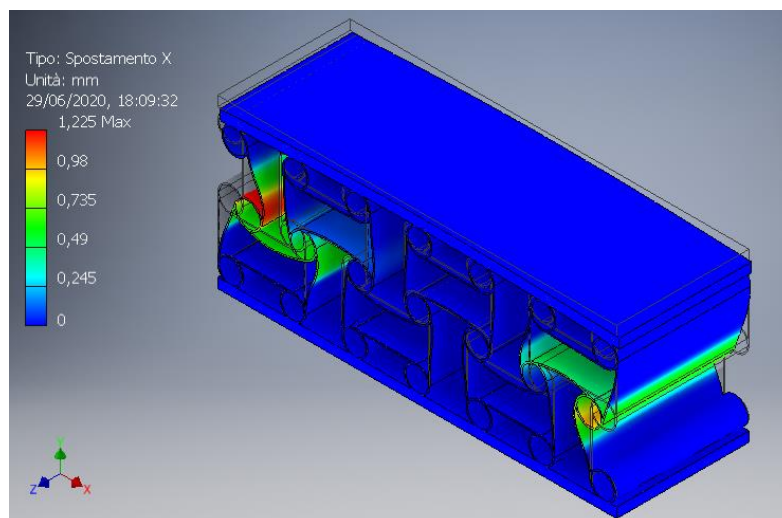


Figure 52 Horizontal deflection of the chiral square symmetric model

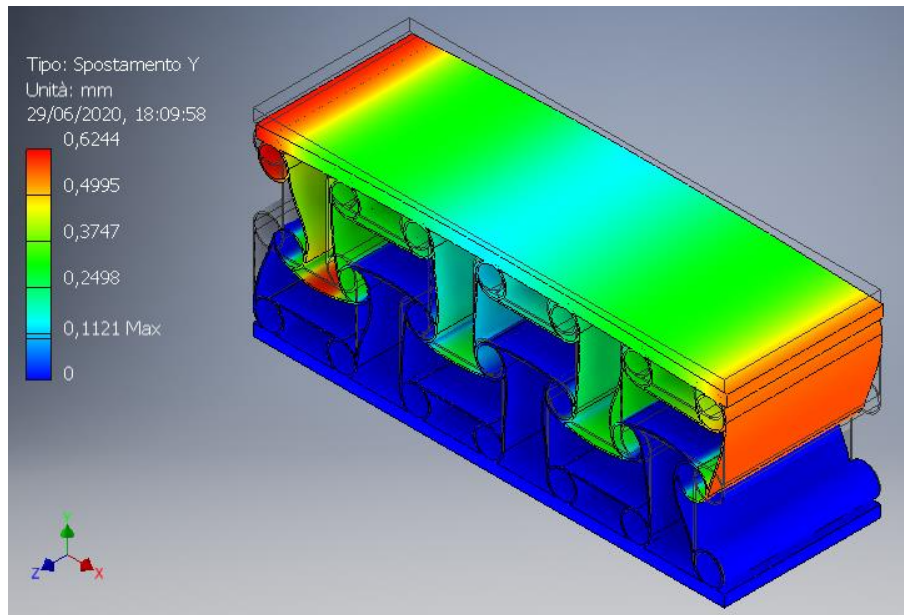


Figure 53 Vertical deflection of the chiral square symmetric model

In this case the structure has a similar behavior to the other chiral models analyzed. There is a torsion movement due to the rotation of the circles that compose the structure. The deflections are very small and the horizontal ones are concentrated only in the outer part of the structure. For the vertical one they are very small and they are not symmetric because of the non symmetry of the structure in the outer part (most deflected).

The second case is the re-entrant triangular model:

(For this case the applied load was 0,005 MPa)

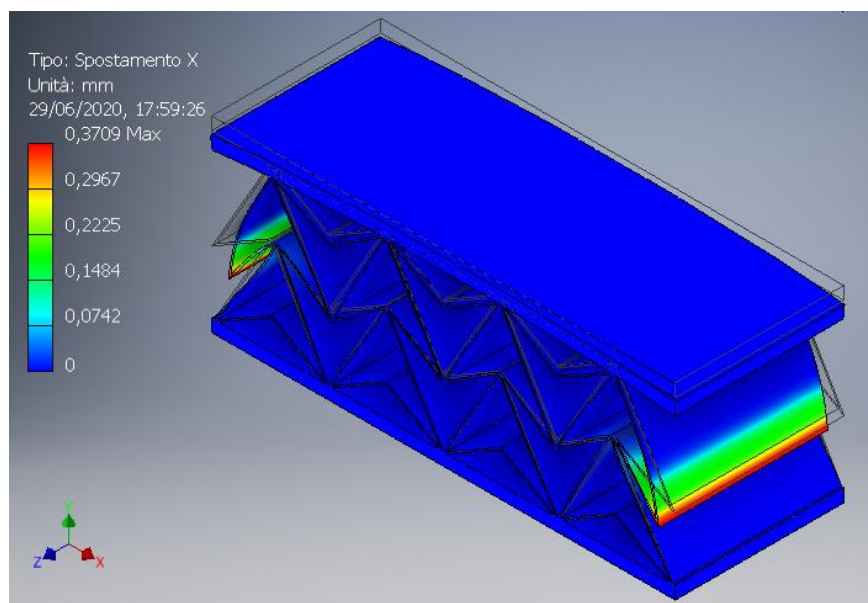


Figure 54 Horizontal deflection of the re-entrant triangular model

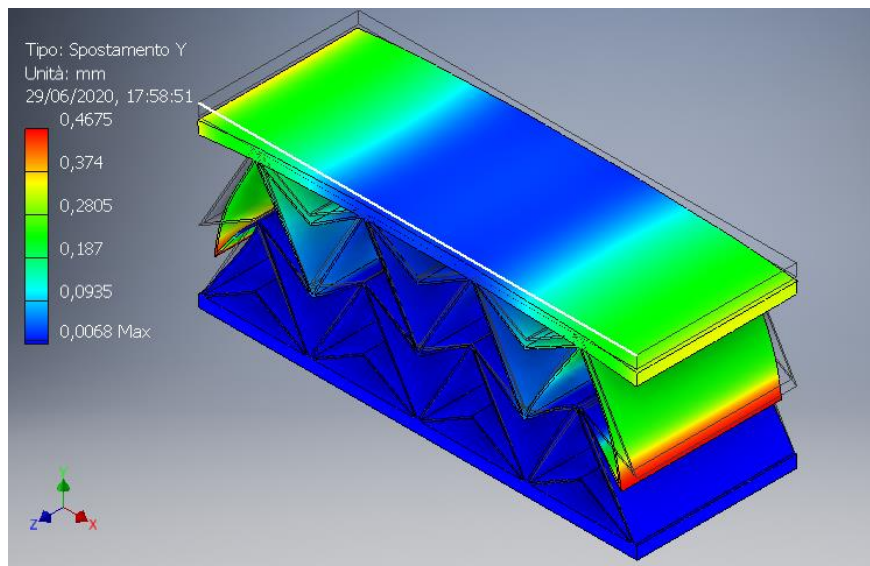


Figure 55 Vertical deflection of the re-entrant triangular model

The behavior of this structure is symmetrical because of the symmetry of the model. As for the first one this structure is highly stiff and the deflections occur only in the outer part of the model. Both horizontal and vertical deflections are very low and are not useful to show the auxetic behavior.

The third case is the re-entrant honeycomb model:

(For this case the applied load was 0,015 MPa)

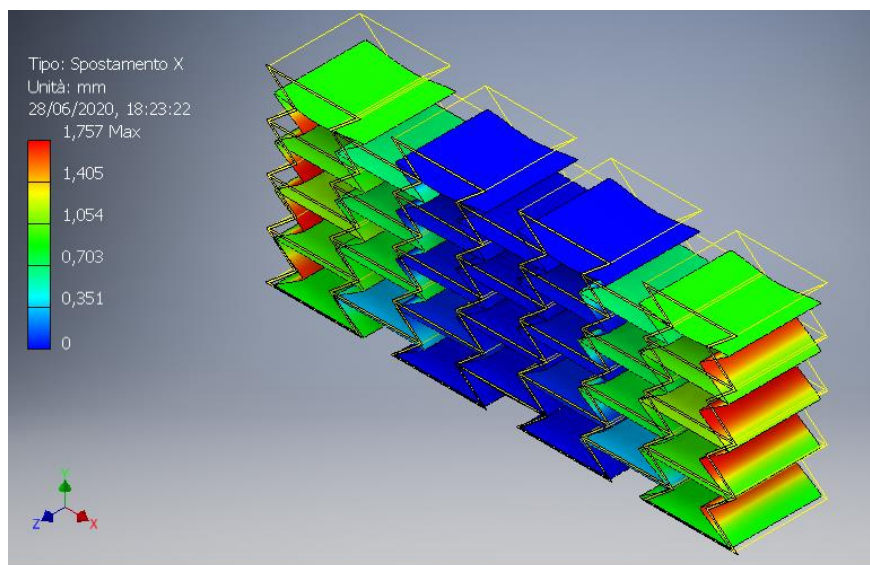


Figure 56 Horizontal deflection of the re-entrant honeycomb model

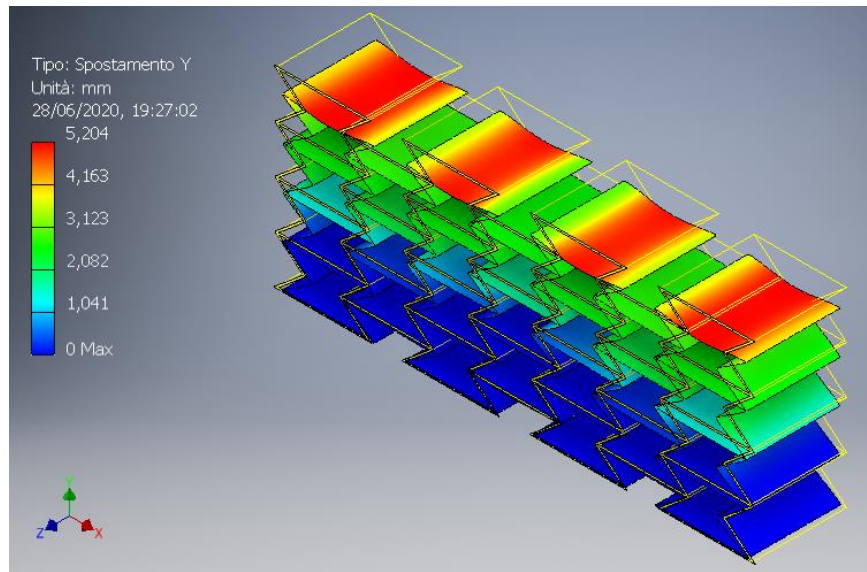


Figure 57 Vertical deflection of the re-entrant honeycomb model

In this last case there are many displacements occurring in the whole structure. The highest are in the outer and upper part. For the vertical displacements they occur especially in the central part of each upper unit cell and they are very high (5 mm). While for the horizontal ones they occur on the edges of each outer unit cell and they are symmetrical. The horizontal displacements are quite high too and due to symmetry they “double” in size and for this reason is very easy to observe the auxetic behavior.

After these considerations it was decided that the re-entrant honeycomb structure is the most convenient to analyze with the laboratory conditions and due to its geometry it’s the easiest to use to calculate the Poisson’s ratio. Before proceeding further it was decided to analyze what would happen if the same unit cell would double in size and double in thickness. For these reason other two re-entrant honeycombs were analyzed. The geometries and the results of the two proposed models are shown in the next figures.

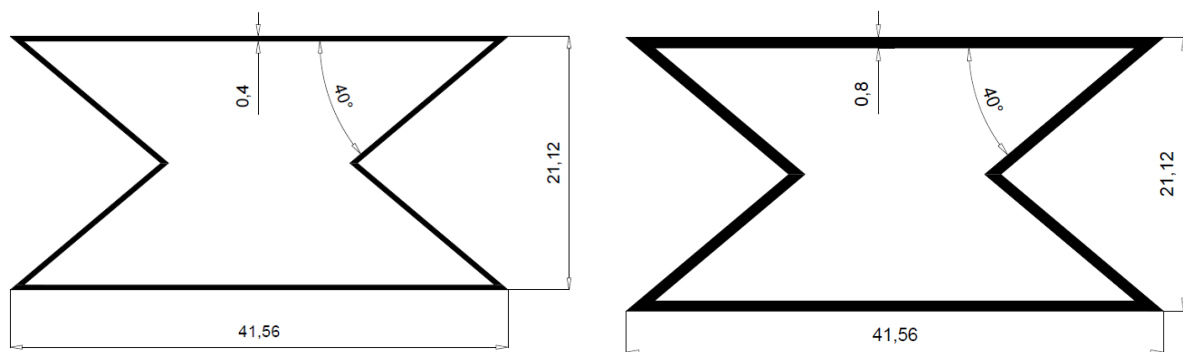


Figure 58 Re-entrant honeycomb unit cell double sizes (left) and double size/thickness (right)

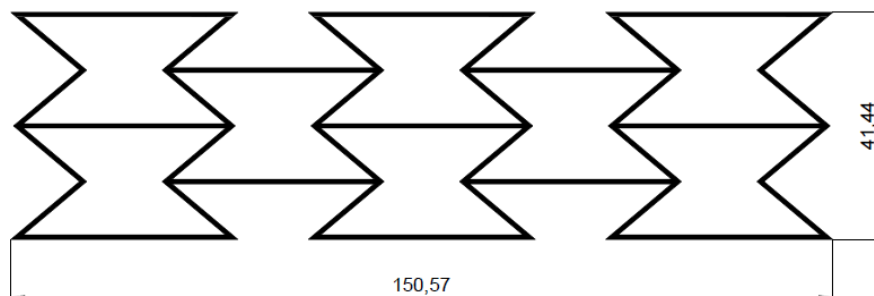


Figure 59 Re-entrant honeycomb double size structure

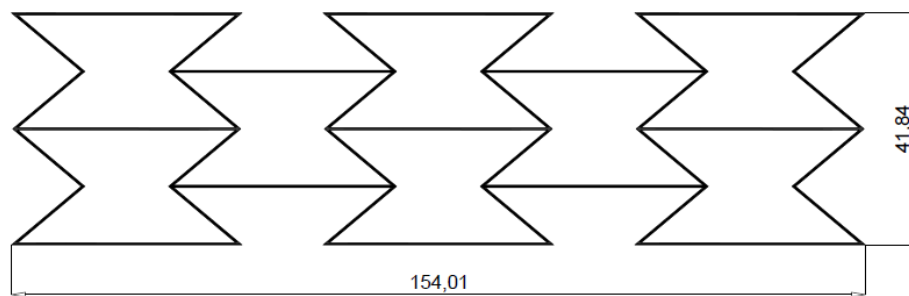


Figure 60 Re-entrant honeycomb double size/thickness structure

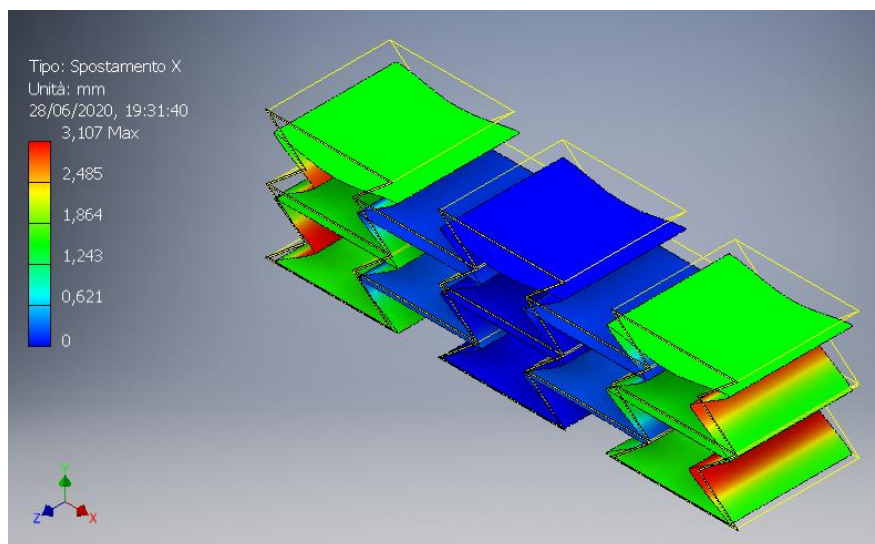


Figure 61 Horizontal displacement re-entrant honeycomb double size

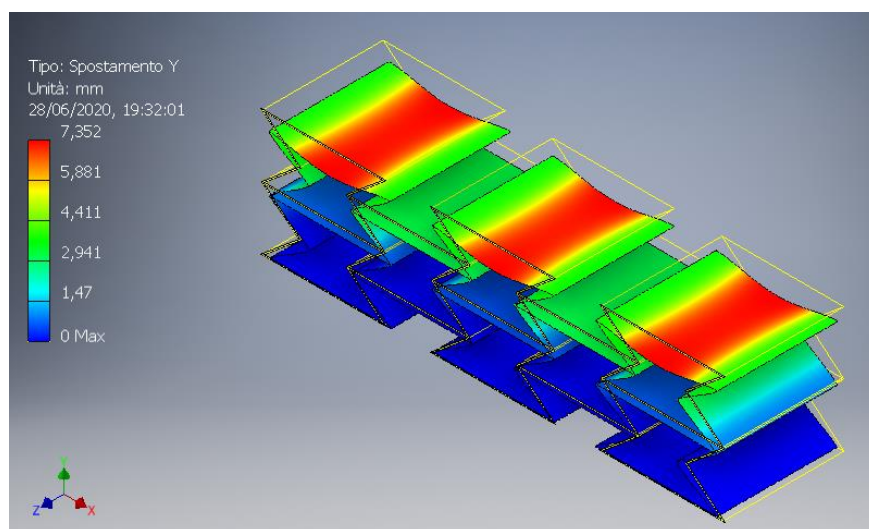


Figure 62 Vertical displacement re-entrant honeycomb double size

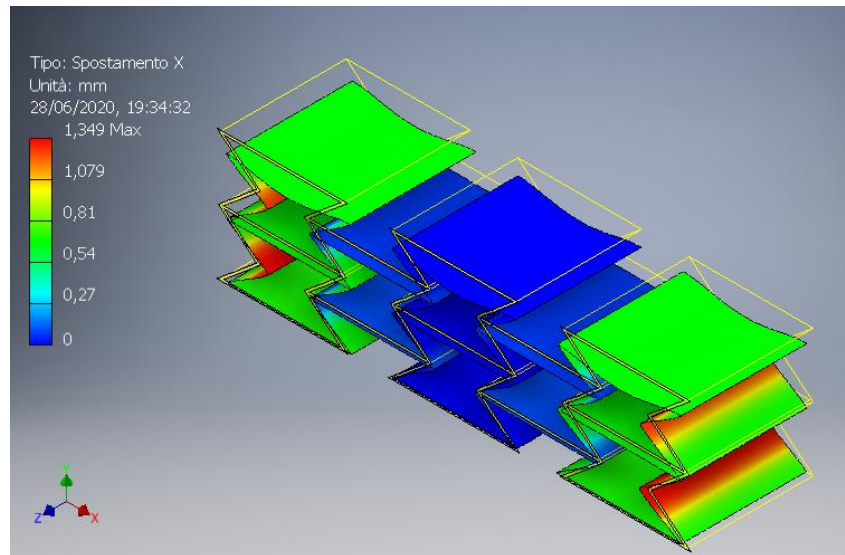


Figure 63 Horizontal displacement re-entrant honeycomb double size/thickness

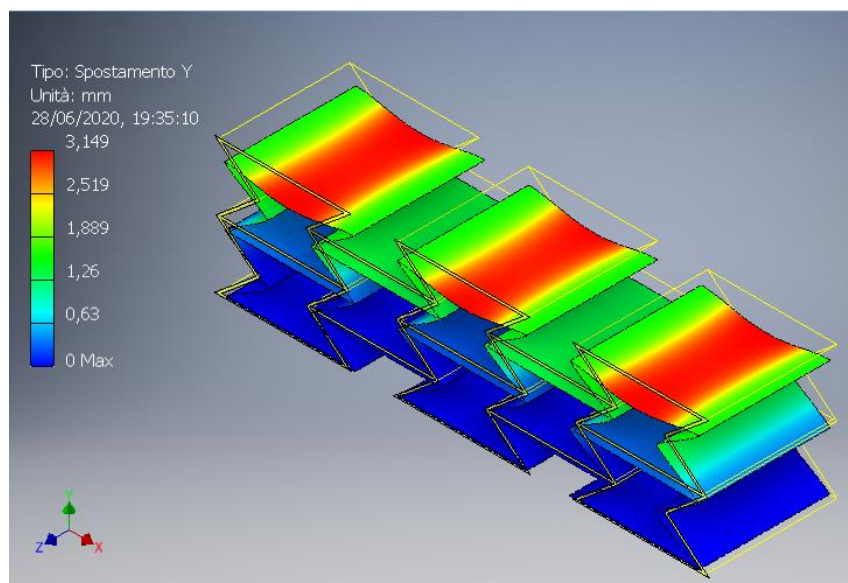


Figure 64 Vertical displacement re-entrant honeycomb double size/thickness

By this analysis it's shown that by doubling the size of the unit cell the whole structure becomes less stiff and there is an increase of the displacements. By doubling both size and thickness the response is not linear, so there is not a perfect scale effect and the displacements that occur are smaller than the first re-entrant honeycomb unit.

After these analyses it was decided to proceed with two re-entrant honeycomb unit cells: the first one analyzed and the same one just doubled in size.

2.3 Dependence between deformation and structural packing

As said before the geometry chosen for the analysis was the re-entrant honeycomb. To understand the difference in behavior due the measures of the single unit cell it was decided to make a comparison between the first re-entrant honeycomb unit cell analyzed and the same unit cell doubled in size, but left with the same thickness. For convenience the two samples will be called "Sample A" for the original unit cell and "Sample B" for the doubled in size. In the next figure are presented the measures of both single unit cells.

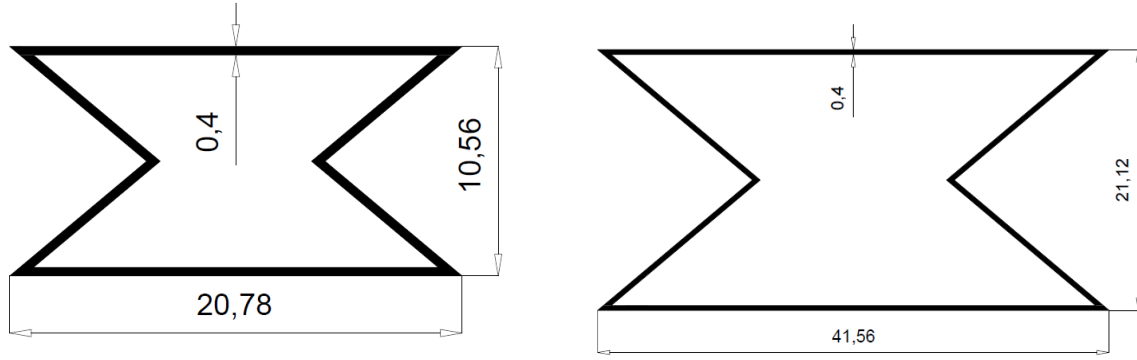


Figure 65 Geometries of sample A (left) and sample B (right)

In this analysis nine different models were realized for each sample to understand the different behavior due to the increase of unit cells. For convenience the models were seen as a matrix $m * n$, with m and n were respectively the number of rows and columns. For the rows is intended the number of layers of unit cells (from 1 to 3). For columns is intended the number of unit cells constrained to the support plane (from 1 to 3).

The measures of the samples 1x1 A and B are already represented by the unit cells. To show the geometries of the other models, are reported the measures of structures 2x2 and 3x3 of each sample.

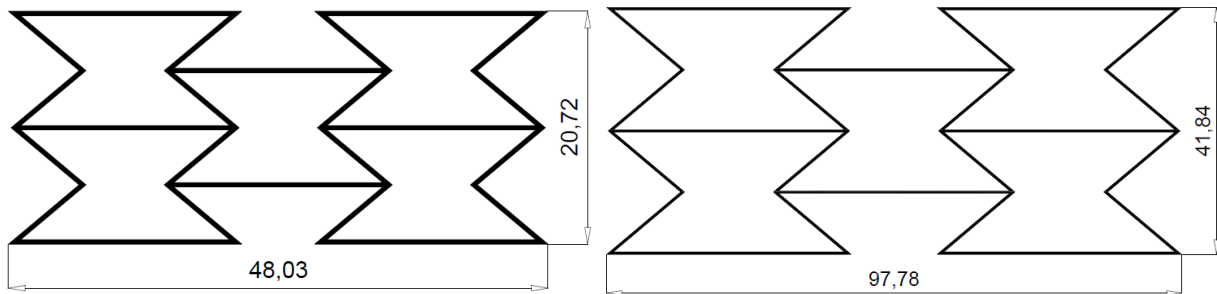


Figure 66 Samples 2x2 A (left) and 2x2 B (right)

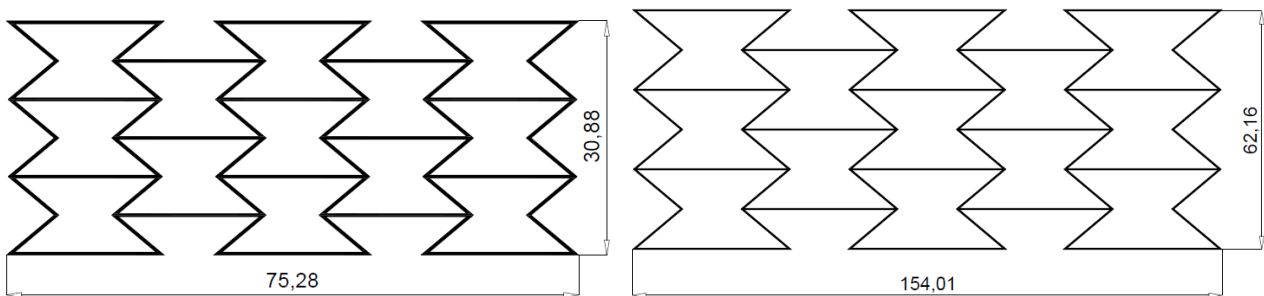


Figure 67 Samples 3x3 A (left) and 3x3 B (right)

For the modeling of the structure were used the same considerations of the previous analyses. The geometries were extruded 40 millimeters, same PLA material, all structures constrained to the base with impossibility of vertical movement and the applied load was chosen by studying the safety factor FS . Immediately it was noticed that the sample A structures were more stiff than the ones of sample B, so it was decided to use two different loads. For all the models of sample A it was used a distributed load of 0,02 MPa and a load of 0,004 MPa for the ones of sample B.

Here is illustrated a graphic comparison of each structure for both samples, showing the horizontal and vertical displacement.

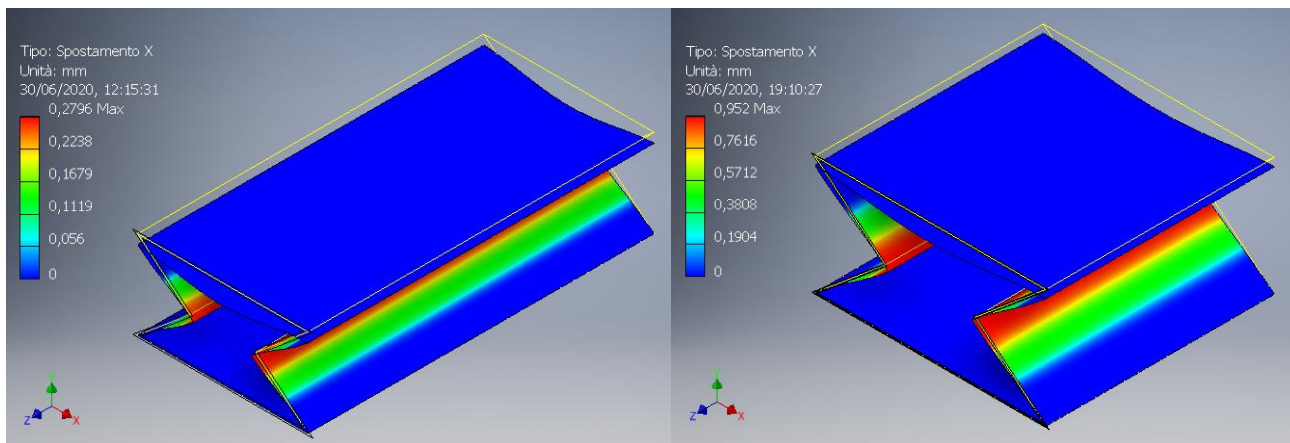


Figure 68 Horizontal displacements model 1x1 sample A (left) and B (right)

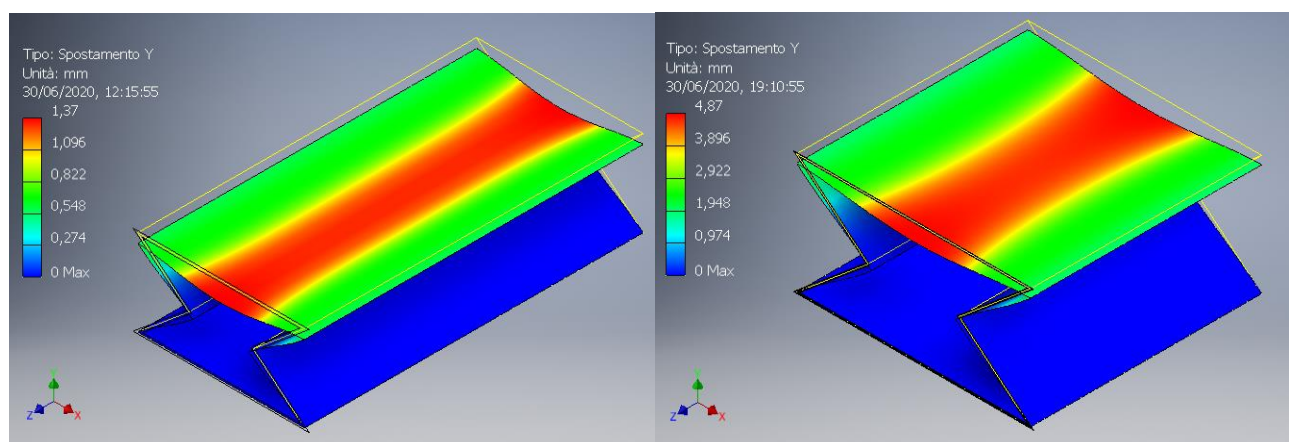


Figure 69 Vertical displacements model 1x1 sample A (left) and B (right)

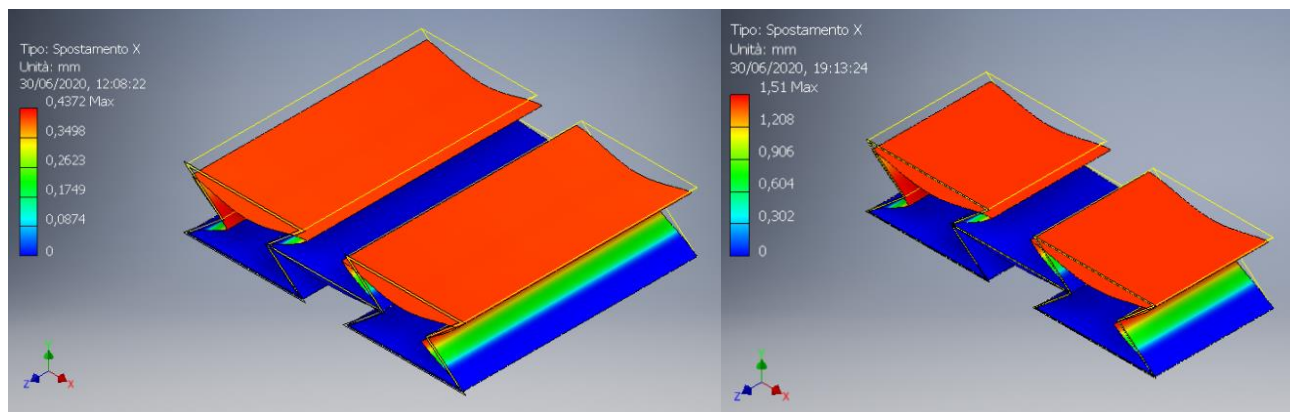


Figure 70 Horizontal displacements model 1x2 sample A (left) and B (right)

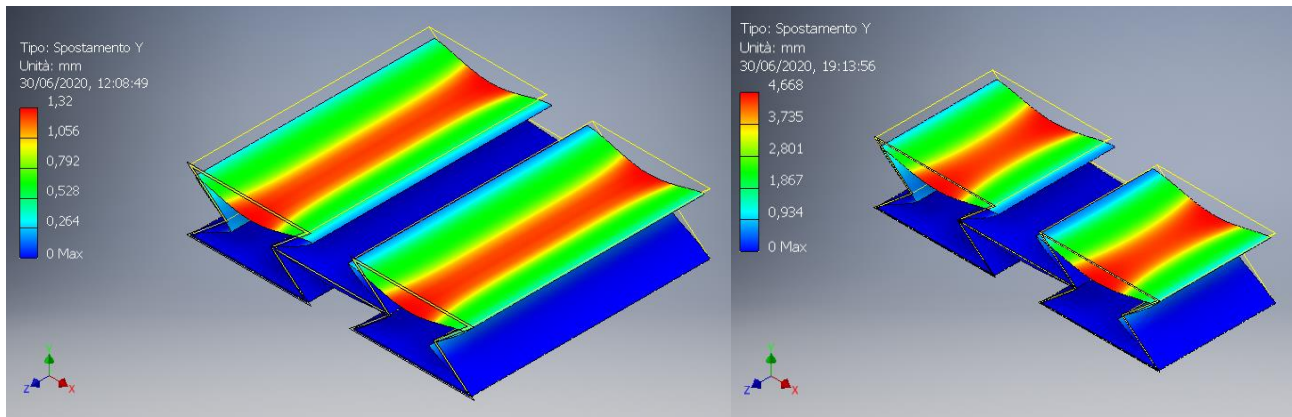


Figure 71 Vertical displacements model 1x2 sample A (left) and B (right)

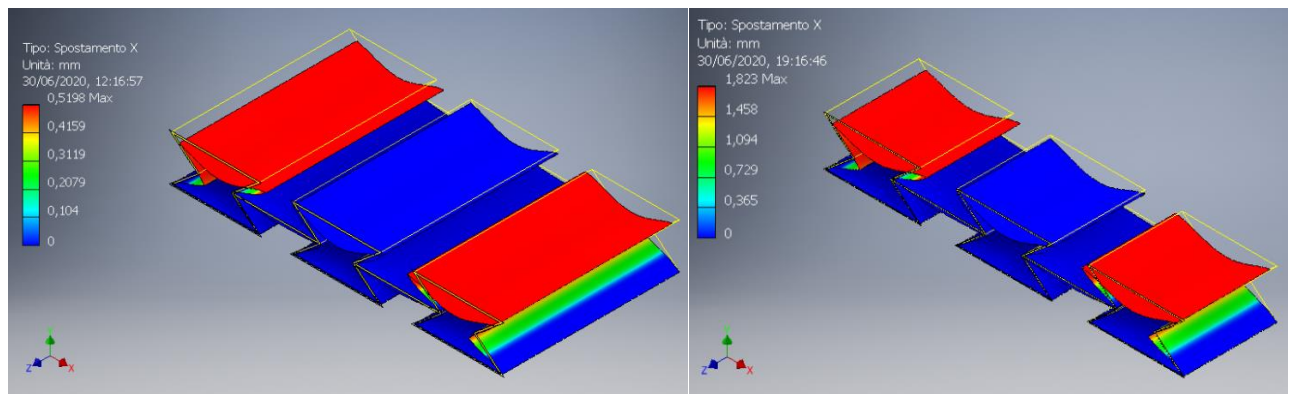


Figure 72 Horizontal displacements model 1x3 sample A (left) and B (right)

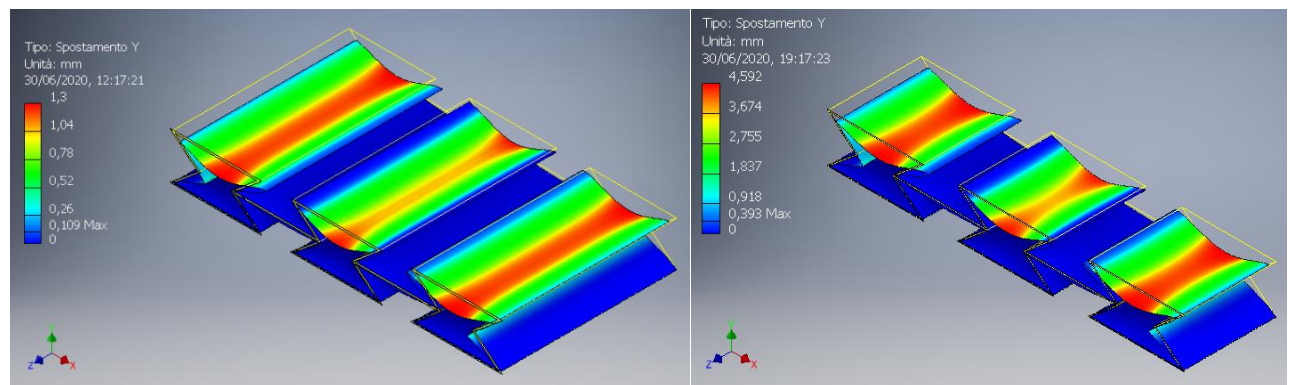


Figure 73 Vertical displacements model 1x3 sample A (left) and B (right)

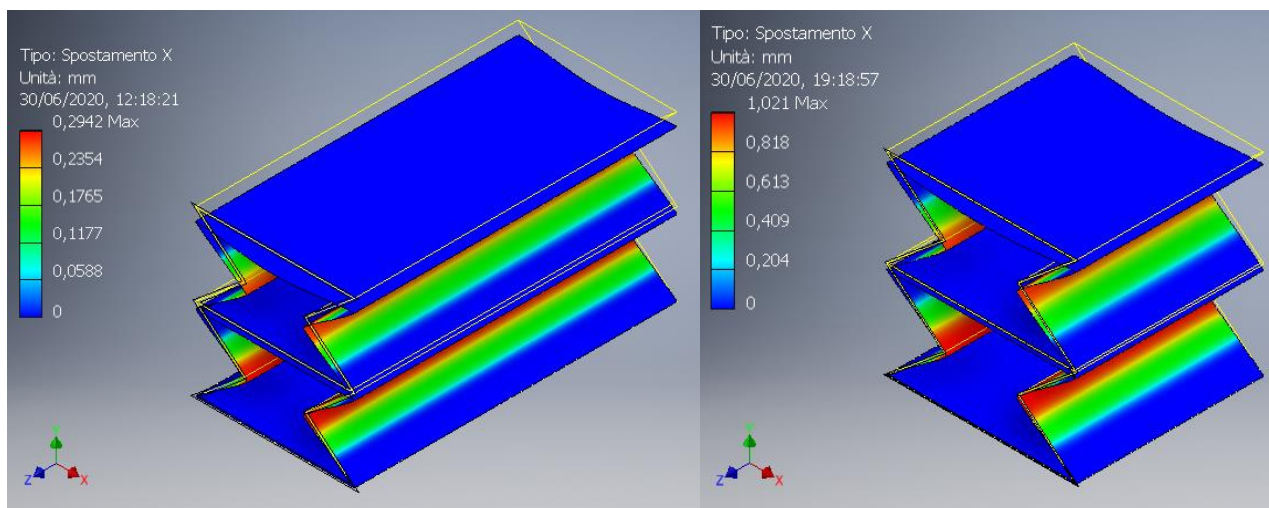


Figure 74 Horizontal displacements model 2x1 sample A (left) and B (right)

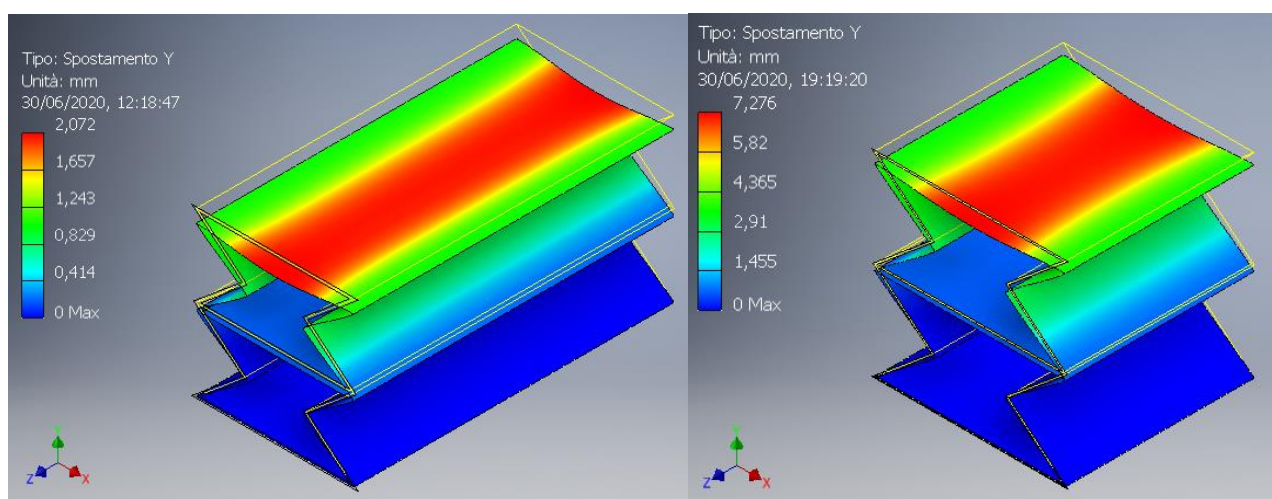


Figure 75 Vertical displacements model 2x1 sample A (left) and B (right)

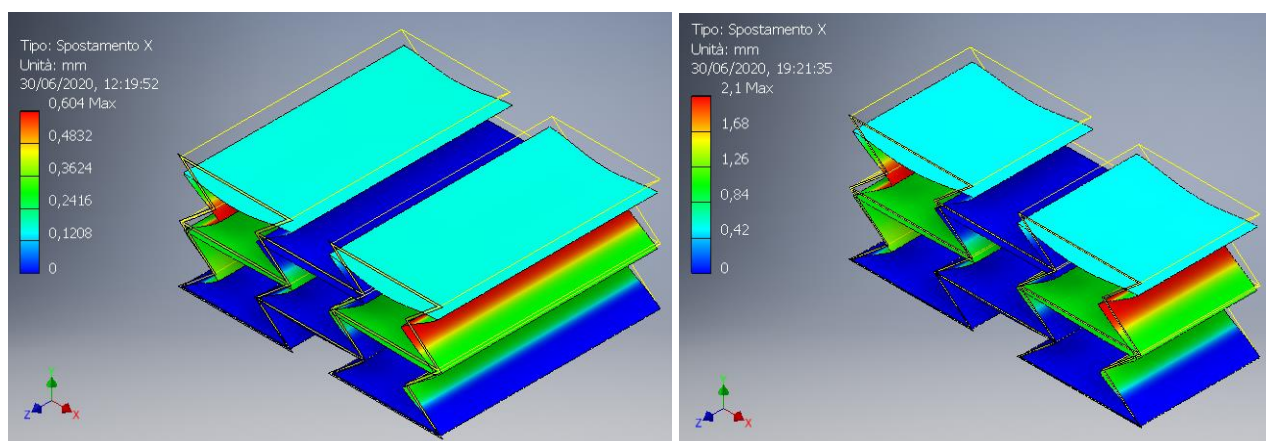


Figure 76 Horizontal displacements model 2x2 sample A (left) and B (right)

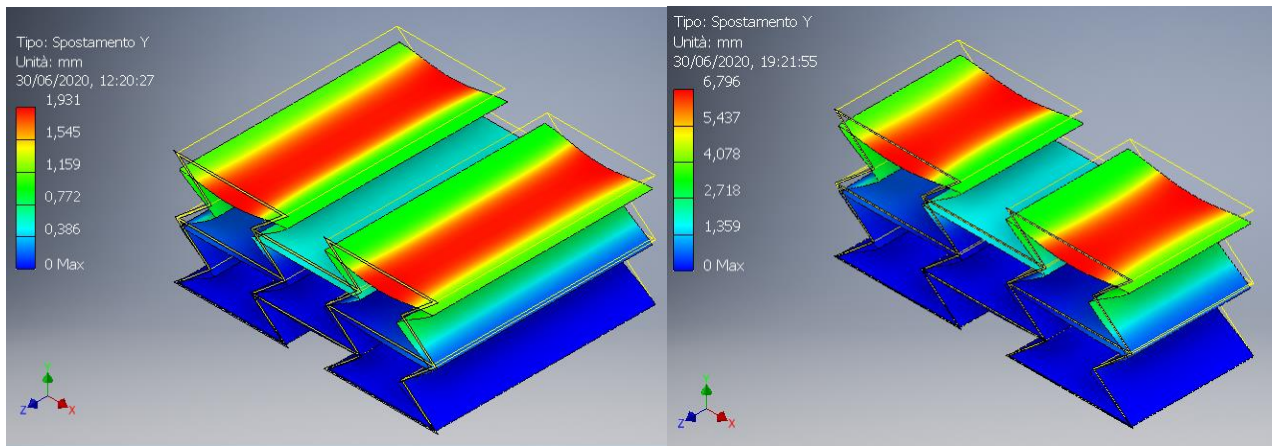


Figure 77 Vertical displacements model 2x2 sample A (left) and B (right)

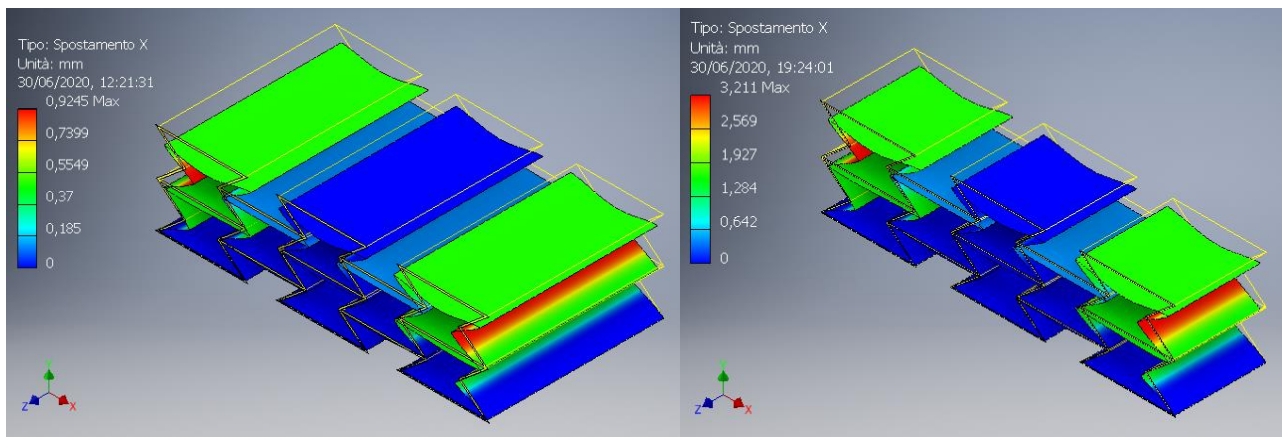


Figure 78 Horizontal displacements model 2x3 sample A (left) and B (right)

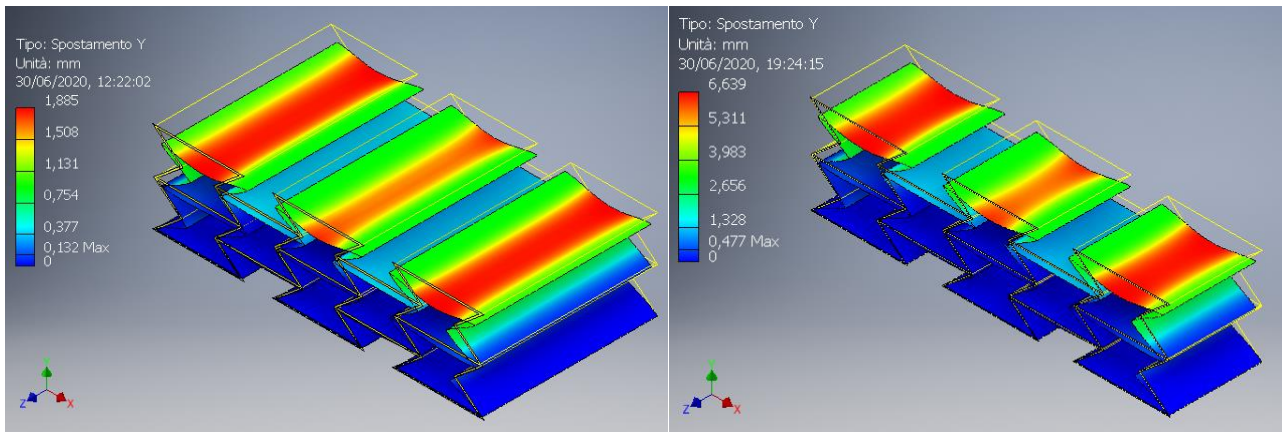


Figure 79 Vertical displacements model 2x3 sample A (left) and B (right)

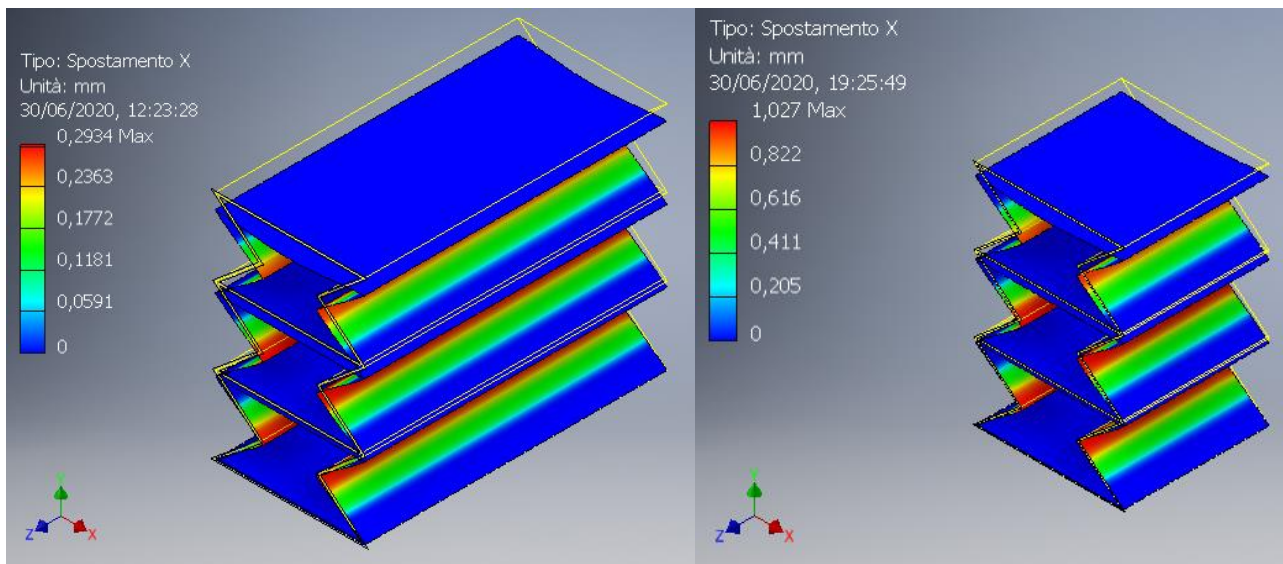


Figure 80 Horizontal displacements model 3x1 sample A (left) and B (right)

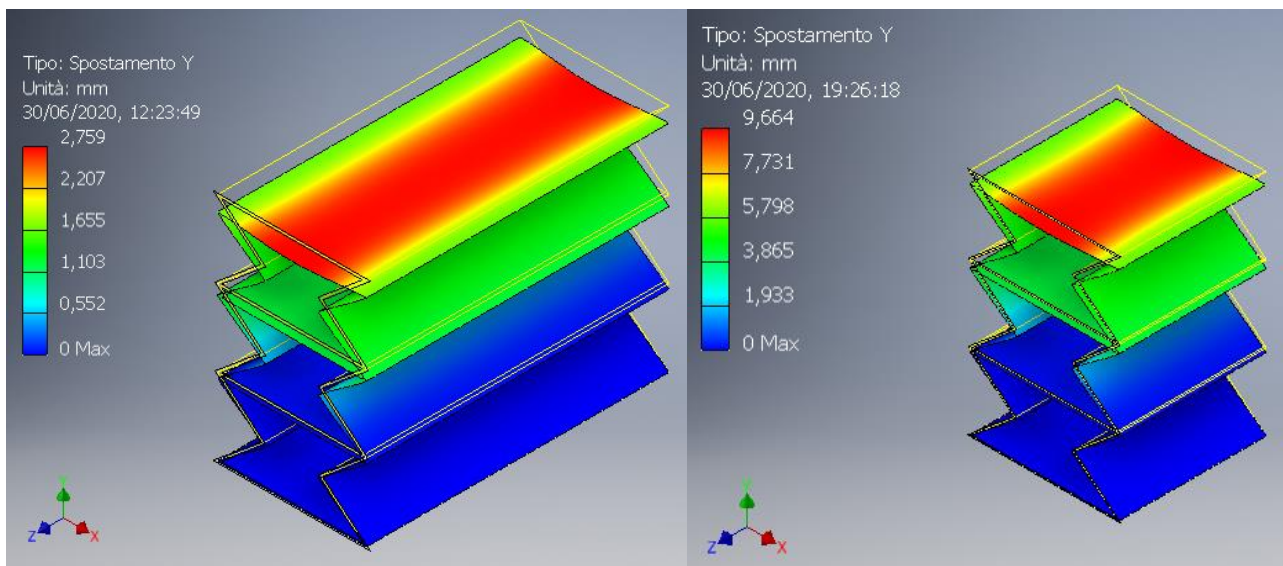


Figure 81 Vertical displacements model 3x1 sample A (left) and B (right)

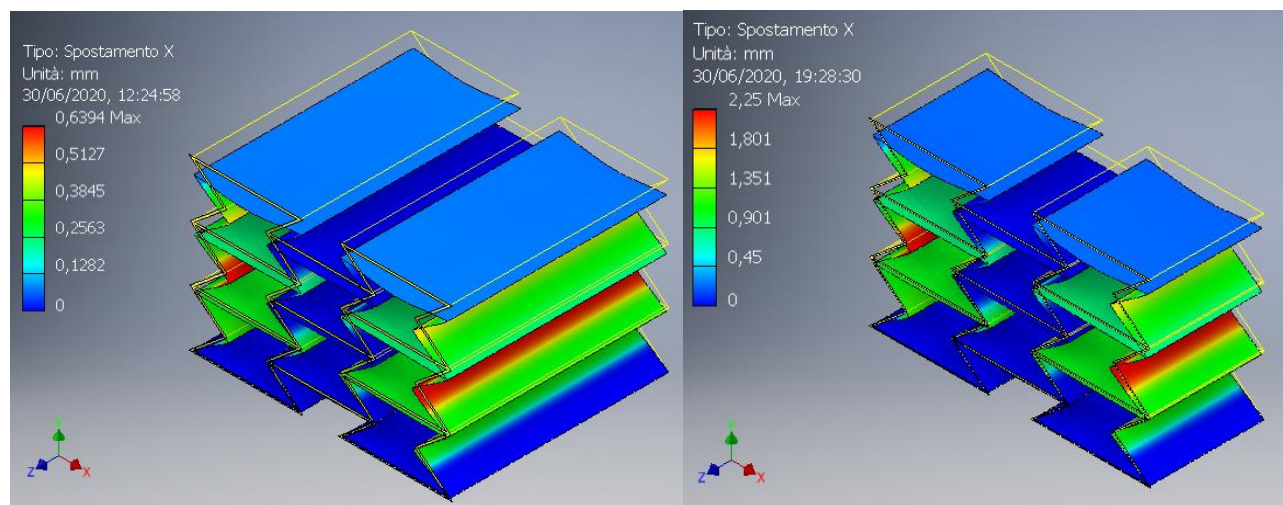


Figure 82 Horizontal displacements model 3x2 sample A (left) and B (right)

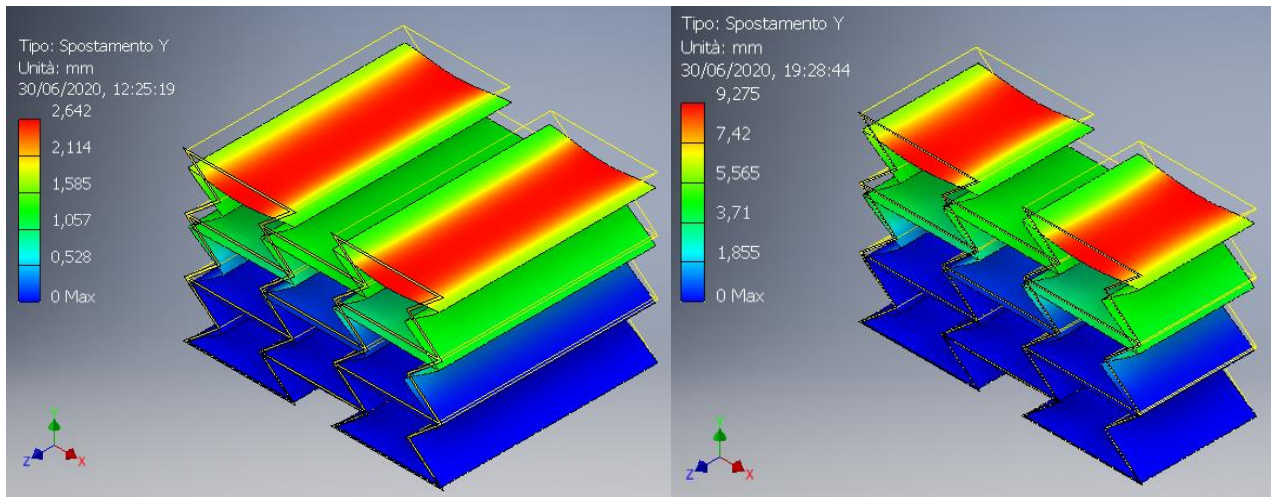


Figure 83 Vertical displacements model 3x2 sample A (left) and B (right)

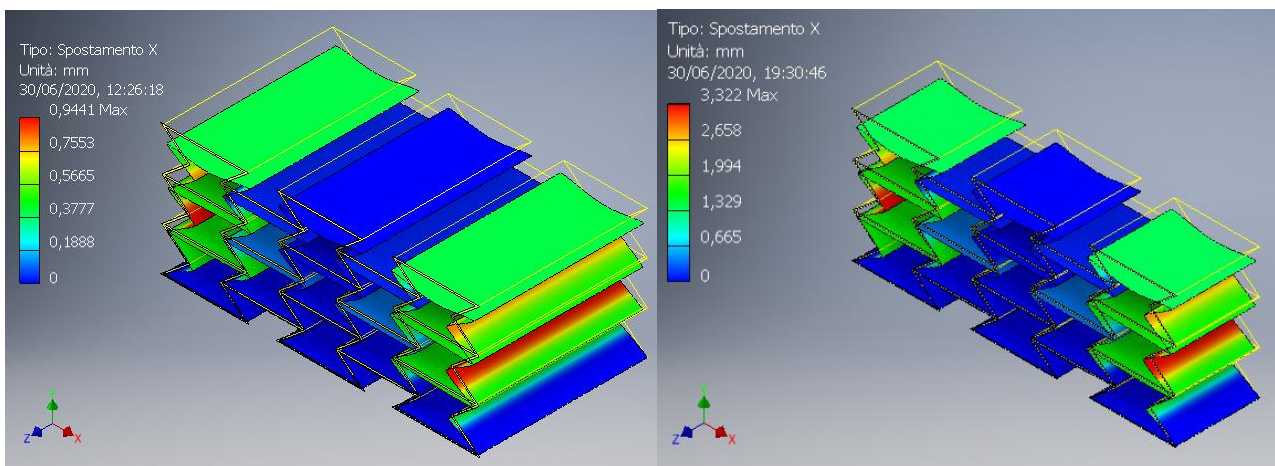


Figure 84 Horizontal displacements model 3x3 sample A (left) and B (right)

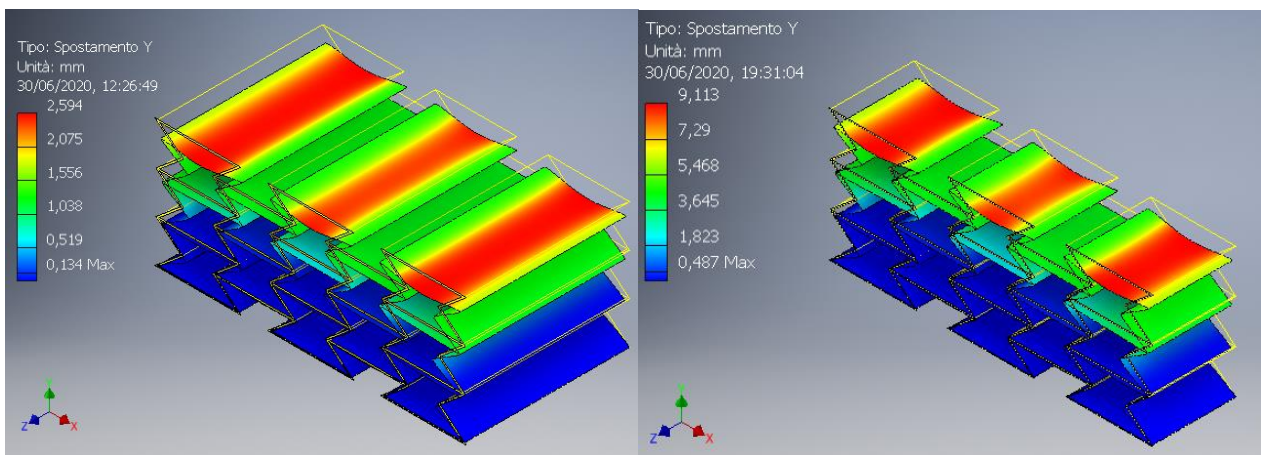


Figure 85 Vertical displacements model 3x3 sample A (left) and B (right)

By comparing the results it's shown that the two samples have the same behavior in every model. For both samples the horizontal displacement is higher in the shorter re-entrant part of the unit cell and the vertical one is higher in the center of each unit cell.

It's possible to make an evaluation by taking into account the increasing of unit cells per row and per column. Here are the two respective graphs that describe this behavior (since the Poisson's ratio are very similar it's

used one graph for both samples).

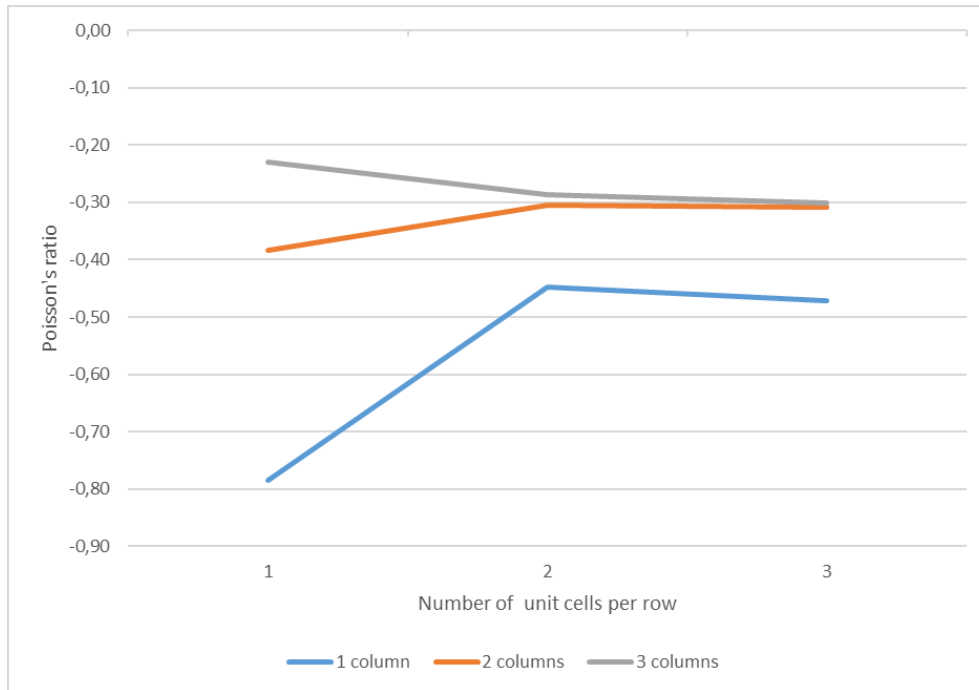


Figure 86 Dependence between Poisson's ratio and number of columns

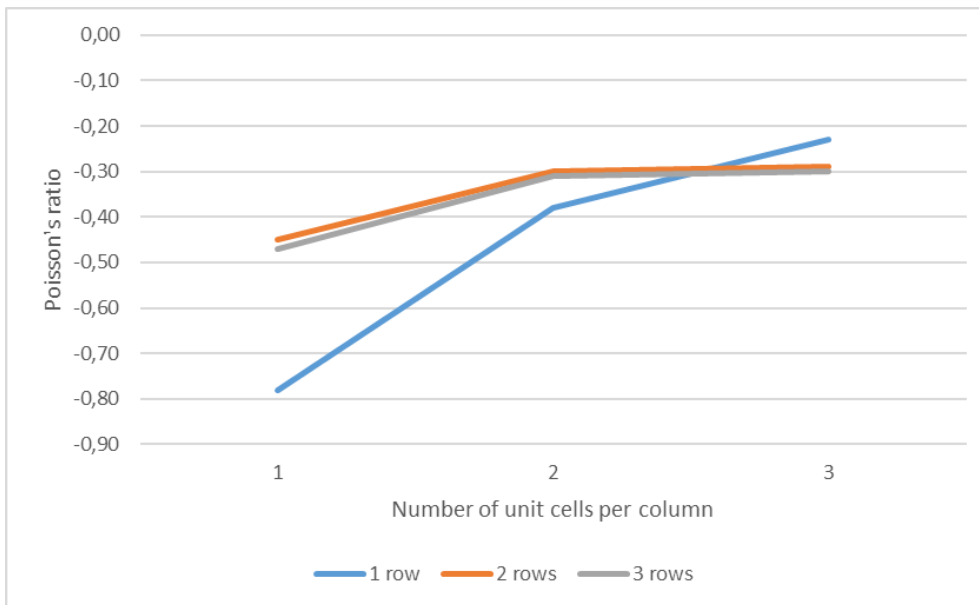


Figure 87 Dependence between Poisson's ratio and number of rows

By analyzing the graphs it's possible to notice that by adding rows or columns generally the Poisson's ratio tends to be lower, so the structure gets stiffer. The only difference is made in the case of adding rows to the three column model. In this case is noticeable that the Poisson's ratio tends to get higher. This difference is given mostly because of the model 1x3 in which the Poisson's ratio is very high (0,23): in fact in models 2x3 and 3x3 the Poisson's ratio is similar. An assumption that could be made is that the 1x3 model is a large structure with low height, therefore is the most stable and stiff model.

By analyzing in details the table it's possible to notice that by leaving the same number of unit cells per row and increasing the columns (having a larger structure), the horizontal displacement tends to increase and the deformation occurs in the outer parts of the structures: in fact in the 1x3, 2x3 and 3x3 models the central

unit cells have displacement close to zero. On the other hand for the vertical displacement there's just a small decrease when columns are added.

By adding layers of unit cells and getting a higher structure the horizontal displacement tends to grow. In this case the displacement is almost the same in each unit cell of each layer. On the other hand the vertical displacement gets higher when layers are added, but it's higher on the top layer and gets lower by going to the bottom layer.

To better understand the auxetic behavior, in this analysis it was measured the Poisson's ratio of each model. To do so, it was defined a number of study points of which was measured both horizontal and vertical displacement. In the next figures are the study points: in green the ones for vertical displacement, in red for horizontal.

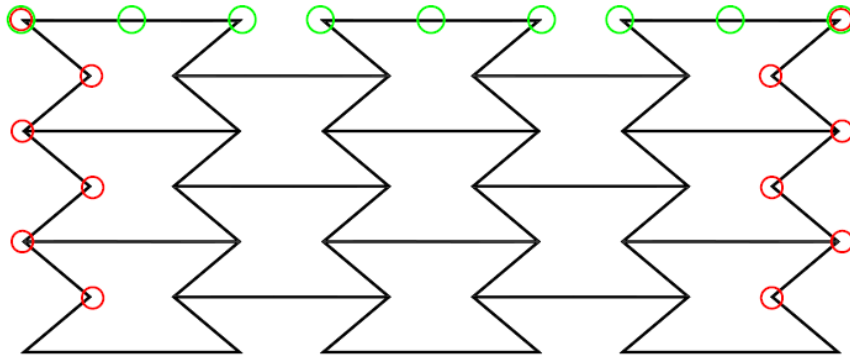


Figure 88 Study points for measure of Poisson's ratio

In the next tables are presented the observed measures, the calculated displacements and the calculated Poisson's ratio. For L_1 is intended the shorter horizontal length of the structure, L_2 is the longer horizontal length, L_z is the height of the structure, ΔL_x is the horizontal average deformation, ϵ_x is the horizontal strain, ΔL_z is the vertical average deformation, ϵ_z is the vertical strain, ν is the Poisson's ratio.

Model/Measures	L_1/L_2 (x)	L_z	ΔL_x	ϵ_x	ΔL_z	ϵ_z	ν
1x1	8,20	10,56	0,54	0,07	0,89	0,08	-0,78
1x2	35,45	10,56	0,99	0,03	0,77	0,07	-0,38
1x3	62,70	10,56	0,91	0,01	0,67	0,06	-0,23
2x1	8,20	20,72	0,56	0,03	1,57	0,08	-0,45
	20,30		0,01				
2x2	35,45	20,72	1,03	0,02	1,46	0,07	-0,30
	47,55		0,66				
2x3	62,70	20,72	1,43	0,02	1,38	0,07	-0,29
	74,81		1,14				
3x1	8,20	30,88	0,57	0,03	2,27	0,07	-0,47
	20,30		0,00				
3x2	35,45	30,88	1,05	0,02	2,14	0,07	-0,31
	47,55		0,63				
3x3	62,70	30,88	1,51	0,02	2,05	0,07	-0,30
	74,81		1,19				

Figure 89 Measures of Poisson's ratio of sample A

Model/Measures	$L_1/L_2 (x)$	L_z	ΔL_x	ϵ_x	ΔL_z	ϵ_z	ν
1x1	16,39	21,12	1,90	0,12	3,13	0,15	-0,78
1x2	72,61	21,12	2,87	0,04	2,70	0,13	-0,31
1x3	128,84	21,12	3,19	0,02	2,34	0,11	-0,22
2x1	16,39	41,84	1,95	0,06	5,52	0,13	-0,45
	40,22		0,01				
2x2	72,61	41,84	3,60	0,04	5,11	0,12	-0,29
	97,31		2,01				
2x3	128,84	41,84	5,00	0,03	4,79	0,11	-0,29
	153,53		4,15				
3x1	16,39	62,56	1,97	0,06	7,89	0,13	-0,48
	40,22		0,01				
3x2	72,61	62,56	3,68	0,04	7,48	0,12	-0,30
	97,31		1,98				
3x3	128,84	62,56	5,27	0,03	7,16	0,11	-0,29
	153,53		3,83				

Figure 90 Measures of Poisson's ratio of sample B

The most important evaluation that comes from these results is that for all the models the Poisson's ratio is negative so the auxetic behavior is proved. Additionally is visible that the Poisson's ratio is very similar between the two samples. This is reasonable because the two samples have the same geometry e proportions, and Poisson's ratio depends on ϵ_x and ϵ_z which are dimensionless characteristics. As seen before at an increasing of unit cells per row or column the deformations are increasing as well, but on the other hand the Poisson's ratio is decreasing. In conclusion it's visible that even if the applied load on sample B models (0,004 MPa) is five times lower than the one applied on sample A (0,02 MPa), the strains in case B are higher. Moreover the deformations in case B are 3-4 times higher than the ones in case A, so they are more visible to the naked eye. For this reason the sample B unit cell is chosen as the one to be used for the laboratory test.

2.4 Models for laboratory tests

The final model chosen to be printed was sample B. The measures of the model that would be printed were the same of sample B, but to have better results on the laboratory test it was decided to analyze two more models that will be printed. The only difference from the original sample was the thickness of the walls. It was decided to proceed with 0,4 (original sample), 0,8 and 1,2 millimeters of thickness for the walls. The measures were decided depending on the 3D printer nozzle diameter which was 0,4 millimeters.

Due to some technical problems related to the first 3D printer, it was decided to use a different printer. Therefore the material used changed too: from a ABS plastic to a PLA (Polylactic Acid) base material, which is a biodegradable (under the correct conditions) thermoplastic derived from renewable resources such as corn starch or sugarcane. For this reason it was done a new analysis for the original sample B too.

For convenience the three samples will be called "B1" for the 0,4 mm thickness, "B2" for the 0,8 mm thickness and "B3" for the 1,2 mm thickness. For the analyses it was decided to use a different load depending on the safety factor. For sample B1 it was used an applied load of 0,01 MPa, for sample B2 a load of 0,04 MPa and for sample B3 a load of 0,09 MPa. In the next figures are shown the mechanical properties of the new material, the results for horizontal and vertical displacement and a table with the calculated Poisson's ratio of the three samples.

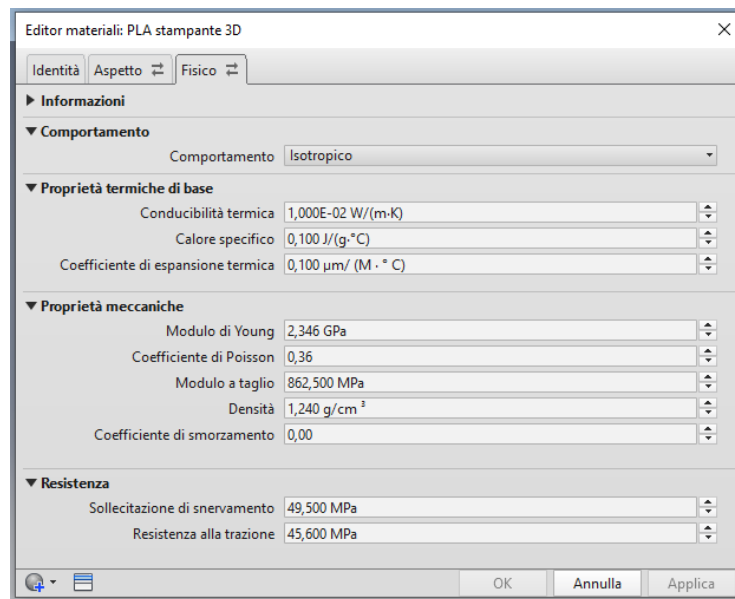


Figure 91 Characteristics of the PLA base material used in the software analysis

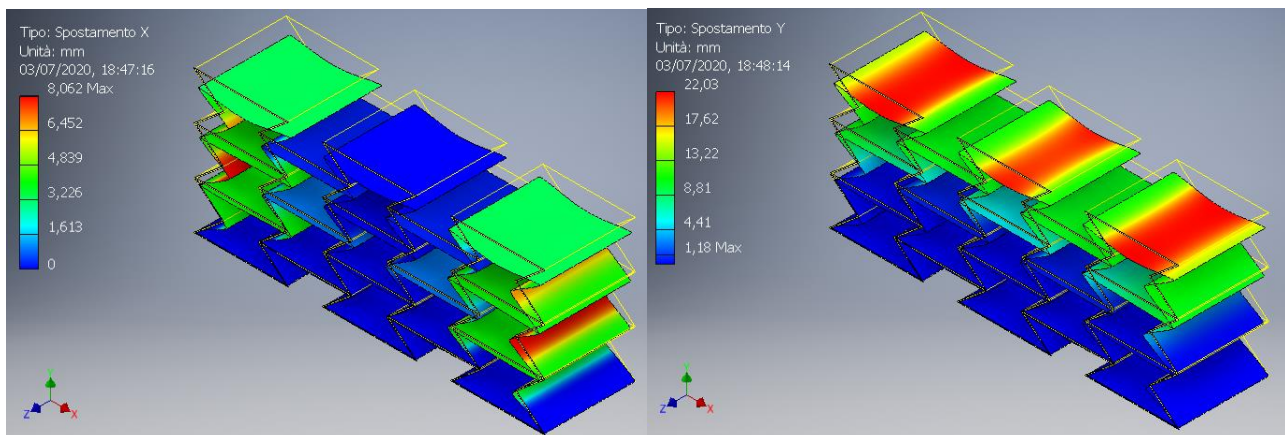


Figure 92 Horizontal (left) and vertical (right) displacement of sample B1

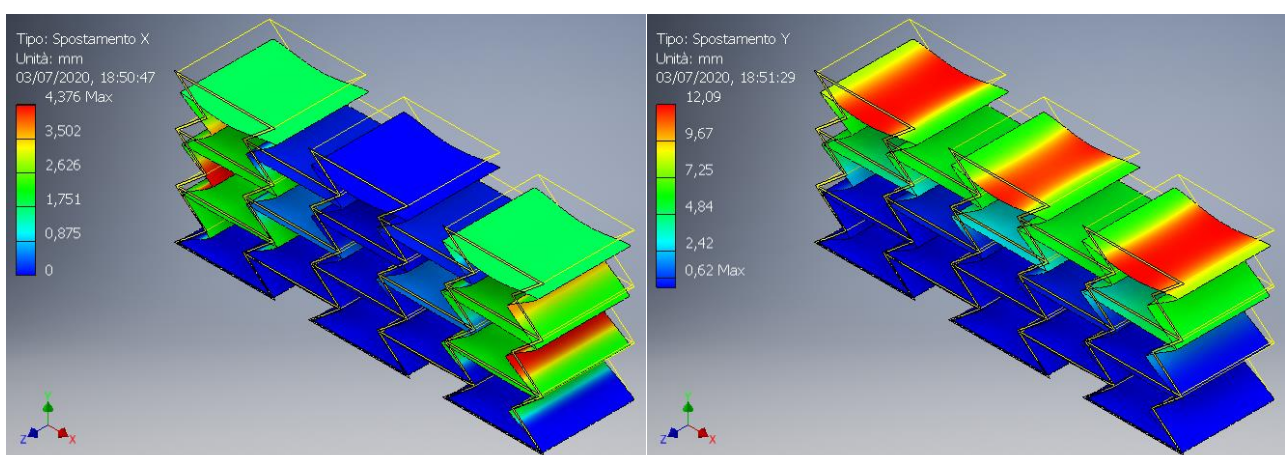


Figure 93 Horizontal (left) and vertical (right) displacement of sample B2

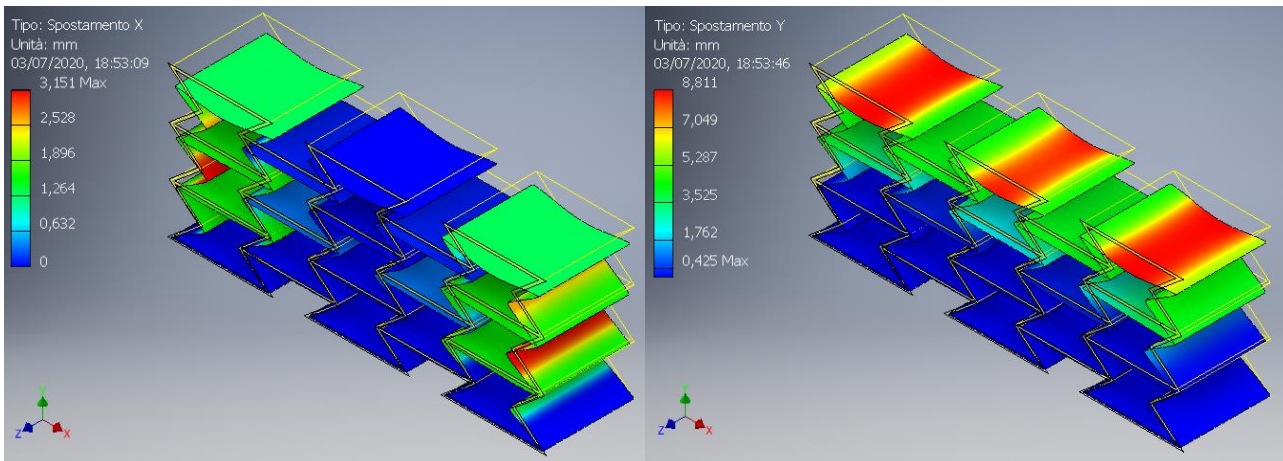


Figure 94 Horizontal (left) and vertical (right) displacement of sample B3

Sample/Measures	L_1/L_2 (x)	L_z	ΔL_x	ϵ_x	ΔL_z	ϵ_z	ν
B1	128,84	62,56	12,78	0,08	17,35	0,28	-0,29
	153,53		9,30				
B2	133,53	64,16	6,93	0,04	9,48	0,15	-0,28
	158,70		5,03				
B3	138,21	65,76	4,99	0,03	6,90	0,10	-0,28
	163,86		3,62				

Figure 95 Measure of Poisson's ratio of samples B1, B2 and B3

2.5 Conclusions

After the tests the three samples showed all the auxetic behavior. As seen before in the comparison between sample A and sample B, the Poisson's ratio is almost the same for the three samples, so the thickness of the wall cells is not relevant on the Poisson's ratio. Although the thickness of the cell walls is very important for the stiffness of the structure. By increasing the thickness, the applied load to reach the tensile strength is much higher and the deformations are decreasing.

3 3D PRINTING

3.1 Introduction

In this chapter is explained the process of 3D printing of the different models by analyzing the material used, the characteristics of the printer and its functioning for the realization of the structures. At the end there is a brief comment on the designed products.

3.2 MakerBot Replicator +

The 3D printer employed to fabricate auxetic models is the “MakerBot Replicator +”. In the next figure is shown the structure of the 3D printer and its main features.

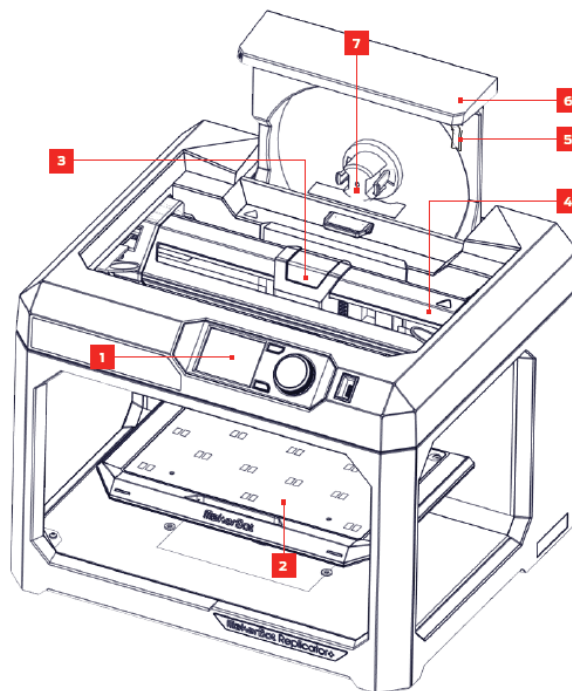


Figure 96 MakerBot Replicator + 3D printer; (1) Control panel, (2) Built plate, (3) Extruder assembly, (4) Gantry, (5) Filament guide tube, (6) Filament drawer, (7) Filament spindle

The MakerBot 3D printer makes three dimensional solid objects by melting a PLA filament. Before starting a print the filament spool has to be positioned in the filament drawer in the correct way. The filament spool has to be placed onto the filament spindle, then the free end of the filament has to be inserted in the filament guide and pushed till the end of it. When it's done the drawer can be closed and the printer can be used.

The PLA filament melting point is at 145-160 degrees and its mechanical characteristics are presented in the next figure:

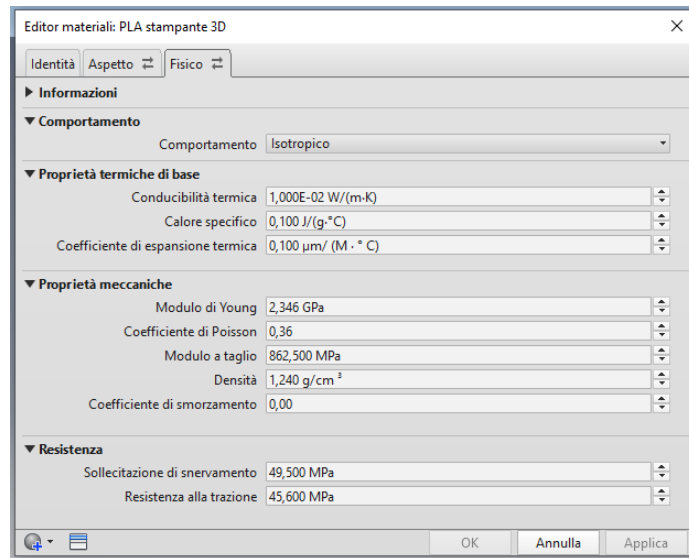


Figure 97 PLA MakeBot filament mechanical characteristics

Here are shown the printer characteristics:

PRINTING

Print Technology:	Fused deposition modeling
Build Volume:	29.5 L x 19.5 W x 16 H cm [11.6 L x 7.5 W x 6.3 H in]
Layer Resolution:	100-300 microns
Filament:	1.75 mm [0.069 in]
MakerBot PLA Filament	
Nozzle Diameter:	0.4 mm [0.015 in]
Print File Type:	.makerbot
Grip Build Surface:	Polycarbonate film

SOFTWARE

Software Bundle:	MakerBot Print
3D Model File Types:	Windows: .stl, .obj, .thing, .sldprt, .sldasm, .ipt, .iam, .iges, .igs, .step, .stp, CATPart, .CATProduct, .prt, .par, .asm, .wrl, .x_t, .x_b Mac: .stl, .makerbot
Supported OS:	Windows (7+), MacOSX (10.9, 10.10, 10.11)

PHYSICAL DIMENSIONS

Printer:	52.8 L x 44.1 W x 41.0 H cm [20.8 L x 17.4 W x 16.2 H in]
Shipping Box:	61.6 X 52.4 X 57.9 [24.3 X 20.7 X 22.9]
Printer Weight:	18.3 kg [40.4 lb.]
Shipping Weight:	22.8 kg [50.2 lb.]

TEMPERATURE:

Ambient Operating	
Temperature:	15-26°C [60-78°F]
Storage Temperature:	0-38°C [32-100°F]

Figure 98 MakerBot Replicator + characteristics

3.3 Printing process

The first step to make a 3D print is to create a design file containing the model structure. The CAD file is converted to a “.stl” and processed through the MakerBot Print application, which is used to manage all the printer settings and to convert the “.stl” file into a “.makerbot” file. Then the file is transferred to the printer through a USB flash drive. By accessing the control panel the file is managed and set to print.

After set to print all the operations are done by the printer. Firstly it starts to preheat the extruder at 180

degrees in order to melt the PLA filament used for the print. Then it levels the built plate, which has to be clean from any debris, on which the structure will be set. Therefore the printer starts to melt the PLA filament and extrude it from the nozzle onto the built plate in thin lines, to built the structure layer by layer. This method of 3D printing is called fused deposition modeling (FDM).

The first layers that are printed are just a raft which is a base that supports the structure and ensures that everything adheres well to the built plate. When the raft is finished the structure starts to be printed. When the print is done, the built plate has to be removed. By simply bending the flexible built plate the structure can be detached. Finally the raft can be peeled off and the print is finalized.

The time taken to print the different models was of 5 hours for sample B1, 7 hours for the sample B2 and 9 hours for sample B3. Here are some pictures of the different samples created with the 3D printer:

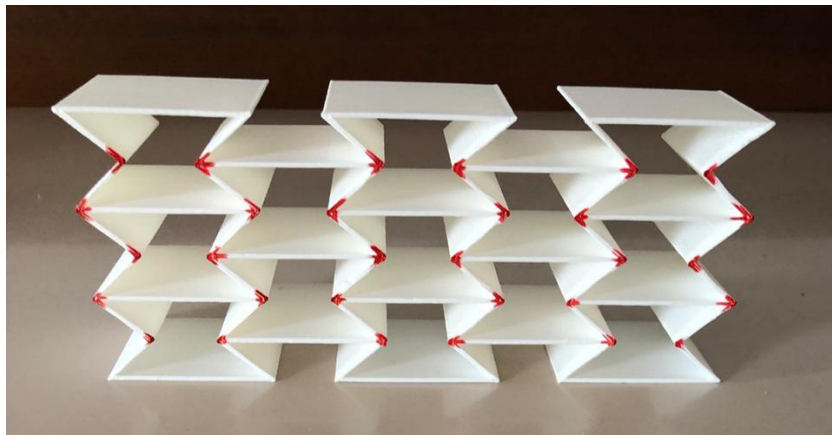


Figure 99 Sample B3 front view

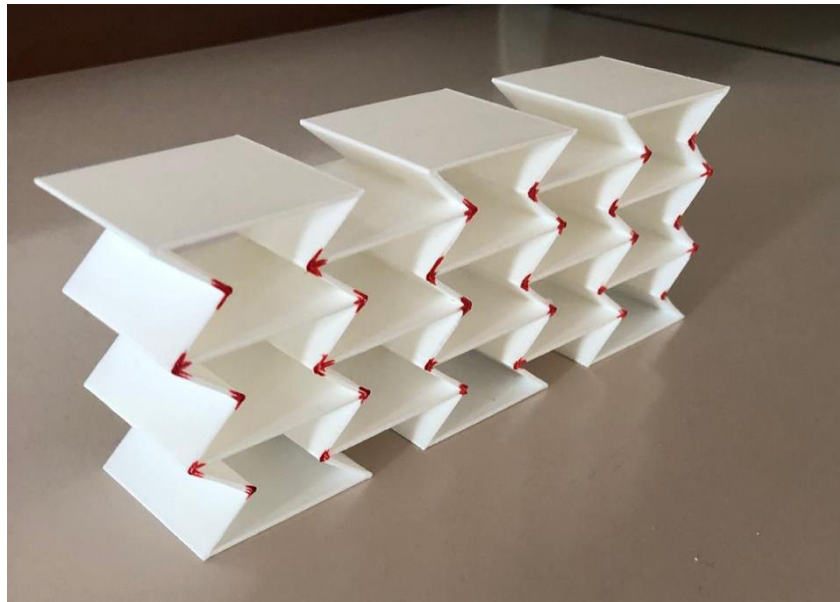


Figure 100 Sample B2 side view



Figure 101 Sample B3 front/side view

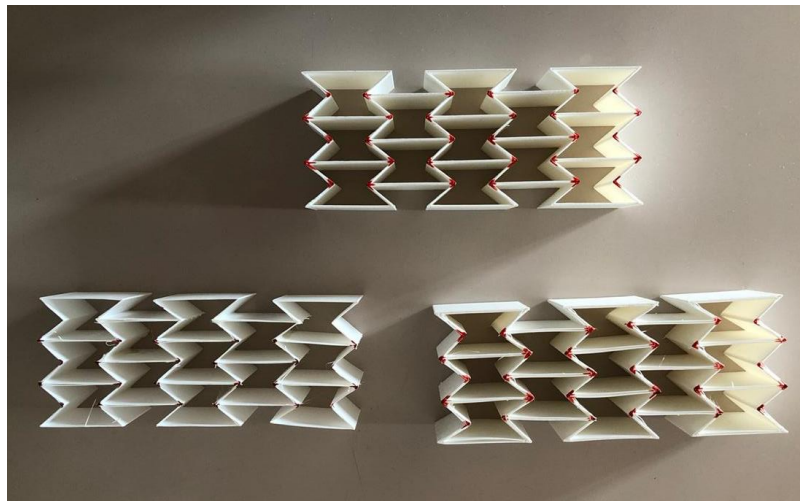


Figure 102 Samples B1, B2 and B3 top view

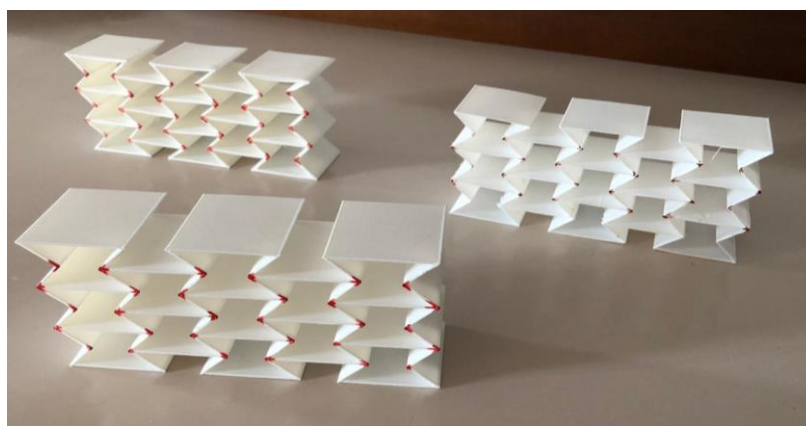


Figure 103 Samples B1, B2 and B3 front/side view

3.4 Conclusions

At the end it was possible to print all the samples needed for the laboratory tests, even the one designed by using the minimum layer thickness of 0,4 millimeters. In some parts of the samples there were some small mistakes done by printer like the one visible on the top right corner of sample B3. However, as a first approach to 3D printing, the result was positive.

4 LABORATORY TEST

4.1 Introduction

In this chapter is described the laboratory test that was done on the three samples previously described, to make an evaluation between the software analysis and the real results. Firstly there's a brief introduction to all the equipment and the software used for the test. Then it's described the laboratory set up and all the different steps of the test itself. Finally are displayed the results of the experiment and it's made a comparison between the previous software analysis results and the ones from the test.

4.2 Equipment and software

The laboratory experiment that was done to determine the Poisson's ratio of the three printed samples (B1, B2 and B3) was divided in two different parts: the first one was the actual compression test that was done on the three different sample; the second one was a video software analysis through which was drawn the Poisson's ratio of each structure.

For all the experiment were used a hydraulic press, a digital camera with a tripod and the software "Tracker", which are described in the next paragraphs.

4.2.1 Laboratory equipment

The actual test was a compression test done with a hydraulic press like the one shown in the picture. On the top of the machine there is a fixed beam that create a contrast to the load which is applied by the piston. At the lower part of the top is inserted a plate that is used to widen the contrast surface. The sample is positioned on a plate on the top of the lower part (black plate on the picture), which then, it's pushed by the piston towards the top. In this way when the sample will reach the top plate there would be a compression of the sample itself. The distance between the two plates can be regulated to ease the maneuver.

The hydraulic press that was used works on control of deformation. The minimum reachable speed of deformation is 0,02 mm/min. The maximum strength that can be applied is of 50KN and the minimum strength readable is 5N. To the machine are connected a transducer to read the vertical displacement and to a laptop which reads step by step the displacement and the applied load.

All the test was recorded with a "Canon 800D" positioned on a tripod. The main features are a 24.2-megapixel CMOS sensor with Dual Pixel CMOS AF, high-speed Continuous Shooting at up to 6.0 fps, 1080p at 60/50 fps video recording capability.



Figure 104 Hydraulic press

4.2.2 Tracker video analysis software

The analysis of the experiment was done by making a video of the samples during the compression test. Then it was used a software called “Tracker”, with which was possible to do a video analysis of the deformation process. The software permits to do an object tracking and to calculate the position, velocity and acceleration of the studied object.

To do so there are a few steps to follow to have a suitable outcome. Firstly the video is uploaded on the software. On the software interface, as shown in the following picture, it is possible to visualize every frame of the video. To start the analysis it has to be chosen which part of the video has to be analyzed, therefore is chosen the starting frame and the ending frame of the analysis. Then it has to be identified a measured object, so the software can measure all the figures in the video by setting the length in pixels of that object as a reference. In this case it was used a bolt of 40,6 millimeters of length (blue line). The next step is to set a cartesian system of coordinates (purple crossing lines) and to identify the points which need to be analyzed. For our case the analyzed points were the same chosen in the software analysis and they were highlighted with a red marker.

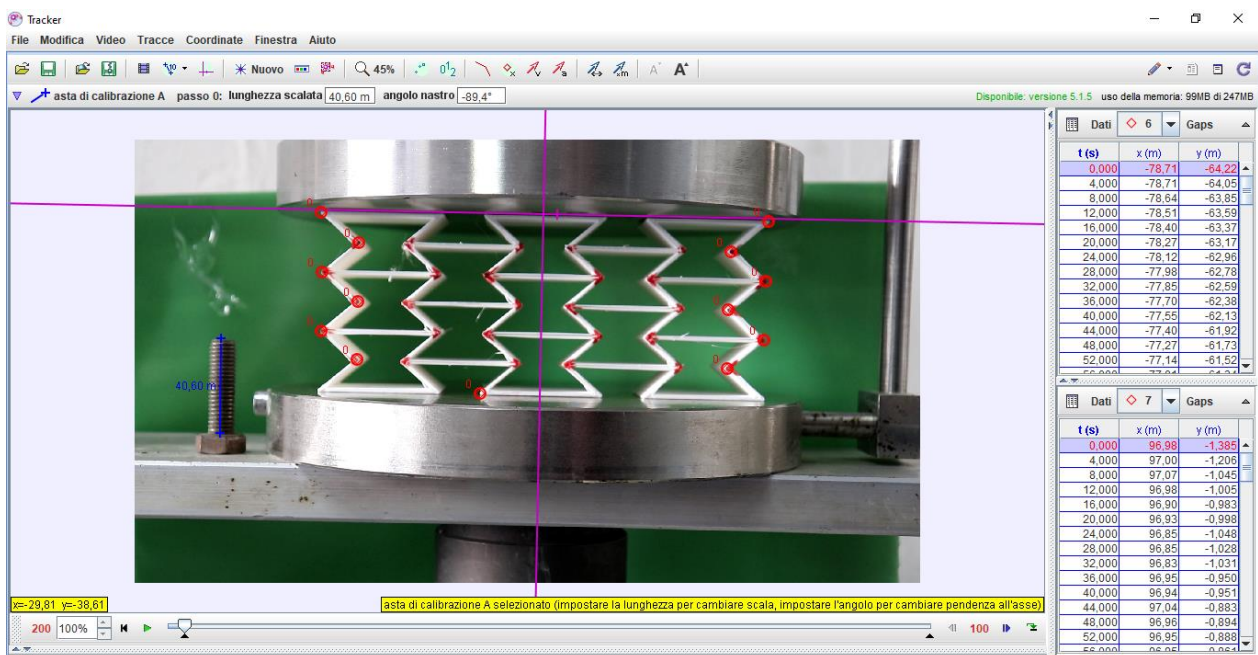


Figure 105 Tracker video analysis software interface

At this point the analysis can be done in two different ways: manually and automatically. These terms address to the way the points selected points will be identified in the following frames. In the starting frame, as shown in the picture, all the points are identified; till the last frame the points will move, so they have to be identified various times to understand which is their path. This action can be done manually or automatically by the software (automatically in this case). Moreover this analysis can be done for each frame from the first to the last one or it can be chosen a different spacing between the frames analyzed. The frame length of the videos recorded for each test was about 10'000 frames. Since the deformation of the structure was very slow it was decided a 1% frame rate for the analysis, so the individuation of the points was done every 100 frames.

At the end of the analysis all the results are displayed (on the right in the picture) and it's possible to visualize the Cartesian coordinates of each point for each analyzed frame. All the results can be manipulated in the software or can be drawn and used on other platforms. In this case they were drawn and copied on Excel for the final calculations.

4.3 Laboratory set up

Before the test could start, all the instruments had to be set up. The upper and bottom plates of the hydraulic press where maneuvered to be at a distance of around 75 millimeters (10 mm higher than the sample's height). The tripod was placed in front of the press and was regulated so that the camera would be at the same height of the samples. The camera zoom and focus were adjusted to have the best resolution of the analyzed samples. To have a better contrast of the later analyzed points (highlighted in red), a green paper was placed behind the samples. Finally it was adjusted the transducer in order to gather the vertical displacement.

The same adjustments were made for each sample and the compression tests were completed. For every sample it was decided to have a deformation speed of 2,5 mm/min. For sample B1 and B2 the test was stopped after a vertical displacement of around 16/17 millimeters. For sample B3 the test was stopped earlier, around 12,5 mm, because it was exhibiting larger displacements.

4.4 Laboratory and software results compared

For each sample the starting configuration and the deformation speed were the same. However the first two samples, B1 and B2, had almost the same mechanism of deformation, while the one of sample B3 was very different. In the next figures are shown the starting configuration and the different ending configurations.



Figure 106 Starting configuration (same for all three samples)

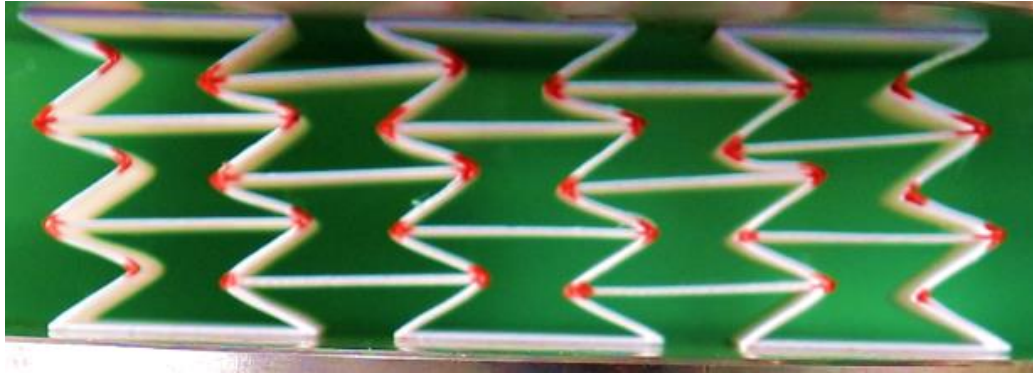


Figure 107 Final configuration of sample B1



Figure 108 Final configuration of sample B2

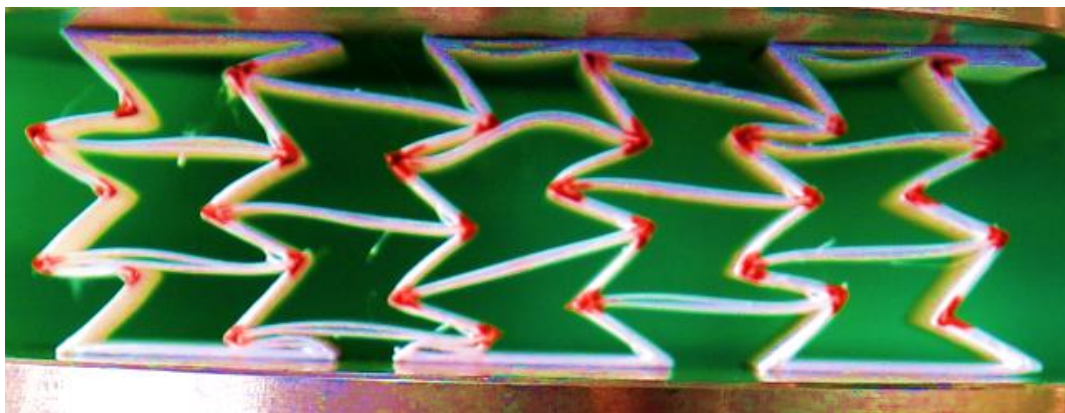


Figure 109 Final configuration of sample B3

For all the samples it was done a video analysis and, by considering the same analysis point used in the “Software analysis” chapter, all the displacements were calculated. By doing this it was possible to calculate the displacements and the Poisson’s ratio of each sample. In the next figure are presented the results.

Sample/Measures	L_1/L_2 (x)	L_z	ΔL_x	ϵ_x	ΔL_z	ϵ_z	ν
B1	128,84	62,56	7,92	0,05	16,31	0,26	-0,19
	153,53		5,54				
B2	133,53	64,16	8,64	0,05	16,57	0,26	-0,20
	158,70		5,84				
B3	138,21	65,76	8,38	0,05	12,52	0,19	-0,27
	163,86		6,71				

Figure 110 Calculated Poisson’s ratio of the three samples used in the laboratory test

As visible from the pictures and from the calculations, all three samples present an auxetic behavior. For the first two samples the deformation behavior is almost identical. Differently from the ideal behavior, in both cases the deformation is nonsymmetrical. The horizontal ligaments don't tend to deform and the other ones tend to deform all in the same way.

For sample B3 the behavior is auxetic but is very different from the expected one. The deformation is nonsymmetrical and all the ligaments tend to deform in almost a random way. The horizontal ones are bending and even opening up. For the other ones, some stay stiff and have almost zero deformation, while others deform completely. This big difference is probably due to lack of stiffness in the nodes and to lack of material in some of the ligaments.

By analyzing the samples before the test was possible to identify some ligaments where the material was not well attached or in some cases there were missing layers. It's possible to notice from the image that the ligaments which are having a bending deformation are exactly those where some layers are missing; while the other ones are having an expected deformation behavior. It's possible to make the same reasoning for those ligaments which deform by going down to complete horizontal position. Probably this behavior is due to lack of stiffness in the nodes, which allows this deformation behavior.

In the next tables are reported the results that were calculated in the chapter "Software analysis" and a comparison between the laboratory ones and them.

Sample/Measures	L_1/L_2 (x)	L_z	ΔL_x	ϵ_x	ΔL_z	ϵ_z	ν
B1	128,84	62,56	12,78	0,08	17,35	0,28	-0,29
	153,53		9,30				
B2	133,53	64,16	6,93	0,04	9,48	0,15	-0,28
	158,70		5,03				
B3	138,21	65,76	4,99	0,03	6,90	0,10	-0,28
	163,86		3,62				

Figure 111 Calculated Poisson's ratio of the three samples used in software analysis

Sample	Laboratory		Software analysis	
	Applied load (N)	Vertical displacement	Applied load (N)	Vertical displacement
B1	24	16,31	48	17,35
B2	90	16,57	202	9,48
B3	628	12,52	475	6,9

Figure 112 Comparison between laboratory and software analysis results

As visible from the tables, the Poisson's ratios calculated in laboratory are quite different from the ones expected from the software analysis. By taking into account the horizontal deformations it's visible that the displacements analyzed in laboratory are higher than the one expected, however the behavior it's the same: the displacements of the shorter sides of the samples are the highest one. By analyzing the horizontal strains it's visible that they make a big difference in the final result of the Poisson's ratio for sample B1 and B3: in fact the horizontal strain is doubled for sample B1, while just half for sample B3. Instead the bigger difference in Poisson's ratio for sample B2 is made by the vertical strains. The difference between laboratory and software strains is almost double.

By analyzing the applied load and the vertical displacements is visible that in the laboratory tests the structures were much more flexible. In fact for sample B1 the vertical displacement is almost the same with

half of the expected applied load; for sample B2 there's a almost doubled displacement with less than 50% of the expected load; while for sample B3 the load was higher than the one used in the software (theoretically over the tensile strength), but the deformation was still much higher.

4.5 Conclusions

After analyzing the differences between laboratory and software results is clear that the main problem is due to the final results of the 3D printing. All the samples have the same geometry, but different thicknesses of the walls. Theoretically they should have all the same deformation behavior but with different results for applied load/displacements. For the first two samples the deformation behavior is the same and it's very similar to the one expected, even if the Poisson's ratios are not the same and the deformation was not completely symmetrical. However there's a big difference between a software analysis and a real one because of two main reasons: the material in the software is just assign to the structure without analyzing the way the structure is composed; by using the 3D printing technique the material is melted and the structure is made by layers, therefore the material characteristics could change. Secondly there were some "mistakes" in the 3D printing process that led to some imperfections; these "mistakes" could be related to the fact that the wall thickness was very close to the minimum layer thickness.

For sample B3, even if the Poisson's ratio was very close to the one expected, there were more visible mistakes. The deformation was not symmetrical and for some parts of the structure completely different from the expected one. In this case, by analyzing the sample, it's clear that the main problem was due to the 3D printing process: in fact many ligaments were not well connected and some joints were not stiff enough.

5 Conclusions

From the analysis made in this thesis it appears the extent of the studies carried about the auxetic materials, even if their discover is not so far in time. The first chapter starts by defining these materials through the Poisson's ratio and by showing their origin. The first notable fact that comes to light is that there are not many natural materials which show this kind of behavior. However, since is a very interesting matter, many studies have been done to understand how to make artificial auxetic structure and it's shown that many are found. In this thesis it's analyzed one of these methods, which is 3D printing.

Moreover it's possible to see how auxetic structures are classified and which are the different properties that these materials share with the regular ones. Therefore the different properties are analyzed and it's shown how auxetic materials exceed in many ways regular materials. The main characteristics which are highlighted are their high resistance and their variable permeability due to their behavior. In fact in the end of the chapter are shown many of the current fields of application of these materials, and most of them have their usage based on these characteristics.

In the second part are examined some of the potential geometries that could lead us to interpret in a better way this unique deformation behavior. It was possible to see that the first geometries which were analyzed didn't give very good results. They were not symmetrical, therefore the deformation was not symmetrical; in addition the deformation of the structures was moving in one direction, so the auxetic behavior was not easily visible. After these models, other geometries were analyzed; all of them had a symmetrical deformation but some of them were very stiff, so the auxetic behavior was visible, but there were not large displacements. At the end it was chosen the re-entrant honeycomb geometry because of its higher deformation and its ease of showing a symmetrical auxetic deformation.

After that it was made an analysis to understand how the cell size and wall thickness were related to the deformation behavior. It was understood that by increasing the cell size, the deformation increases too and the applied load to reach the tensile strength of the structure is much lower (by 3-4 times). On the other hand if both cell size and wall thickness are doubled, the results are very similar to the original structure. The next step to understand the auxetic behavior was to realize how the unit cell packing affects the deformation behavior. There were found important results for both horizontal and vertical deformation. For the horizontal deformation, when the model would get larger, the deformation will tend to happened in the outer unit cells; while when the model would get higher, the deformation will stay almost the same for every unit cell layer. For the vertical deformation, when the model gets larger there are not significant differences because the deformation tends to be the same for all the unit cells; instead when the model would get higher, the deformation will get higher and it will concentrate on the top unit cells. Finally by using these results it was possible to choose the best models for the laboratory test.

In the last part all the assumptions and predicted results were tested with the laboratory experiment. The most important result was to understand if the 3D printing would be a good method to make auxetic structures. At the end, by analyzing all the samples it was understandable that with the 3D printing method it's possible to make structures with auxetic behavior. However the results that were reported were not identical to the one expected by the software analysis. By analyzing the three samples, the first two (samples B1 and B2) had almost the same behavior; the deformation mechanism was similar to the one expected, but with some differences: the deformation was not symmetrical, the correlation between displacements and applied load was very different and, therefore, the Poisson's ratio was not the one expected. The third sample (sample B3) had an auxetic deformation, but it was completely different from the one expected: the deformation was not symmetrical, many of the ligaments which should stay horizontal started bending and many of the hinges were not stiff enough and permitted rotations. The main characteristics that led to this difference in behavior could be identified in the printing method, which provided some flaws in the

ligaments, and the material characteristics, which, most probably, were different from the software model, because of the production method, which consists in melting the material and composing the structure with different layers.

As said, one of the flaws was the absence of material between some of the structure's layers. This could be due to some errors of the 3D printer or probably to the layer's pattern design. The third sample had a wall thickness of 1,2 millimeters and the minimum thickness of the walls was 0,4 millimeters because of the printer nozzle. The machine works by melting the material and positioning it by doing a path which firstly covers one thickness (0,4 millimeters) of the whole structure, and then it runs the model again for the second and third thickness. Probably, since it's a complex structure, the time that passes from the first pass to the second is enough to cool down the first layer; therefore when the second and third layer are added there is not perfect adhesion between the horizontal layers. Understanding if there is a connection between the layer's pattern design and the final structure, could be an interesting topic to analyze in future works, to better understand the 3D printing process.

In conclusion, when reached a well 3D printed structure, it would be very interesting to make a comparison between two identical models: one made by 3D printing and one by using a mold. In this way it could be achieved a better knowledge of how the 3D printing meting method affects the final material characteristics.

6 APPENDIX

In this appendix is described the functioning of the software Autodesk Inventor Nastran, used for the structural analysis of the auxetic models described in the chapter “Software analysis”.

Autodesk Inventor Nastran software is a general purpose finite element analysis (FEA) tool embedded in Autodesk Inventor. It is powered by the Autodesk Nastran solver, and offers simulation capabilities that span across multiple analysis types, such as linear and nonlinear stress, dynamics, and heat transfer.

6.1 FEA

Finite element analysis (FEA) is a computerized method for predicting how a structure responds to real-world forces physical effects, such as forces, vibrations and heat. FEA works by breaking down a real structure into a large number (from thousands to hundreds of thousands) of finite elements, such as little cubes. Mathematical equations help forecast the behavior of each element. Then a computer adds up all the individual behaviors to predict the actual structure’s behavior.

This section summarizes the assumptions needed when defining an FEA analysis. These include the analysis geometry, materials, meshing, loads, constraints and choosing the appropriate physics for the situation. The next assumptions are the one that are used in the software analysis:

- Modelling idealization: shell models
- Mesh element types: triangular shell elements (average mesh element dimension equal to 0,1 mm)
- Material: PLA edited material with characteristics described in fig. 89
- Material properties: linear and isotropic
- Geometry: imported from CAD model and extruded into a 3D model

The boundary conditions are described in the “Software analysis” chapter as for the analysis type.

6.2 Linear and nonlinear analysis

The defining line between linear and nonlinear is gray at best. Traditionally, in finite element analysis, there has been a set of criteria that determines if nonlinear effects are important for the analysis of a particular model. If any of these criteria are present, a nonlinear analysis is needed to simulate an accurate real-world behavior. While this criteria continue to apply, new capability such as linear contact and new materials such as composites further blur the line on when it is necessary to carry out a full nonlinear analysis.

In Linear static analysis we assume the following:

- Displacements and rotations are small
- Supports do not settle
- Materials remains linear, and stress is directly proportional to strain
- Loads (magnitude, orientation, distribution) remain constant as the structure deforms

Most problems can usually be considered linear because they are loaded in their linear elastic, small deflection range. For these types of problems, the slight nonlinearity does not affect the results and the difference between a linear and nonlinear solution is negligible.

While many practical problems can be solved using linear analysis, some or all of its inherent assumptions may not be valid:

- Displacements and rotations may become large enough that equilibrium equations must be written for the deformed rather than the original configuration. Large rotations cause pressure loads to change in direction, and also to change in magnitude if there is a change in area to which they are applied
- Elastic materials may become plastic, or the material may not have a linear stress-strain relation at any stress level
- Part of the structure may lose stiffness because of buckling or material failure
- Adjacent parts may make or break contact with the contact area, changing as the loads change

Thus a Nonlinear effect can be broken down into three main categories:

- Geometric (large displacements)
- Material (plasticity, nonlinear stress-strain curves)
- Boundary condition (loads and constraints, contact interaction)

The corresponding FEA equations are as follows:

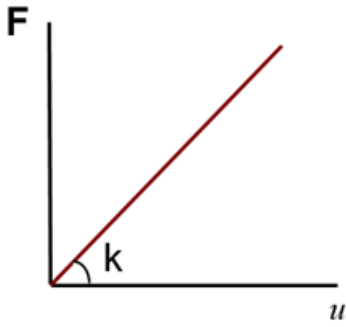
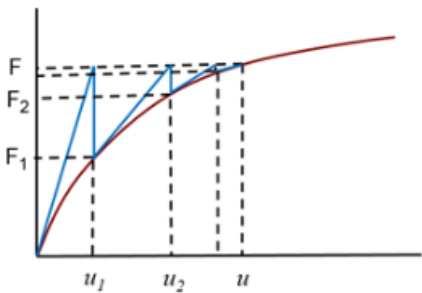
Linear Analysis	Nonlinear Analysis
$[K]\{U\} = \{F\}$ 	$[K(U)]\{\Delta U\} = \{\Delta F\}$  <p>The difference $(F - F_i)$ is called residual force.</p> <p>The process is repeated until $F = F_i$.</p>

Figure 113 Linear and Nonlinear analysis

Where K is the global target stiffness matrix, U is the global displacement vector, ΔU is the global incremental displacement vector, F is the global load factor, ΔF is the global incremental load factor.

6.2.1 Geometric nonlinearity

The geometric nonlinearity becomes a concern when the part(s) deform in such a way that the small strain assumptions are no longer valid. The large displacements effects are a collection of different nonlinear properties, such as large deflections, stress stiffening/softening, snap-thru, buckling, large strain.

6.2.2 Material nonlinearity

There can be a significant difference between the linear and nonlinear material responses. The simplified model of stress-strain curves used in Autodesk Inventor Nastran are:

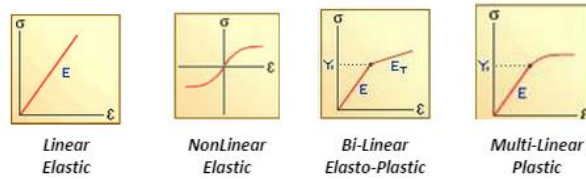


Figure 114 Simplified model of stress-strain curves

A linear model can provide valid data for many materials at low strains and for trend comparisons. A linear analysis can only predict the onset of yielding. Once the limits of the analysis are exceeded, correlation degrades with the complexity of the stress state.

A nonlinear plasticity analysis can only predict the onset of fracture. The nonlinear material effects can be important when you want to find out what happens past the initial yield of the material.

Alternatively, non-metal materials like rubber and plastic can show a highly nonlinear stress-strain curve even at low strain values. Therefore, getting a more accurate picture of the stiffness of the material through its strain range is important to accurately predicting the stiffness of the overall model.

Brittle materials such as cast iron have little inelastic deformation before failure, so a linear analysis approach for these types of materials is generally okay.

However, the majority of materials and even metals have some amount of ductility. This ductility allows hot-spots to locally yield thus reducing the stresses compared to what a linear analysis would predict.

6.2.3 Boundary condition nonlinearity

A model exhibits boundary nonlinearity when the loads, constraints, or load paths change throughout the solution. If the orientation, distribution, or magnitude of applied loads or the load path changes as loading is increased, a nonlinear model may be required. The most common boundary nonlinearities are contact and follower forces.

7 REFERENCES

- [1] Lakes, R. S. and Witt, R., "Making and characterizing negative Poisson's ratio materials", International Journal of Mechanical Engineering Education, 30, 50-58, Jan. (2002)
- [2] V. H. CARNEIRO, J. MEIRELES, H. PUGA, Auxetic Materials – A Review, (2013)
- [3] ROH J.H., GILLER C.B., MOTT P.H., ROLAND C.M., AIP Advances, 3 (2013), 042126
- [4] GREAVES G.N., GREER A.L., LAKES R.S., ROUXEL T., Nat. Mater., 10 (2011), 823
- [5] STREK T., MARUSZEWSKI B., NAROJCZYK J.W., WOJCIECHOWSKI K.W., J. Non-Cryst. Solids, 354 (2008), 4475
- [6] WOJCIECHOWSKI K.W., NOVIKOV V.V., Task Quarterly, 5 (2001), 5
- [7] GERCEK H., Int. J. Rock Mech. Min., 44 (2007), 1
- [8] GLIECK J., The New York Times, 14th April 1987
- [9] MILTON G.W., J. Mech. Phys. Solids, 40 (1992), 1105
- [10] EVANS K.E., NKANSAH M.A., HUTCHINSON I.J., ROGERS S.C., Nature, 353 (1991), 124
- [11] PRAWOTO Y., Comp. Mater. Sci., 58 (2012), 140
- [12] WOJCIECHOWSKI K.W., J. Phys. Soc. Jpn., 72 (2003), 1819
- [13] KOCER C., MCKENZIE D.R., BILEK M.M., Mater. Sci. Eng. A – Struct., 505 (2009), 111
- [14] MOTT P.H., ROLAND C.M., Phys. Scripta, 87 (2013), 055404
- [15] LAKES R.S., LEE T., BERSIE A., WANG Y.C., Nature, 410 (2001), 565
- [16] TOKMAKOVA S.P., Phys. Stat. Sol. B, 242 (2005), 721
- [17] NAROJCZYK J.W., WOJCIECHOWSKI K.W., Phys. Stat. Sol. B, 245 (2008), 606
- [18] BRANKA A.C., HEYES D.M., MACKOWIAK SZ., PIEPRZYK S., WOJCIECHOWSKI K.W., Phys. Stat. Sol. B, 249 (2012), 1373
- [19] KIMIKUZA H., OGATA S., SHIBUTANI Y., Mat. T. JIM, 46 (2005), 1161
- [20] NAROJCZYK J.W., WOJCIECHOWSKI K.W., J. Non- Cryst. Solids, 356 (2010), 2026
- [21] BRANKA A.C., HEYES D.M., MACKOWIAK SZ., PIEPRZYK S., WOJCIECHOWSKI K.W., Phys. Stat. Sol. B, 248 (2011), 96
- [22] BAUGHMAN R.H., SHACKLETTE J.M., ZAKHIDOV A.A., STAFSTRÖM S., Nature, 392 (1998), 362
- [23] TING T.C.T., CHEN T.Y., Q. J. Mech. Appl. Math., 58 (2005), 73
- [24] NORRIS A.N., J. Mech. Mater. Struct., 1 (2006), 793
- [25] ATTARD D., GRIMA J.N., Phys. Stat. Sol. B, 245 (2008), 2395
- [26] EVANS K.E., Membr Tech., 137 (2001), 9
- [27] VOIGT W., Annalen der Physik, 16 (1882), 273
- [28] LOVE A.E.H., A Treatise on the Mathematical Theory of Elasticity, Dover Publications, United States of America, 1944
- [29] KIMIZUKA H., KABURAKI H., KOGURE Y., Phys. Rev. Lett., 84 (2000), 5548
- [30] GRIMA J.N., EVANS K.E., J. Mater. Sci., 41 (2006), 3193
- [31] GRIMA J.N., GATT R., ALDERSON A., EVANS K.E., J. Mater. Chem., 15 (2005), 4003
- [32] VERONDA D.R., WESTMANN R.A., J. Biomech., 3 (1970), 111
- [33] LEES C., VINCENT J.F.V., HILLERTON J.E., Bio- Med. Mater. Eng., 1 (1991), 19
- [34] WILLIAMS J.L., LEWIS J.L., J. Biomech. Eng., 104 (1982), 50
- [35] PIKHITSA P.V., Phys. Rev. Lett., 93 (2004), 015505
- [36] PASTERNAK E., DISKIN A.V., Int. J. Eng. Sci., 52 (2012), 103
- [37] LAKES R.S., Science, 235 (1987), 1038
- [38] GRIMA J.N., Auxetic Metamaterials, Strasbourg, France, 2010
- [39] Yeganeh-Haeri A, Weidner DJ, Parise JB. Elasticity of α -cristobalite: a silicon dioxide with a negative Poisson's ratio. Science 1992;257(5070):650-2
- [40] Keskar NR, Chelikowsky JR. Negative Poisson ratios in crystalline SiO₂ from firstprinciples

calculations. *Nature* 1992;358(6383):222

- [41] Gibson, L. J., Ashby, M. F., Schajer, G. S., and Robertson, C. I. The mechanics of two-dimensional cellular solids. *Proc. R. Soc. Lond.*, 1982, A382, 25–42
- [42] Gibson, L. J. and Ashby, M. F. *Cellular solids: structure and properties*, 1988 (Pergamon Press, London)
- [43] Evans, K. E., Alderson, A., and Christian, F. R. Auxetic 2-dimensional polymer networks – an example of tailoring geometry for specific mechanical-properties. *J. Chem. Soc. Faraday Trans.*, 1995, 91, 2671–2680
- [44] Masters, I. G. and Evans K. E. Models for the elastic deformation of honeycombs. *Compos. Struct.*, 1997, 35, 403–422
- [45] Prall, D. and Lakes, R. Properties of a chiral honeycomb with Poisson's ratio -1 . *Int. J. Mech. Sci.*, 1996, 39, 305–314
- [46] Theocaris, P. S., Stavroulakis, G. E., and Panagiotopoulos, P. D. Negative Poisson's ratios in composites with star-shaped inclusions: a numerical homogenization approach. *Arch. Appl. Mech.*, 1997, 67(4), 274–286
- [47] Larsen, U. D., Sigmund, O., and Bouwstra, S. Design and fabrication of compliant micromechanisms and structures with negative Poisson's ratio. *J. Microelectromech. Syst.*, 1997, 6, 99–106
- [48] Paulhac, A., Perrot, D., Scarpa, F., and Yates, J. R. Flatwise compressive behaviour of novel chiral honeycomb concept. DFC-7 Conference, Sheffield, 22–24 May 2003
- [49] Spadoni, A., Ruzzene, M., and Scarpa, F. Global and local linear buckling behaviour of a chiral cellular structure. *Phys. Status Solidi B*, 2005, 242, 695–709
- [50] Paulhac, A., Scarpa, F., Perrot, D., and Yates, J. R. Transverse shear strength of chiral cellular core. In *Proceedings of ICEM12*, Bari, Italy, 29 August to 1 September 2004
- [51] Sahab Babaee, Jongmin Shim, James C. Weaver, Elizabeth R. Chen, Nikita Patel, and Katia Bertoldi, "3D Soft Metamaterials with Negative Poisson's Ratio", (2013)
- [52] Lakes R.S. 1987. Foam structure with a negative Poisson's ratio. *Science* 235:1038–40
- [53] Friis E.A., Lakes R.S., Park J.B. 1988. Negative Poisson's ratio polymeric and metallic foams. *J. Mater. Sci.* 23:4406–14
- [54] Li D., Dong L., Lakes R.S. 2013. The properties of copper foams with negative Poisson's ratio via resonant ultrasound spectroscopy. *Phys. Status Solid. B* 250(10):1983–87
- [55] Alderson, A. A triumph of lateral thought. *Chem. Ind.*, 1999, 10, 384–391
- [56] Caddock, B. D. and Evans, K. E. Microporous materials with negative Poisson's ratios. I: Microstructure and mechanical properties. *J. Phys. D: Appl. Phys.*, 1989, 22, 1877–1882
- [57] Evans, K. E. and Caddock, B. D. Microporous materials with negative Poisson's ratios. II: Mechanisms and interpretation. *J. Phys. D: Appl. Phys.*, 1989, 22, 1883–1887
- [58] Alderson, A. and Evans, K. E. Modelling concurrent deformation mechanisms in auxetic microporous polymers. *J. Mater. Sci.*, 1997, 32, 2797–2809
- [59] Alderson, K. L., Alderson, A., Smart, G., Simkins, V. R., and Davies, P. J. Auxetic polypropylene fibres. Part 1. Manufacture and characterisation. *Plast. Rubbers Compos.*, 2002, 31(8), 344–349
- [60] Simkins, V. R., Alderson, A., Davies, P. J., and Alderson, K. L. Single fibre pullout tests on auxetic polymeric fibres. *J. Mater. Sci.*, 2005, 40, 4355–4364
- [61] L.J. GIBSON, M. F. ASHBY, G. S. SCHAJER and C. I. ROBERTSON, *Proc. Roy. Soc. Lond.* A382 (1982) 25
- [62] L.J. GIBSON and M. ASHBY, "Mechanics of cellular solids" (Pergamon, Oxford, New York, 1988)
- [63] A.G. KOLPAKOV, *Prikl. Mat. Mekh.* 59 (1985) 969
- [64] K. BERGLUND, *Arch. Mech.* 29 (1977) 383
- [65] HALL L.J., COLUCI V.R., GALVÃO D.S., KOZLOV M.E., ZHANG M., DANTAS S.O., BAUGHMAN R.H., *Science*, 320 (2008), 504

- [66] LIU Q., Literature Review: Materials with Negative Poisson's Ratios and Potential Applications to Aerospace and Defense, Defense Science and Technology Organization, Victoria, Australia, 2006
- [67] BEER F.P., JOHNSTON E.R., Mechanics of Materials, 3rd ed., MAKRON Books, S^o Paulo, Brazil, 1967
- [68] M.H. Fuetal, "International Journal of Solids and Structures", 80 284–296, (2016)
- [69] EVANS K.E., ALDERSON A., Adv. Mater., 12 (2000), 617
- [70] ARGATOV I.I., D'IAZ R.G., SABINA F.J., Int. J. Eng. Sci., 54 (2012), 42
- [71] COENEN V.L., ALDERSON K.L., Phys. Stat. Sol. B, 248 (2011), 66
- [72] CRITCHLEY R., CORNI I., WHARTON J.A., WALSH F.C., WOOD R.J.K., STOKES K.R., Phys. Stat. Sol. B, (2013), 1
- [73] TETRIAKOV K.V., WOJCIECHOWSKI K.W., J. Chem. Phys., 136 (2012), 204506
- [74] NAROJCZYK J.W., ALDERSON A., IMRE A.R., SCRAPA F., WOJCIECHOWSKI K.W., J. Non-Cryst. Solids, 354 (2008), 4242
- [75] CHOI J.B., LAKES R.S., Int. J. Fracture, 80 (1996), 73
- [76] BEZAZI A., BOUKHAROUBA W., SCARPA F., Phys. Stat. Sol. B, 246 (2009), 2102
- [77] DONOGHUE J.P., ALDERSON K.L., EVANS K.E., Phys. Stat. Sol. B, 246 (2009), 2011
- [78] MIATI S., ASHBY M.F., GIBSON L.J., Scripta Metall, 18 (1987), 213
- [79] HABERMAN M.R., HOOK D.T., TIMOTHY D., J. Acoust. Soc. Am., 132 (2012), 1961
- [80] HOWELL B., PRENDERGAST P., HANSEN L., Acoustic Behavior of Negative Poisson's Ratio Materials, Ship Materials Engineering Department – United States Navy, Arlington, United States of America, 1991
- [81] ALDERSON K.L., WEBBER R.S., MOHAMMED U.F., MURPHY E., EVANS K.E., Appl. Acoust., 50 (1997), 23
- [82] RUZZENE M., SCARPA F., Phys. Stat. Sol. B, 242 (2005), 665
- [83] GRIMA J.N., Modelling Auxetic Materials, Gdansk, Poland, 2009
- [84] CHEN Y.J., SCARPA F., FARROW I.R., LIU Y.J., LENG J.S., Smart Mater. Struct., 22 (2013), 045005
- [85] LAKES R.S., WITT R., Int. J. Mech. Eng. Edu., 30 (2002), 50
- [86] LORATO A., INNOCENTI P., SCARPA F., ALDERSON A., ALDERSON K.L., ZIED K.M., RAVIRALA N., MILLER W., SMITH S.W., EVANS K.E., Compos. Sci. Technol., 70 (2010), 1057
- [87] Y. LIU, H. HU., Sci. Res. Essays., 5 (2010), 1052
- [88] HASSAN M.R., SCARPA F., MOHAMED N.A, RUZZENE M., Phys. Stat. Sol. B, 245 (2008), 2440
- [89] JACOBS S., COCONNIER C., DIMAIO D., SCARPA F., TOSO M., MARTINEZ J., Smart Mater. Struct., 21 (2012), 075013
- [90] BIANCHI M., SCARPA F., SMITH C.W., Acta Mater., 58 (2010), 858
- [91] BIANCHI M., SCARPA F., SMITH C.W., WHITTEL G.R., J. Mater. Sci., 45 (2010), 341
- [92] ALDERSON A., ALDERSON K.L., MCDONALD S.A., MOTTERSHEAD B., NAZARE S., WITHERS P.J., YAO Y.T., Macromol. Mater. Eng., 298 (2013), 318
- [93] BIANCHI M., FRONTONI S., SCARPA F., SMITH C.W., Phys. Stat. Sol. B, 248 (2011), 30
- [94] UZUN M., PATEL I., Arch. Mater. Sci. Eng., 44 (2010), 120
- [95] KOPYT P., DAMIAN R., CELUCH M., CIOBANU R., Compos. Sci. Technol., 70 (2010), 1080
- [96] XU B., ARIAS F., BRITAIN S.T., ZHAO X.-M., GRZYBOWSKI B., TORQUATO S., WHITESIDES M., Adv Mater., 11 (1999), 1186
- [97] ALDERSON A., RASBURN J., EVANS K.E., GRIMA J.N., Membr. Tech., 137 (2001), 6
- [98] EVANS K.E., ALDERSON A., Adv Mater., 12 (2000), 617
- [99] Hong Hu, Minglonghai Zhang, Yamping Liu, "Auxetic textiles", 2019
- [100] CHOI J.B., LAKES R.S., Cell Polym., 10 (1991), 205
- [101] ALDERSON K.L., ALDERSON A., ANAND S., SIMKINS V., NAZARE S., RAVIRALA N., Phys. Stat. Sol. B, 249 (2012), 1322

- [102] ALDERSON A., ALDERSON K.L., Tech. Textiles Int., 77 (2005), 29
- [103] Hudson K, East G. Geotextiles; 1991, No. 6, ARRB